Spring 5-15-2018

Understanding Stroke in the Connected Human Brain

Joshua Sarfaty Siegel
Washington University in St. Louis

WASHINGTON UNIVERSITY IN ST. LOUIS
Division of Biology and Biomedical Sciences
Neurosciences

Dissertation Examination Committee:
David Van Essen, Chair
Maurizio Corbetta, Advisor
Nico Dosenbach
Jin-moo Lee
Abraham Snyder
Michel Thiebaut de Schotten

Understanding Stroke in the Connected Human Brain

by
Joshua Sarfaty Siegel

A dissertation presented to
The Graduate School
of Washington University in
partial fulfillment of the
requirements for the degree
of Doctor of Philosophy

May 2018
St. Louis, Missouri

Table of Contents

List of Figures

**References to figures made in chapter text will only give the figure number within that chapter. For example, if the notation 'Fig. 2' appears within the text of chapter 5, it refers to Figure 5-2.

List of Tables

List of Abbreviations

R-fMRI – resting state functional magnetic resonance imaging

BOLD – blood oxygenation level dependent

FC – Functional connectivity

DVARS –frame-to-frame fMRI signal intensity change (mean of whole-brain differentiated BOLD time series)

MTL – multi-task learning;

BVMT – brief visuospatial memory test;

HVLT – hopkins verbal learning test;

RSNs – Resting State Networks:

VIS = Visual network; PO = parieto-occipital; SMD = dorsal somato-motor; SMV = ventral somato-motor; AUD = auditory; CON = cingulo-opercular; VAN = ventral attention; SAL = Salience; CP = Cingulo-parietal; DAN = dorsal attention network; FPN = frontoparietal network; DMN = default mode network; NON = no assigned network.

Acknowledgments

I think about how lucky I am to be where I am, and be doing what I am doing, just about every single day. For that, and for everything written in this dissertation, the credit goes to the people that I have had the fortune to learn from, work with, and play with. I am humbled in my gratitude for their support. Here are those who have helped me the most through my career, in roughly chronological order.

Carla Lankford – a warm and kind soul, my first scientific mentor from my first scientific research position at the NIH, and still my friend today.

Carl Craver - When I got to Washington University in St. Louis as a freshman, undecided about what path to pursue, I took an introductory cognitive sciences class. By the end of every class, after an hour and a half of animated and provocative lecturing and debate, Dr. Craver would often leave the class drenched in sweat. His sweat was disturbing, but energy and inspiration was contagious. Over the next four years he was an inspiring teacher, my major advisor, thesis advisor, and a tremendous mentor in every sense. I very distinctly remember asking him if he would recommend me to go work in Steve Petersen's lab. "I'll do it, but don't fuck this up." - Having taught me during my freshman year, he had good reason for concern. But he recommended me… and I did my best not to. And so it goes.

Steve Petersen - for giving me the opportunity to work in his lab as an undergraduate and take a hands-on role in a neuroimaging experiment. From the beginning, Steve expected me to take the reins with almost every aspect of experimentation and to work though them thoughtfully and

carefully. But perhaps most importantly, joining Steve's lab changed my perception of what it means to be a scientist – because of the environment that he creates. He remains an excellent mentor, teacher, and scientific role model to me.

Brad Schlaggar – for taking time out of his busy schedule for me many times over the past 7 years. Brad is exceptional as a man who treats everyone fairly, treats every problem thoughtfully and never lets anything cloud his judgement and values.

Hristina Lessov-schlaggar - for just being a caring, inspirational, and fun person to be around.

Maurizio Corbetta – my thesis advisor. He has taught me that value of bringing clinical knowledge and experience to the intellectual and scientific pursuit of understanding the human brain. He has also taught me that art of taking small facts – one experiment or one paper – and fitting them in to large models that help us understanding how the brain works and help us to see what is the next experiment that needs to be done.

Avi Snyder – the incomparable. He is at once a bulldog and a puppy. And by this I don't mean that he walks on all fours, but that he fights for truth and clarity in science above all else, and he has been a great friend to me and to so many other graduate students that have passed through the neuroimaging labs. There would literally be no neuroimaging labs without Dr. Snyder. Despite this, he remains humble, down-to-earth, and patient with any student hungry to learn.

Gordon Shulman – who has kept the Corbetta lab grounded. He is a careful and thoughtful scientist, and my PhD work would not have been possible without his advice, mentorship, and collaboration.

Nick Metcalf – who has been so incredibly helpful as the ahh… senior data managing bioinformati..… the problem solver. I can't praise Nick enough for what he has given to the Corbetta lab, and to me. And just as importantly, Nick is just a great guy to work with and to hang out with.

Alex Carter – for being a clinical role model and a 'good guy' role model, and pushing me to always think about how our research relates to clinical care.

The members of my thesis committee - Jin-moo Lee, David Van Essen, Nico Dosenbach, Michel Thiebaut de Schotten – picking a thesis committee was honestly one of the most fun parts of this whole process for me. It was like putting together my scientific dream team. I got the all stars of stroke and of brain networks, the up and coming rookie, and even some guy in London (now Paris) – I just read his book on brain connections, thought it brilliant, and then called him up the next week and said "Hey, want to be on my thesis committee?" Beyond committee meetings, I have now had the opportunity to collaborate with every one of them, and it has been a pleasure.

Next, let me thank all of the students that I have had the pleasure to work with and play with in my years in the NIL.I will give a special thanks to Lenny Ramsey, who was really a great person to work with and just an impressive personality in so many ways. But I also thank the students before me – Steve Nelson, Alecia Vogel, Tim Laumann, Alex Cohen, Matt Brier, Mario Ortega – and the students of my cohort - Anish Mitra, Ben Seitzman, Haoxin Sun, and Dohyun Kim. I couldn't ask for a better group of people to work with.

Finally, there are many friends and family members who have support me thoughout the time I spent working on my dissertation. Here are a few that deserve special thanks.

My parents deserve the largest credit for allowing me to reach this point in my career. I definitely won the lottery on this one. No other way to put it. I learned a love of science and numbers from my dad. From my mom, I learned the value and the reward of finding something that you are passionate about and then pouring your heart in to it. But more importantly than any lesson, they have provided for me and supported me tirelessly and limitlessly.

Lastly, a special thanks to my beautiful wife, Jeannette Wong-Siegel. For patiently accepting my occasional long nights in the lab or at the computer. For providing me with the emotional and culinary support that I needed. For always pushing me to live up to my own expectations of myself. For making life a thrill and a joy. For often knowing what was best for me, even when I didn't … like getting a dog (boy, was I wrong about that one). This work is not my accomplishment, but our accomplishment.

Thank you.

Joshua S Siegel, Washington University, May 2018

Dedicated to Sophie.

Abstract

Structural and functional disconnection following stroke
by
Joshua Siegel
Doctor of Philosophy in Biology and Biomedical Sciences
Neurosciences
Washington University in St. Louis, 2016
Professor Maurizio Corbetta, Principal Investigator
Professor David Van Essen, Chair

Although structural damage from stroke is focal, remote dysfunction can occur in regions of the brain distant from the area of damage. Lesions in both gray and white matter can disrupt the flow of information in areas connected to or by the area of infarct. This is because the brain is not an assortment of specialized parts but an assembly of distributed networks that interact to support cognitive function. Functional connectivity analyses using resting functional magnetic resonance imaging (fMRI) have shown us that the cortex is organized into distributed brain networks. The primary goal of this work is to characterize the effects of stroke on distributed brain systems and to use this information to better understand neural correlates of deficit and recovery following stroke. We measured resting functional connectivity, lesion topography, and behavior in multiple domains (attention, visual memory, verbal memory, language, motor, and visual) in a cohort of 132 stroke patients. Patients were followed longitudinally with full behavioral and imaging batteries acquired at 2 weeks, 3 months, and 1 year post-stroke. Thirty age- and demographic-matched controls were scanned twice at an interval of three months.

In chapter 1, we explore a central question motivating this work: how is behavior represented in the brain? We review progressing prospective – from basic functional localization to newer theories connecting inter-related brain networks to cognitive operations. In so doing, we attempt

to build a foundation that motivates the hypotheses and experimental approaches explored in this work.

Chapters 2 and 3 serve primarily to validate approaches and considerations for using resting fMRI to measure functional connectivity in stroke patients. In chapter 2, we investigate hemodynamic lags after stroke. 'Hemodynamic lag' is a local delay in the blood oxygen level dependent (BOLD) response to neural activity, measured using cross-correlation of local fMRI signal with some reference brain signal. This work tests assumptions of the BOLD response to neural activity after stroke, but also provides novel and clinically relevant insight into perilesional disruption to hemodynamics. Significant lags are observed in 30% of stroke patients sub-acutely and 10% of patients at one-year. Hemodynamic lag corresponds to gross aberrancy in functional connectivity measures, performance deficits and local and global perfusion deficits. Yet, relationships between functional connectivity and behavior reviewed in chapter 1 persist after hemodynamic delays is corrected for. Chapter 3 provides a more extended discussion of approaches and considerations for using resting fMRI to measure functional connectivity in stroke patients. Like chapter 1, the goal is to motivate experimental approaches taken in later chapters. But here, more technical challenges relating to brain co-registration, neurovascular coupling, and clinical population selection are considered.

In chapter 4, we uncover the relationships between local damage, network wide functional disconnection, and neurological deficit. We find that visual memory and verbal memory are better predicted by connectivity, whereas visual and motor deficits are better predicted by lesion topography. Attention and language deficits are well predicted by both. We identify a general pattern of physiological network dysfunction consisting of decrease of inter-hemispheric

integration and decrease in intra-hemispheric segregation, which strongly related to behavioral impairment in multiple domains.

In chapter 5, we explore a case study of abulia – severe apathy. This work ties together principles of local damage, network disruption, and network-related deficit and demonstrates how they can be useful in understanding and developing targeted treatments (such as transcranial magnetic stimulation) for individual stroke patients.

In chapter 6, we explore longitudinal changes in functional connectivity that parallel recovery. We find that the topology and boundaries of cortical regions remains unchanged across recovery, empirically validating our parcel-wise connectivity approach. In contrast, we find that the modularity of brain systems i.e. the degree of integration within and segregation between networks, is significantly reduced after a stroke, but partially recovered over time. Importantly, the return of modular network structure parallels recovery of language and attention, but not motor function. This work establishes the importance of normalization of large-scale modular brain systems in stroke recovery.

In chapter 7, we discuss some fundamental revisions of past lesion-deficit frameworks necessitated by recent findings. Firstly, anatomical priors of structural and functional connections are needed to explain why certain lesions across distant locations should share behavioral consequences. Secondly, functional priors of connectomics are needed to explain how local injury can produce widespread disruption to brain connectivity and behavior that have been observed.

1 Introduction

A central question in neuroscience for nearly two centuries has been 'how behavior is represented in the brain?' Since the times of Wernicke and Broca in the late 19th century, the principle of localization of function – according to which different parts of the brain are specialized for different functions – has been center stage in our thinking about how the brain enables behavior. By the late 1980's, principles of cognitive neuroscience were emerging, bolstered by the advent of functional neuroimaging. Instead of the posited correspondance between one brain region and one function, the paradigm for studying brain function shifted to the idea that brain regions housed 'mental operations', and that behavior was mediated by ensembles of mental operations organized in 'networks' of brain regions. Research in the last 20 years has pushed us even further from a strict localizationist view. It has been shown that even single operations recruit distributed neural systems, and that even small lesions can cause functional alterations among distant regions of cortex with no structural connections to the lesion. The next paragraphs reviews in more detail these different theories about brain-behavior relationships, specifically in relation to lesion studies, with the goal of setting up a set of issues that I will address experimentally in my thesis.

1.1 The localization of human behavior

1.1.1 One area one function

Much of our understanding of brain function comes from over 140 years of studies that describe specific deficits following lesions to specific parts of the brain (Broca, 1861; Wernicke, 1874).

Maps of different behaviors (executive function, vision, movement, language, etc) onto different brain regions, as extrapolated from lesion-behavior studies, represent the most common framework for understanding the behavioral effect of focal or diffuse injuries to the brain (Fig. 1A).

From an historical perspective it is interesting to realize that the principle of localization of function, as any other theory in science, won the battle of cultural evolution through the natural selection offered by conference communications, papers, and political/sociological influence. When Broca first presented his theory and evidence in Paris in 1861, the reception was skeptical to say the least[1]. But by the early decades of the 1900's his views were dominant. This framed the work of the 20th century, with many researchers identifying abnormal behaviors that could be engendered by lesions in different locations, and few reporting observations that questioned the localizationist dogma.

But the conclusions drawn from studies were often circular consequences of the approaches and assumptions of the study. For example, most localization findings were based either on case series with a shared deficit of interest (e.g. a deficit of speech production or speech

---

[1] Pierre Flourens claims that, by ablation of various brain regions, he has disproven localization of function. In this very same year of 1861, a young surgeon named Paul Broca receives word of a patient named Leborgne in the Bicetre hospital with a processive loss of speech, but not a loss of language comprehensions. He is nicknames Tan due to his inability to say any words other than Tab. Misseure Leborgne dies a few years later and Broca performs an autopsy. He determines that, as predicted, Leborgne did in fact have a lesion in the frontal lobe in the left cerebral hemisphere. From a comparative progression of Leborgne's loss of speech and motor movement, the area of the brain important for speech production was determined to lie within the third convolution of the left frontal lobe, next to the lateral sulcus. This case finally gives him the edge over Pierre Flourens. In the following two years, Broca is able to find autopsy evidence for 8 more cases in support of the localization of articulated language to the left frontal lobe. Broca's findings were formally published in 1865 (Finger, 2004).

understanding), or else a comparison between a group of patients with and a group without a deficit of interest. Such approaches were designed to localize a 'function' by finding patients with a unique behavioral profile after a lesion to a specific location in the brain. The interpretation was that the deficient function was housed in the damaged part of the brain, thus leading to the creation of maps of normal functions in the brain based on their disruption after damage. The most successful examples of this approach were the demonstration that language was localized to specific regions of temporal and frontal cortex (Broca, 1861; Wernicke, 1874), and that memory encoding could be devastated by focal damage of the hippocampus (Scoville and Milner, 1957).

The advent of CT and MRI scans in the 1960's and 1970's allowed imaging of lesions in vivo. Along with the development of improved statistical techniques (Bates et al., 2003), this led to even finer mapping of deficits onto specific parts of the brain. These methods called 'voxel-based lesion-symptom mapping' are based on the same assumptions as the classical clinical studies. However, they take advantage of the increased spatial resolution of CT/MRI scans comparing often large groups of patients with or without a specific deficit down to the level of a small part of the brain, i.e. a voxel (a volume tipically 1-2 mm3). Voxel-based lesion-symptom mapping has been applied not only to basic sensory, motor, and cognitive functions or operations, but also to very complex cognitive constructs like theory of mind (Blanke et al., 2004; Saxe and Powell, 2006), body schema (Buxbaum et al., 2000; Buxbaum and Coslett, 2001), risk taking (Clark et al., 2008), the gist of language comprehension, and recognition of emotions in facial expression (Adolphs et al., 1994).

These approaches still included many of the same biases as the traditional anatomo-clinical method of single case studies, notably that disruption of behavior after a specific lesion implied a key contribution of that region of the brain to normal function. Additionaly, standard voxel-wise lesion-deficit methods use univariate statistics that assume statistical independence of neighboring voxels in their contribution to behavior. Especially with regard to stroke, this assumption is invalid. Damage frequently co-occurs in neighboring voxels or even more distant voxels within a common vascular distribution will frequently. This systematically distort precision and displace results of lesion-deficit maps (Mah et al., 2014; Phan et al., 2010). These biases can be attenuated by using multivariate approaches. A more significant problem is that statistical association methods like logistic regression begin with a deficit measured on some scale (independent variable), and then predict if a voxel is damaged or not (dependent variable). This precludes asking how much variance in a given behavior is explained by lesion location. A strict localizationist theory would predict that most of the variability of behavioral performance across of a group of patients would be explained by lesion location. This claim is not only important, but empirically falsifiable using machine learning models that predict deficit based on lesion. If the amount of variance accounted for in such a model is relatively small, then other explanations for the severity of behavioral disruption must be considered.

Another problem for lesion-symptom mapping studies is the interpretative bias toward cortex. Researchers have focused on the cortical damage, and have largely ignored the white matter. This bias is not surprising in the historical context of neuroanatomy. Initially, physiological studies electrical stimulation of cortex had a large influence on early neuroanatomical thinking (Gustav Fritsch and Edvard Hitzig, 1870, dog's motor cortex; Penfield, 1949 human cortex).

Moreover, the availability of a systematic way to identify cortical areas (Brodmann, 1909), and the corresponding lack of an atlas of the white matter, made it convenient to correlate behavioral deficits with damage of specific cortical areas. When CT scans became available for mapping lesions, lack of stereotactical methods of lesion analysis favored the projection of lesions onto a Brodmann's atlas. Despite availability of stereotactical lesion normalization, more recent voxel-based lesion-symptom mapping studies often remain biased toward cortex by focusing interpretation on troves of cognitive neuroimaging data showing cortical activation for different tasks.

But this 'cortico-centric' view of brain-behavior relationships was not so pronounced early on in the history of neuroanatomy. In 1874 Karl Wernicke described the 'conduction aphasia', resulting from damage to the arcuate fasciculus connecting temporal auditory centers to the frontal speech area (Wernicke, 1874). This became the prototype for the disconnection syndrome. Wernicke later hypothesized that connections from and to locations of the brain are as critical, and in some cases, even more critical than cortical localization to understanding deficit (Wernicke, 1885). Similarly, alexia and other syndromes were hypothesized to arise from disconnection (e.g. Dejerine, 1891). In the 1960's Norman Geshwind elaborated on these early views to propose disconnection as a major mechanism accounting for neurological deficits. However, the emphasis on the role of the white matter was largely lost in the decades that followed.

More recently, there has been a resurgence of the potential importance of white matter damage on behavior. For instance, the two brains that Broca initially described to support the importance of the left inferior frontal cortex for speech production later on were found to have extensive

damage of the frontal-temporo-parietal white matter, as well as damage of neighboring insular cortex and subcortical nuclei (Dronkers et al., 2007). Similar arguments apply for other famous cases that have been used as examples of localization of function (see Thiebaut de Schotten et al., 2015 for a re-consideration of important cases in the language of white matter damage). And both lesion and awake intraoperative stimulation approaches have enabled extensive description of the functional role of numerous large white matter bundles (Duffau, 2015).

More generally, even taking a cortico-centric view of lesion-behavior relationships, it became apparent in the 1970's that the traditional 'one area one function' approach was fallible. Studies of aphasia by the Boston VA group showed that the localization of lesion to specific 'language' regions did not produce the expected deficits. For instance damage to Broca's area did not produce a chronic linguistic problem (Mohr et al., 1978). Lesions anywhere in the large perisylvian cortex could produce linguistic deficits, and not even the distinction between anterior/speech output and posterior/speech understanding could be confirmed all the time (Mazzocchi and Vignolo, 1979; Vignolo et al., 1986).

Efforts to localize hemispatial neglect – a syndrome present in on third of acute stroke patients in which a deficit in awareness of one side of space (contralateral to the lesion) is observed – provided a further example of limitations to the localizationist model. Neglect was initially classified as a 'parietal sign' (Brain, 1941; Critchley, 1953; McFie et al., 1950; Paterson and Zangwill, 1944). Ensuing investigations pointed out that spatial neglect can also arise from damage to frontal cortex (Heilman and Valenstein 1972; Damasio et al. 1980), temporal cortex (Beume et al., 2016; Karnath et al., 2001) thalamus (Cambier et al., 1980; Watson et al., 1981; Watson and Heilman, 1979), and to the basal ganglia (Damasio et al., 1980; Hier et al., 1977;

Kumral et al., 1999; Leibovitch et al., 1998; Sapir et al., 2007). And studies by De Renzi and collaborators showed that the laterality of spatial functions to the right hemisphere was relative and not absolute (De Renzi, 1982).

1.1.2 Mental Operations and the Modular Organization of the Brain

By the late 1980's, emerging principles of cognitive neuroscience, originating from the fusion of cognitive science and neuroscience, led to the idea that behavior results from a series of mental operations carried out by an ensemble of distributed brain regions (Fig. 1B). This was thanks in large part to the advent of functional neuroimaging in 1980-1990's (Belliveau et al., 1991; Fox and Raichle, 1986; Posner et al., 1988). Functional brain images showed that even simple tasks engaged numerous widely distributed brain areas, and that behavior requires the orchestration of multiple cortical and sub-cortical regions organized in networks (Mesulam, 1990; Posner et al., 1988). For example in a landmark study Petersen and colleagues used PET activation methodology with O15-water to show that simple language tasks engaged not only left but also right hemisphere regions, and that even cerebellar regions were involved in the cognitive aspect of word selection (Petersen et al., 1988).

In the cognitive neuroscience way of thinking, a brain region is conceptualized as a processor that performs a specific operation on an input, and generates a specific output to another region. A complex behavior is putatively represented by the sequential and precise temporal recruitment of different processing operations, hence brain regions. Brain regions specialized for different functions are organized in dedicated networks (attention, memory, language) (Mesulam, 1990;

Posner et al., 1988). Fairly abstract cognitive functions could now be understood as a combination of simpler operations.

This led researchers to try to identify the key sites of dysfunction of specific complex cognitive systems by combining psychometric tasks able to isolate specific cognitive components with accurate structural imaging of lesions using MRI. A parallel agenda in healthy subjects involved *mapping specific operations onto brain areas* using functional neuroimaging in combination with carefully designed psychological paradigms in which a single element of the task was manipulated either dichotomously or parametrically.

Early notable attempts involved, for instance, the localization of three putative components of the orienting attention system: disengage, move, engage to posterior parietal cortex, superior colliculus/frontal eye field, and pulvinar of the thalamus (Posner and Cohen, 1984). Another attempt was the separation of the three sub-sytems of attention: an orienting network involving posterior parietal cortex; an arousal network involving right inferior frontal cortex and inferior parietal cortex; and, a response selection involving anterior cingulate and dorsolateral prefrontal cortex (Posner and Petersen, 1990). Yet efforts to find corresponding anatomical and behavioral dissociations in stroke patients have not yielded robust dissociations (Rengachary et al., 2011; Verdon et al., 2009) [reviewed in Corbetta and Shulman, 2011]. On the contrary, most patients with hemispatial neglect suffer from a combination of deficits of visuospatial attention, motor exploration, arousal, and sustained attention.

There are several reasons why a simple mapping of one brain region to one mental operation (one-to-one) does not represent a satisfactory model of brain-behavior relationships. A first fundamental problem is that patterns of activation that include multiple distant brain areas appear

to correspond to even a single cognitive operation like a shift of attention, or the detection of a mismatch in response (many-to-one) (Dosenbach et al., 2006). A second possible problem is that certain regions are driven by many cognitive tasks, and thus damage to a region can cause deficits in multiple domains (one-to-many).

A third problem is that a lesion in the brain causes distributed functional abnormalities to structurally normal regions of the brain. Appreciation for this phenomenon gained considerable momentum in the late 1990- early 2000s. fMRI studies showed that functional abnormalities correlate with acute deficits, and tend to normalize in parallel with recovery of function (Buckner et al., 1996; Corbetta et al., 2005; Saur et al., 2006; Ward et al., 2003). These imaging observations provide the provocative suggestion that a lesion can broadly alter neural function across many brain regions, and that this widespread functional alteration may be the best correlate of abnormal behavior in the presence of a brain lesion.

This idea is also not novel as it corresponds to the principle of '*diaschisis'*, first enunciated by Konstantin Von Monakoff in 1914 (von Monakow, 1914). Diaschisis is the principle that neurophysiological changes can occur distant from a focal brain lesion. De-afferentations, or loss of input to a cortical area, can produce immediate changes in metabolism, blood flow, resting neural activity, and evoked neural activity. Consider a straightforward anatomical illustration of this principle; destruction of ascending dopaminergic nigrostraital pathways results in a reduction of glucose metabolism in the basal ganglia (Schwartz, 1978). For more extensive reviews of focal diaschisis, we direct the reader to (Feeney and Baron, 1986) and (Carrera and Tononi, 2014). More complex relationships have been proposed between subcortical damage and cortical blood flow and glucose metabolism (Hillis et al., 2002). However, the relationship of

hypoperfusion or hypometabolism to behavior remains uncertain. More generally, analogously to lesion information, it is entirely unclear how much of behavioral variability functional alterations of any type explain. This major gap is largely due to lack of any large-scale studies of stroke patients in which behavior, structure, and function have been systematically examined.

1.1.3 Hierarchical network models of brain function

Finally, we have begun to move towards a framework in which the brain is not an assortment of specialized parts but an assembly of distributed networks that flexibly interact to support cognitive function. Brain activation and the flow of information in response to a stimulus is highly dependent on a functional backbone of brain synchrony occurring in the absence of stimulus. Concepts such as brain synchronization have taken center stage in our thinking, and we have come to appreciate that in order to understand human behavior, we must understand functional brain systems that remain active, interdependent and balanced even in the absence of behavior.

It is fair to say that a new theory of brain function and behavior has not yet emerged, but a growing body of evidence points to the importance of ongoing activity and network organization for behavior. This new framework has gained traction largely as a result of studies analyzing the temporally correlated spontaneous activity in the blood-oxygenation level dependent (BOLD) signal, which has emerged as a powerful tool for mapping the brain's functional organization. Resting functional magnetic resonance imaging (R-fMRI) measures BOLD fluctuations and has been used to define distributed and modular brain systems (Doucet et al., 2011; Carl D Hacker et al., 2013; Power et al., 2011; Yeo et al., 2011) that correspond to the functional domains in the

brain (Bertolero et al., 2015; Smith et al., 2009). Using this approach, several important advances have been made toward understanding the functional architecture of the human brain. Individual differences in brain connectivity at rest correlate with differences in behavior (Baldassarre et al., 2012; Smith et al., 2015; Vaidya and Gordon, 2013). Moreover, learning and therapeutic intervention produce measurable changes in FC in relevant cortical circuits (Albert et al., 2009; Lewis et al., 2009; Tambini et al., 2010).

Learning not only modulates activation within a brain area, but also alters the strength of functional connections between brain areas. And conversely, a stroke not only damages brain tissue and de-afferents anatomically connected regions, but also alters communication in the functional network in which the lesion is embedded, and can even disrupt the dynamic balance between other networks in the brain (Fig. 1,C/D). Thus, the resulting behavioral deficit reflects not only the local effects of the lesion, but also disruptions of other networks that communicate with the one that is predominantly affected.

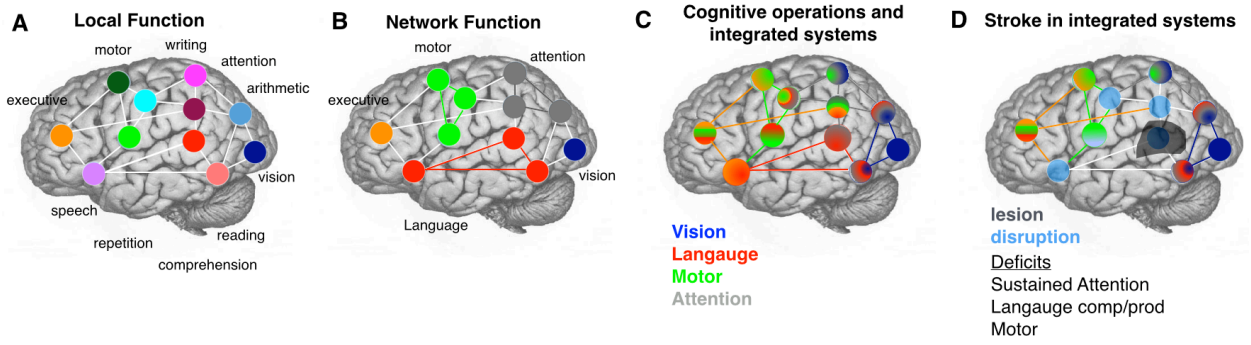

Figure 1-1. Progression views of brain-behavior relationships
At left, the localizationist model is depicted. Specific behaviors such as speech, arithmetic, and motor function are carried out by specific foci. Next, an association or network model is depicted. Networks of areas are responsible for broader domains of behavior such as 'attention'. Next, an integrated system is depicted. While a brain area may carry out a specific 'cognitive operation', that operation may be simultaneously important to motor, attention, and language functions. Finally, the effect of a lesion to the integrated system is depicted. The loss of a single node disruptes the functional of multiple connected nodes and produces deficit in multiple behavioral domains.

Given the presence of multiple networks, an important issue is the relative specificity of the behavioral dysfunction in relation to the alteration of network function. Before my work began our laboratory had provided evidence in small case series' that alterations of communication (FC) in specific networks (e.g. dorsal attention) was associated with network specific impairment (e.g. spatial attention deficits) (He et al., 2007; Carter et al., 2010). However, the specificity of such relationships across brain networks and across multiple behavioral domains was unknown. Moreover, it was unknown if these network abnormalities remain encapsulated in the network of interest or 'spread' and with what rules to other networks? More importantly, it was entirely unknown how relevant were these abnormalities for behavior, i.e. how much behavioral variance did they account for by structural damage versus network disruption? Finally, the relationship of network disruption to recovery was entirely unknown.

The primary goals of the research described in this thesis is to generate a holistic understanding of the relationship between local damage, global connectivity changes, and the behavioral deficits [and recovery] that follows. I aim to use this information to update the principles described above – namely, neural correlates of deficit and recovery following stroke and models of how networks in the human brain interact to support cognitive functions.

1.2 Approach

Our goals is to elucidate the relationship between stroke and deficit without *a priori* assumption of functional localization or isolation of deficit. This means designing experiments to answer questions such as: Do behavioral deficits tend to occur in isolation, in clusters with other deficits,

or along a single axis of domain-general deficit? To what extent is a behavioral deficit predicted by the location of the lesion – and does this differ between behaviors? Are deficits (and recovery) better predicted in the individual by the location of their lesion or by disruptions to their brain connectivity? Do common network principles emerge in FC-deficit models across behavioral measures? To answer these questions, we recruited a heterogeneous sample of stroke patients and examined a wide range of neuropsychological measures (Fig. 2). This is in contrast to prior lesion-deficit and FC-deficit mapping studies that have typically recruited groups with presence or absence of a common deficit or lesion. In addition, we implement multivariate approaches (such as a multi-task learning model described in chapter 4) to remove hidden biases, quantitatively assess not just localization, but *localizability*, and disentangle domain-specific versus domain-general deficit-related changes in brain connectivity.

This project involves a large cohort (n=132 completing timepoint 1) of patients tested longitudinally at 3 time points that span one year, and includes 1) a behavioral battery that provides a broad and deep assessment of neurological function 2) structural scans to measure anatomy and 3) resting-state fMRI and ASL scans to measure physiology. Importantly, control subjects were matched to patients both in age, demographics, and stroke predisposition (to our best approximation). In the below work, we first determine the degree to which post-stroke hemodynamics are altered and the impact this has on measuring FC using R-fMRI. We then use lesion location and functional connectivity to test predictions about the three-way relationship between disconnection, networks disruption and clinical deficit. Finally, we attempt to understand how damage and FC changes are associated with recovery from stroke.

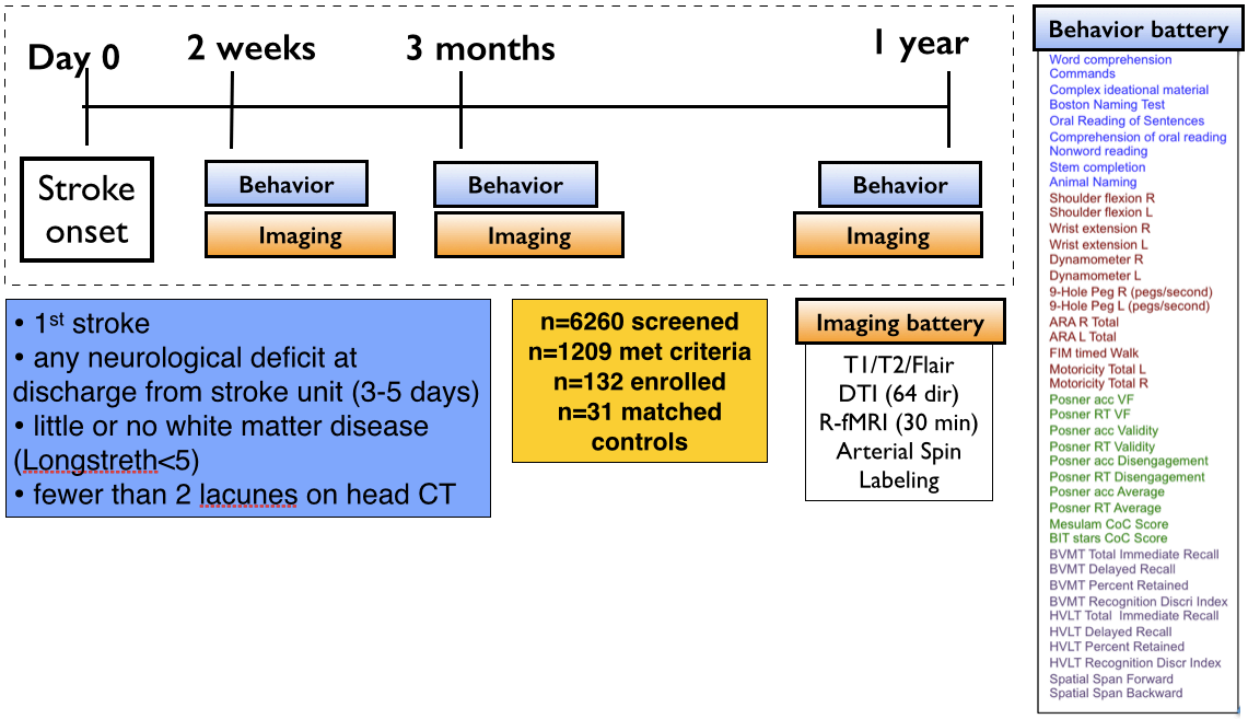

Figure 1-2. Longitudinal stroke study recruitment, behavioral and imaging batteries.

2 The effects of hemodynamic lag on functional connectivity and behavior after stroke.

This chapter has been published as a journal article. The citation is:

Siegel, J.S., Snyder, A.Z., Ramsey, L., Shulman, G.L., and Corbetta, M. (2015). The effects of hemodynamic lag on functional connectivity and behavior after stroke. Journal of Cerebral Blood Flow and Metabolism 0271678X15614846.

2.1 Abstract

Stroke disrupts the brain's vascular supply, not only within but also outside of areas of infarction. We investigated temporal delays (lag) in resting state functional magnetic resonance imaging signals in 130 stroke patients who were scanned 2 weeks, 3 months and 12 months post stroke onset. 30 controls were scanned twice at an interval of 3 months. Hemodynamic lag was determined using cross-correlation with the global gray matter signal. Behavioral performance in multiple domains was assessed in all patients. Regional cerebral blood flow and carotid patency were assessed in subsets of the cohort using arterial spin labeling and carotid Doppler ultrasonography. Significant hemodynamic lag was observed in 30% of stroke patients sub-acutely. Approximately 10% of patients showed lag at 1-year post-stroke. Hemodynamic lag corresponded to gross aberrancy in functional connectivity measures, performance deficits in multiple domains and local and global perfusion deficit. Correcting for lag partially normalized abnormalities in measured functional connectivity. Yet post-stroke FC-behavior relationships in the motor and attention systems persisted even after hemodynamic delays were corrected. Resting state fMRI can reliably identify areas of hemodynamic delay following stroke. Our data reveal that hemodynamic delay is common sub-acutely, alters functional connectivity, and may be of clinical importance.

2.2 Introduction

The front matter includes all material that appears before the beginning of the body of the text. Number all front matter pages (except the title page and the optional copyright page) with lowercase roman numerals, starting with ii, centered just above the bottom margin. Each of the following sections should begin on a new page. Stroke causes a disruption to the brain's vascular supply that leads to infarction and structural damage of gray/white matter, but also remote physiological and metabolic effects in structurally normal regions of the brain. It is becoming increasingly apparent that an understanding of behavioral deficits post-stroke and their recovery will require a complete description not only of lesion topography, but also of the complement of metabolic, structural and functional connectivity abnormalities, which in turn may relate to abnormal neuronal dynamics at the level of whole brain networks (Corbetta, 2012; Grefkes and Fink, 2014). Functional MRI is the primary tool to examine network level abnormalities caused by focal or diffuse brain diseases based on the premise of a normal coupling between neuronal activity and related blood flow/volume changes (hemodynamic response, HDR).

However, when studying disease states, a normal hemodynamic response cannot be assumed (D'Esposito et al., 2003). For instance, prior work has established that the hemodynamic response can be altered following stroke (Pineiro et al., 2002; Salinet et al., 2013). In patients with cerebrovascular disease, peak BOLD response delays of up to 20 seconds have been reported in the affected hemisphere (Carusone et al., 2002; Bonakdarpour et al., 2007; Amemiya et al., 2012). Such responses are said to exhibit hemodynamic lags.

In resting state MRI (R-fMRI), functional connectivity between regions of the brain is estimated by the temporal correlation of the spontaneous BOLD signal. Two recent studies observed BOLD signal delays in R-fMRI in small cohorts (Amemiya et al., 2013; Lv et al., 2013). These studies raise concerns about how hemodynamic lags might be affecting measurement of functional connectivity after stroke.

In this study we address fundamental questions concerning cerebrovascular physiology in stroke, specifically concerning the importance of hemodynamic lags in relation to changes of functional connectivity (FC), regional cerebral blood flow (rCBF) or diaschisis, as well as behavior and recovery. We report on a longitudinal study of hemodynamic lag in a cohort of 130 first time ischemic and hemorrhagic stroke patients. We consider the longitudinal trends, physiological correlates, and clinical implications of hemodynamic lag. We demonstrate a relationship between lag, and decrements of blood flow, and severity of clinical deficits after stroke. We also demonstrate that lag profoundly affects measures of FC and we investigate the effects of hemodynamic lag on previously reported FC-behavior relationships. Finally, we test a method for correcting for hemodynamic lag in measures of functional connectivity.

2.3 Methods

2.3.1 Patient Enrollment

All aspects of this study were approved by the Washington University School of Medicine (WUSM) Internal Review Board. Written informed consent was obtained from all participants in accordance with the Helsinki Declaration and procedures established by the Washington University in Saint Louis Institutional Review Board and all participants were compensated for their time. First time stroke patients were recruited by a research coordinator through the in-patient service at Barnes-Jewish Hospital (BJH) and the Rehabilitation Institute of St. Louis (TRISL). Inclusion criteria for stroke patients were: 1) Age 18 or greater, 2) first symptomatic stroke, ischemic or intraparenchymal hemorrhagic etiology, 3) clinical evidence of motor, language, attention, visual, or memory deficits based on neurological examination, and 4) time of enrollment < 2 weeks post-stroke onset. Exclusion criteria were: 1) the inability to maintain wakefulness during testing, 2) the presence of other neurological, psychiatric or medical conditions that preclude active participation in research and/or may alter the interpretation of the behavioral/imaging studies (e.g., dementia, schizophrenia), or limit life expectancy to less than 1 year (e.g., cancer or congestive heart failure class IV), 3) evidence of clinically significant periventricular white matter disease (equal or above grade 5 of Longstreth and colleagues(Longstreth et al., 1996)), and 4) contraindications for MRI including claustrophobia or scanner incompatible implants. In total, 6260 charts were screened; 130 patients met all inclusion criteria and completed the entire sub-acute protocol (mean age 52.8 with range 22-77,

119 right handed, 61 female, 64 right hemisphere). Of those, 101 had ischemic strokes, 21 hemorrhagic, 5 ischemic with later hemorrhagic conversion, and 3 carotid or vertebral dissection. Other features of the patient cohort and lesion distribution were described previously(Corbetta et al., 2015).

2.3.2 Stroke Source Population

We conducted a control analysis to determine whether our stroke sample was representative of the general stroke population. The demographic and medical characteristics of the patients in our sample were compared to those of a large control group (n = 1,209) that was selected from the Cognitive Rehabilitation Research Group database(Wolf et al., 2009) of all patients seen at Barnes Jewish Hospital between 2008 and 2013 (n = 6,260) using the same inclusion/exclusion criteria. All included stroke and control subjects provided informed consent according to procedures approved by the Institutional Review Board at Washington University.

2.3.3 Healthy Control Enrollment

Thirty healthy, demographically matched control subjects were recruited and underwent the same behavioral and imaging exams. Inclusion criteria for control subjects were: healthy adult matched to stroke study population by age, gender, handedness, and level of education. Exclusion criteria were: 1) a positive history of neurological, psychiatric, or medical abnormalities preventing participation in research activities, 2) a history of atherosclerotic (coronary, cerebral, peripheral) artery disease, 3) an abnormal neurological examination with

signs of CNS dysfunction. The average age at the time of enrollment was 55.7 years (SD=11.5) with a range from 21 to 83 years.

2.3.4 R-fMRI acquisition and analysis

Patients were studied 2 weeks (mean=13.4 days, SD=4.8 days), 3 months (mean=112.5 days, SD=18.4 days), and 1 year (mean=393.5 days, SD=55.1 days) post-stroke onset. Controls were studied twice at an interval of 3-months. All imaging was performed using a Siemens 3T Tim-Trio scanner at the Washington University School of Medicine (WUSM) and the standard 12-channel head coil. The MRI protocol included structural, functional, pulsed arterial spin labeling (PASL) and diffusion tensor scans. Structural scans included: (1) a sagittal T1-weighted MP-RAGE (TR=1950 msec, TE=2.26 msec, flip angle=90°, voxel size=1.0×1.0×1.0 mm); (2) a transverse T2-weighted turbo spin-echo (TR=2500 msec, TE=435 msec, voxel-size=1.0×1.0×1.0mm); and (3) sagittal FLAIR (fluid attenuated inversion recovery) (TR=7500 msec, TE=326 msec, voxel-size=1.5×1.5×1.5mm). PASL acquisition parameters were: TR=2600 msec, TE=13 msec, flip angle=90°, bandwidth 2.232 kHz/Px, and FoV 220mm. 120 volumes were acquired (322 seconds total), each containing 15 slices with slice thickness 6 mm and 23.7mm gap. Resting state functional scans were acquired with a gradient echo EPI sequence (TR=2000 msec, TE=27 msec, 32 contiguous 4 mm slices, 4×4mm in-plane resolution) during which participants were instructed to fixate on a small cross in a low luminance environment. Central fixation and wakefulness were monitored with an eye tracker and recorded. Six to eight R-fMRI runs, each including 128 volumes (30 min total), were acquired.

Participants with less than five minutes of retained R-fMRI data after strict motion scrubbing were excluded from further analysis. The fraction of participants providing useful fMRI data was 107/130 patients at 2 weeks, 86/94 patients at 3 months, 74/82 patients at 1 year, 24/30 controls at scan 1, and 24/29 controls at scan 2 (Table S1).

2.3.5 R-fMRI Data Preprocessing

R-fMRI data underwent preprocessing as previously described by Baldassarre and colleagues(Baldassarre et al., 2014a). Briefly, this included: 1) compensation for asynchronous slice acquisition using sinc interpolation; 2) elimination of odd/even slice intensity differences resulting from interleaved acquisition; 3) whole brain intensity normalization to achieve a mode value of 1000; 4) spatial realignment within and across R-fMRI runs; and 5) resampling to 3mm cubic voxels in atlas space including realignment and atlas transformation in one resampling step. Cross-modal (e.g., T2-weighted to T1-weighted) image registration was accomplished by aligning image gradients(Rowland et al., 2005). Cross-model image registration in patients was checked by comparing the optimized voxel similarity measure to the 97.5 percentile obtained in the control group. In some cases, structural images were substituted across sessions to improve the quality of registration.

2.3.6 Lesion Segmentation

Lesions were manually segmented using Analyze (www.mayo.edu) by inspection of the structural images (T1-weighted, T2- weighted, FLAIR), simultaneously displayed in atlas space. All segmentations were reviewed by two neurologists (Maurizio Corbetta and Alexandre Carter)

with special attention to distinguishing lesion from CSF and hemorrhage from surrounding vasogenic edema. The lesions ranged from 0.02cm^3 to 82.97cm^3 with a mean of 10.15cm^3 (SD=13.94cm^3).

2.3.7 Pulsed ASL and Carotid Doppler

Pulsed arterial spin labeling (PASL) measures of regional cerebral blood flow (rCBF) were acquired in a subset of patients (27 sub-acute patients and 20 controls). Two proximal inversion with control for off-resonance effects (PICORE Q2) PASL-MRI perfusion scans were collected. PASL data were processed as described previously(Arbeláez et al., 2013). Normalized perfusion (percent of control average) was determined for a set of 169 regions of interest (ROIs) described below. Bilateral carotid Doppler was also acquired at initial post-stroke hospital admission for 66 of the included patients. Carotid Doppler velocity values were converted to categories of 1) ≤50% occlusion, 2) 51-79% occlusion, or 3) ≥80% occlusion, based on guidelines from the Society of Radiologists in Ultrasound Consensus Conference(Grant et al., 2003). PASL and carotid Doppler were compared with R-fMRI measures of local (region of interest) and global (affected hemispheric) lag to determine how perfusion measures associate with lag.

2.3.8 Behavioral Testing

All subjects and controls underwent a behavioral battery that included assessment of motor, language, attention, memory, and visual function following each scanning session. Overall clinical deficit was also assessed in each patient using the NIH stroke scale (NIHSS)(Brott et al., 1989). Imaging and behavioral testing session usually were performed on the same day.

Dimensionality reduction was performed on the behavioral performance data as described previously(Corbetta et al., 2015). Principal components analysis was performed on all tests within a behavioral domain to produce a single score that predicted the majority of variance across tasks. The 'Motor' score describes contralesional deficits that correlated across shoulder flexion, wrist extension/flexion, ankle flexion, hand dynamometer, nine hole peg, action research arm test, timed walk, functional independence measure, and the lower extremity motricity index. The 'Attention (visual field)' score describes contra-lesional visual field effects in Posner, Mesulam, and BIT center of cancellation tasks. A separate 'Attention (sustained)' score loaded on non-spatial measures of overall performance, reaction time, and accuracy on the same tests. The 'Spatial Memory' score loaded on the Brief Visuospatial Memory Test and spatial span. The 'Verbal Memory' score loaded on the Hopkins Verbal Learning Test. The 'Language' score loaded on both comprehension (complex ideational material, commands, reading comprehension) and production (Boston naming, oral reading).

2.3.9 ROIs

A set of 169 regions of interest (ROIs), which was defined based on Hacker and colleagues(Carl D Hacker et al., 2013), were used in post hoc analyses. Briefly, the ROIs were selected based on a meta-analysis of task fMRI studies and refined to optimally represent 7 resting state networks. ROI-based analysis was used for 1) lag laterality measurement, 2) resting BOLD power analysis, and 3) FC analyses. ROIs partially or entirely overlapping with the infarct were excluded from all analyses (excepting the within-lesion BOLD power analysis).

Gray matter, white matter, and CSF ROIs were defined in individual subjects using automated segmentation by FreeSurfer(Fischl, 2012) and excluding any voxels that overlapped with the manual segmented lesion masks.

2.3.10 Lag measure

The R-fMRI data were first temporal bandpass filtered, retaining frequencies between 0.009-0.09Hz. Next, frame censoring identified volumes with a DVARS measure > 0.6% or a framewise displacement > 0.5mm to be excluded from the R-fMRI computations(Power et al., 2012). A shift mask was then generated by removing every frame within 4TR of masked frames. A minimum of 150 usable frames was required for subject inclusion in the present results. Thus, 23/130 sub-acute patients and 6/30 controls were excluded. In the retained data, on average, 570 out of 870 frames remained in sub-acute patients, and 495 of 851 frames remained in controls (Table S1). Next, a reference signal was generated from the average timecourse in each subject's [non-lesion] gray matter ROI.

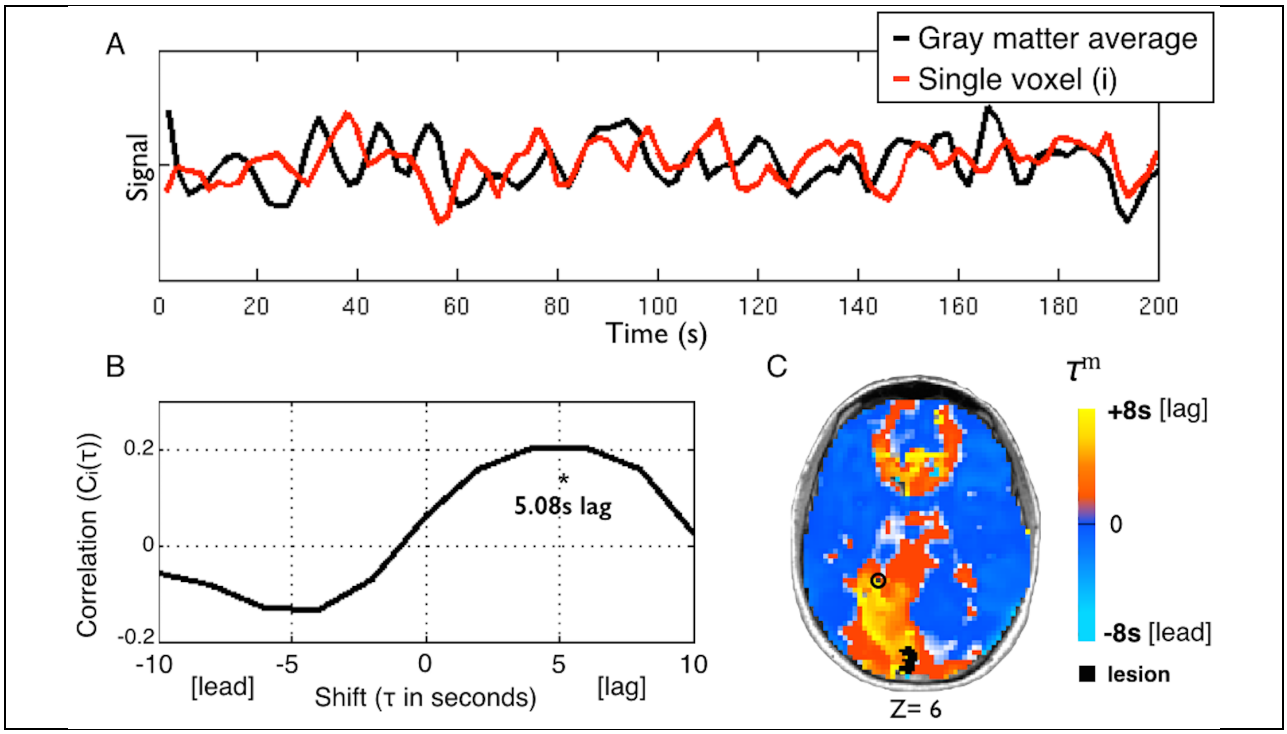

Figure 2-1 Using temporal cross-correlation to measure lag in resting state fMRI.
A) The global reference signal (black line, top panel) is measured by averaging all non-lesioned gray matter voxels. Each voxel timecourse (red line, top panel) is then compared to the reference signal. The exemplar voxel is circled in C. B) The voxel timecourse is shifted forward and backward 8s (±4 TR) and shift correlation is computed (Eq. 1). 5.08s is the optimal shift determined by parabolic interpolation. C) Voxelwise hemodynamic lag image. Orange/yellow indicates a lag behind the reference signal, cyan indicates a lead. Lesioned areas are shown in black. A small caudal infarct in left posterior cerebral artery (PCA) territory shows associated lag in the entire left PCA distribution. A full lag map for this individual is shown in row 5 of Figure 2.

Lagged cross-correlation analysis with reference to the global gray matter reference signal was performed for each voxel over the range ±4 TRs (±8 seconds) (Figure 1):

$$C_i(\tau) = (1/n_\tau) \sum_t \left[\frac{g(t) \cdot s_i(t+\tau)}{\sigma_{s_i} \sigma_g} \right], \qquad (1)$$

where g is the gray matter signal, s_i is the signal in voxel i, and σ_{s_i} and σ_g are the standard deviations of the two signals. The summation runs over frames indexed by t, and n_τ is the number of frames included after a shift of τ (-8s to +8s). To determine the shift that maximizes

the cross-correlation function at a temporal resolution finer than 1TR, the lag (τ) corresponding to the maximum of $C_i(\tau)$ was identified. $C_i(\tau)$ at this lag, as well as one step forward and backward, were fit with a parabolic function and the peak value, $C_i(\tau^m)$, and corresponding temporal shift (τ^m) were computed(Mitra et al., 2014). Positive and negative values of τ^m correspond, respectively, to a lag or lead relative to the mean gray matter signal. The lag measure, τ^m, was computed for every voxel within the brain. Voxels within the lesion as well as voxels not positively correlated with the global signal on the interval, $-8 < \tau < +8$ (in units of seconds), were excluded from region of interest and FC analyses. For visualization, lag maps were smoothed with a 3mm full width at half maximum kernel.

2.3.11 Lag Laterality

Inspection of lag maps demonstrated that lags > 2 sec almost always were confined to the lesioned hemisphere. Thus, it was possible to compute lag laterality scores as a measure of average lag difference in the affected versus unaffected hemisphere. Lag laterality was computed for each patient by finding the average lag for each of the 169 ROIs (excluding those intersecting the lesion) and then computing the difference between all right hemisphere ROIs (78/169) and all left hemisphere ROIs (78/169). The reliability of measured lag maps as well as laterality scores theoretically depends on the quantity of available data(Lv et al., 2013). These relationships were estimated using data subsamples of duration 40s to 800s.

The lag laterality score was used to compare lag severity to clinical variables. Because lag laterality values were not normally distributed, lag laterality was compared with categorical variables using a Mann-Whitney U test, and to continuous variables using Spearman's rank test.

2.3.12 Resting state BOLD power analysis

The BOLD signal power across the low frequency range typically used for resting state FC (0.009-0.09Hz) was computed on all ROI timecourses in all sub-acute subjects. ROIs were then subdivided into three categories: 1) ROIs partially or wholly within a lesion, 2) ROIs that show greater than 2 seconds of lag, 3) all other ROIs. The average power spectrum was then computed for each category.

2.3.13 Correcting functional connectivity measures for hemodynamic lag

Hemodynamic lags theoretically distort FC measures in a manner that is potentially correctible. To address this question, corrected FC measures were computed by shifting regional timeseries according to the previously determined hemodynamic lags. In greater detail, for any pair of signals, one of the timeseries was shifted by the lag difference and this difference was rounded to the nearest TR to avoid timeseries interpolation. FC was then computed using the standard formula (Fisher z-transformed Pearson correlation $\equiv z(r)$). The correction procedure was used to create corrected FC maps for selected ROIs. In addition, indices of interhemispheric FC in the motor system were computed with and without correcting for hemodynamic lag. This index was computed as the average z(r) over multiple motor ROI pairs (10 in the left hemisphere, 12 in the right hemisphere), excluding any ROI compromised by lesion.

To determine if correcting lag improves FC, aberrancy of FC relative to controls was determined for all ROIs in all patients(Siegel et al., 2014). Functional connectivity aberrancy was first quantified for each connection (169-choose-2) by comparing to the mean and standard deviation for that connection in controls. Z-normed FC aberrancy was computed as $(FC_{sub} - \overline{FC}_{control})/SD$, where the over-bar indicates mean over controls and SD is standard deviation over controls. Finally, to determine aberrancy of a given ROI, the Z-score for all of its connections was averaged.

2.4 Results

Subjects (n=130) with first symptomatic stroke anywhere in the brain and evidence of neurological impairment were recruited. To assess whether the study sample was representative of a the larger stroke population, it was compared to a larger source population of 1,209 patients. The study sample was well matched to the source population on stroke variables (etiology, tPA, mechanical thrombectomy, NIHSS in hospital), but showed some differences in demographics and clinical predisposing factors (age, race, coronary artery disease and atrial fibrillation) (Table S2). Further details of this comparison are reported in the supplement. Of the 130 patients studied, 107 had adequate R-fMRI and behavioral data. Of those, 87 had ischemic strokes and 15 had hemorrhagic strokes. Patients with ischemic stroke were further classified based on TOAST criteria(Adams et al., 1993). Regarding ischemic subtypes, large-artery atherosclerosis was observed 16 patients, cardioembolism in 12; small-vessel occlusion in 8, and undetermined etiology (two or more causes identified, stroke is cryptogenic, or evaluation is incomplete) in 45.

Table 2-1. Clinical and behavioral correlates of lag.

	P-value (uncorrected)	Relationships
Neurological History		
Migraine (5)	0.48	
Other neurological history (5)	0.11	
Psychological History		
Depression (5)	0.15	
Substance abuse (13)	0.29	
Cardiac History		
Hypertension (74)	0.70	
Coronary artery disease (9)	0.98	
Diabetes Mellitus (33)	0.18	
Atrial Fibrillation (5)	0.46	
Other		
Smoker within past year (53)	0.79	
tPA (13)	**0.028**	tPA > none
Age	0.75	
Type (ischemic=87, hemorrhagic=14)	0.28	
Lesion size	**7E-04**	0.34
Post-stroke Deficit		
NIHSS	**0.035**	0.26
Motor	0.09	
Attention (visual field)	**0.0018**	-0.31
Attention (sustained)	**0.0048**	-0.28
Spatial Memory	**0.015**	-0.24
Verbal Memory	0.17	
Language	**0.016**	-0.21
Lag Recovery (1yr-acute) vs Deficit Recovery (1yr-acute)		
NIHSS (1yr-acute)	0.053	
Motor	0.92	
Attention (visual field)	**0.020**	-0.30

Attention (Nonspatial)	0.44	
Spatial Memory	0.46	
Verbal Memory	0.75	
Language	0.30	

Note: For categorical variables, relationships to lag laterality were assessed using a Mann-Whitney U test. The number of included patients in that category is given in parenthesis. For continuous variables, relationship to lag laterality was assessed using Spearman's rank test. For tests with $p<0.05$ (not corrected for multiple comparison), the relationships with lag laterality is given in the right column (direction of difference for categorical, Spearman's Rho for continuous).

2.4.1 Lag analysis reveals sizeable delays in the hemodynamic response

To determine the topographic extent and biological correlates of hemodynamic lag following stroke, we performed a longitudinal study of a cohort of stroke patients and age-matched controls. The cohort of 130 patients was selected as a representative sample from a larger sample of 1,209 stroke patients admitted to Barnes-Jewish Hospital in a five-year span that met all study inclusion criteria (see supplemental results and Table S2). Lag in the resting BOLD signal was measured across the brain relative to the global gray matter signal as described in Figure 1. Figure 1A-B illustrates our approach for measuring lag cross-correlation in every voxel. Figure 1C shows the lag map for one subject. The subject's lesion is shown in black and the voxel used in Figure 1B is circles. Lag severity was quantified by comparing the lag laterality – a global measure of lag severity – to the distribution of 24 healthy controls. At 1-2 weeks post-stroke, 32 out of 107 sub-acute stroke patients (30%) exhibited lag measures >2 SD of the control mean (~95% confidence interval) and 19 out of 107 (17.8%) were >3 SD (99.7% confidence interval).

Lag laterality also was measured in voxels restricted to white matter; this quantity was highly correlated ($r=0.7221$, $p=1x10^{-4}$) with lag laterality measured in gray matter voxels, although the magnitude of gray matter lag measures was larger (Fig S1). We also computed the average lag

difference over all homotopic ROI pairs. This quantity was significantly correlated with lag laterality as defined above ($R = 0.55, P < 10^{-9}$).

Figure 2 illustrates hemodynamic lag in our cohort. Figure 2A illustrates lag maps obtained in five representative patients at the sub-acute period. Figure 2B shows a histogram of lag value frequencies measured in the set of 169 ROIs in all patients and all controls. By convention, negative shift values indicate a lead ahead of the reference signal and positive values indicate a lag behind it. Both groups exhibited ROIs that lead the gray matter signal (τ^m <0), but the patients exhibited more ROIs with significant positive lag (patients: 4.0%>2s, 1.7%>4s; controls: 1.9%>2s, 0.2%>4s).

Figure 2C shows subgroup average lag maps generated by subtracting contralesional from ipsilesional hemisphere and then grouping subjects by stroke arterial territory (middle vs. posterior cerebral artery). Figure 2C suggests that distribution of hemodynamic lag tends follow the arterial territory of the stroke. Whereas severity of hemodynamic lag showed no significant relationships to either lesion size (Table 1) or location, the topographic distribution of lesions that produced severe lag did not visually differ from the distribution of lesions in the entire cohort.

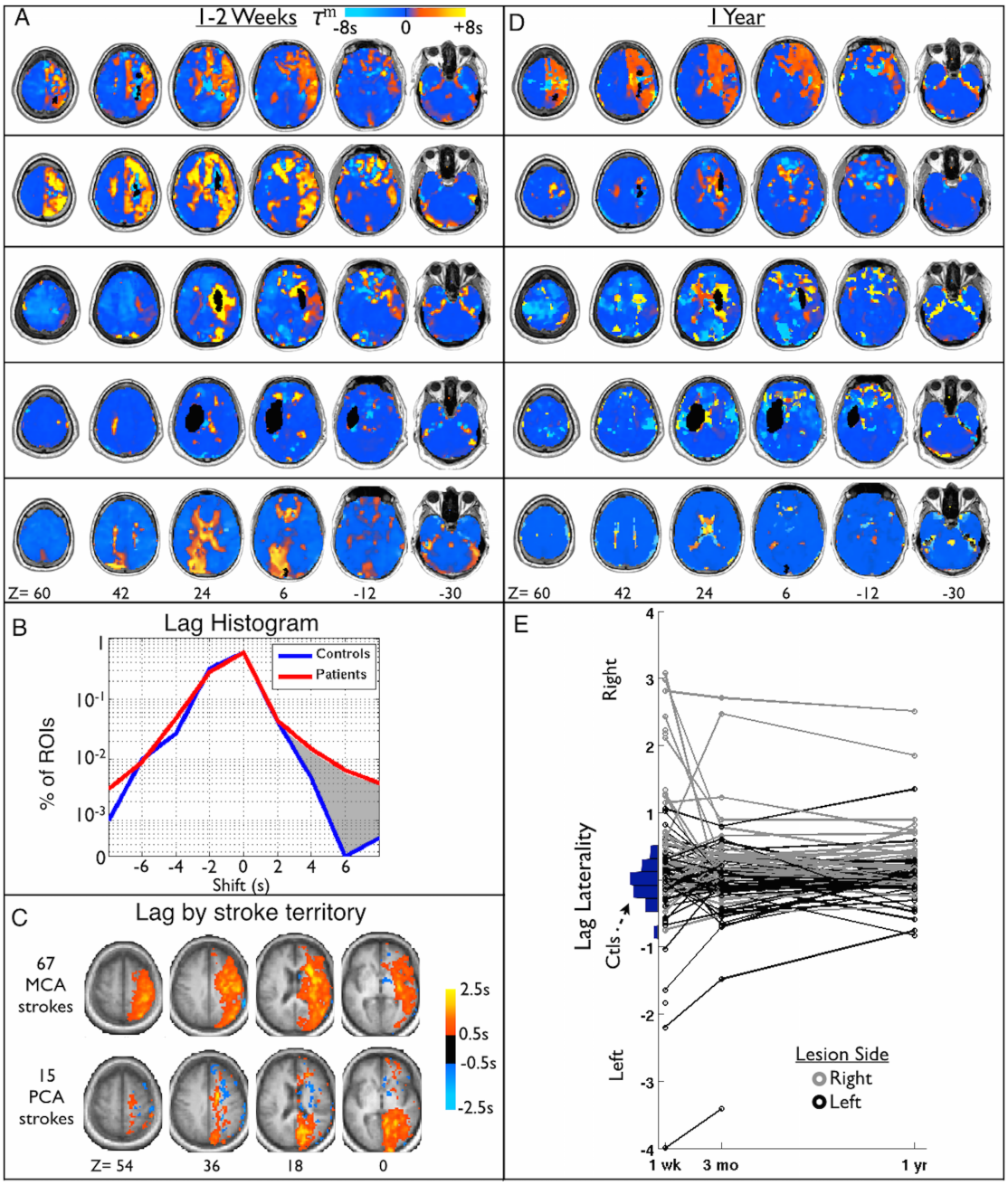

Figure 2-2 Delay in the resting hemodynamic response (lag) is observed after stroke.
A) Lag maps for 5 sub-acute stroke patients overlaid on MP-RAGE. Lesion locations are shown in black. **B)** Histogram of lag value frequencies measured in a set of 169 ROIs in both patients and controls. Both contain some regions that appear to lead the gray matter signal, but the patients show more regions that lag behind it than controls (shaded gray – 1.7% vs 0.2% of ROIs > +4s). **C)** To generate a group average, subjects were grouped be stroke arterial territory and the contralesional hemisphere was subtracted from the ipsilesional hemisphere. Average lag maps for two largest groups; middle cerebral artery (MCA), and posterior cerebral artery (PCA) are shown. **D)** Lag maps at the 1 year follow-up from the same patients shown in A). Lag appears to largely resolve by 1year post-stroke onset in many but not all cases. **E)** Lag laterality scores for all patients included in the study at all timepoints.

Patients with only one timepoint are shown as a single circle. Patients are divided by lesion side to show the frequent correspondence with lag side.

To exclude the possibility that eyes open/closed during the R-fMRI scan biased our results, we measured the percent of time with eyes open for each R-fMRI session. In the first R-fMRI session, patients maintained eyes open 66% of the time on average, and controls maintained eyes open 77% of the time. However, a two way ANOVA found no significant effect of group ($P = 0.846$) or of timepoint ($P = 0.677$) on eyes open. Moreover, a Spearman's correlation of eyes open with lag laterality measured at the sub-acute timepoint did not identify a significant relationship ($R = 0.02$, $P = 0.8$).

2.4.2 Lag recovery

Figure 2D illustrates lag maps for the same five patients at 1year follow-up. A variety of outcomes is evident, ranging from no change (top) to complete resolution (bottom row). Figure 2E shows lag laterality scores over all available data, illustrating the trend of lag over time for all patients. A vertical histogram of lag laterality scores in 24 age-matched controls is shown in blue on the left (mean=-0.046, SD=0.268). The patient lag laterality scores are shown to the right, shaded by lesion side (left-black, right-gray). Figure 2E demonstrates that lag tends to occur on the side of the lesion and most often recovers over time. Only 7 out of 86 (8.0%) patients at 3 months post-stroke and 5 out of 74 (6.1%) patients at 1 year showed lag laterality >3 SD of controls (Table S1).

2.4.3 Lag predicts performance deficits

Lag laterality – difference in lag values between the left and right hemisphere – provided an objective measure of lag severity that was compared to several clinical and demographic measures. (Table 1). We did not find a significant correlation between lag and neurologic history (TIA, Migraine, other), psychiatric history (depression, substance abuse, other), cardiac history (hypertension, CAD, DM, other), smoking history. None of the patients assessed received thrombectomy. And 12% (13) of patients received tissue plasminogen activator (tPA). Patients receiving tPA showed greater lag than those who had not ($P = 0.028$).

Next, associations between lesion type and characteristics and lag laterality were investigated. No significant different in lag was identified in hemorrhagic versus ischemic strokes ($P = 0.28$). Additionally, no difference was found between stroke subtypes defined based on TOAST criteria (ANOVA $P = 0.13$). However, lag laterality was correlated with lesion size ($R = 0.34$, $P = 5.5x10^{-5}$).

Finally lag laterality was compared to behavioral deficit. Lag laterality was correlated with overall deficit measured by NIHSS ($R = 0.26$, $P = 0.035$) and deficit in numerous behavioral domains; spatial attention ($R = -0.31$, $P = 0.0018$), sustained attention deficit ($R = -0.28$, $P = 0.0048$), spatial memory deficit ($R = -0.24$, $P = 0.015$), and language ($R = -0.21$, $P = 0.016$). Recovery of lag by 1-year post-stroke was correlated with recovery of spatial attention ($R = -0.30$, $P = 0.02$). All P-values are not corrected for multiple comparisons.

2.4.4 Areas of lag show reduced blood flow

Figure 3 shows regional lag in stroke patients relative to regional cerebral blood flow (rCBF) and lag laterality relative to internal carotid artery occlusion. rCBF in areas of hemodynamic lag less than 1 second was, on average, 92.46% that of controls. Areas with lag greater than ~2 seconds showed significantly lower rCBF and a monotonic decrease in perfusion with increasing lag (Figure 3). An analysis of variance (ANOVA) showed an effect of carotid occlusion on lag ($P = 8.32 \times 10^{-4}$), with the ≥80% occlusion group showing greater lag than the ≤50% occlusion ($t[58] = -3.76$, $P = 1.97 \times 10^{-4}$) and 51-79% occlusion groups ($t[11] = -2.25$, $P = 0.023$).

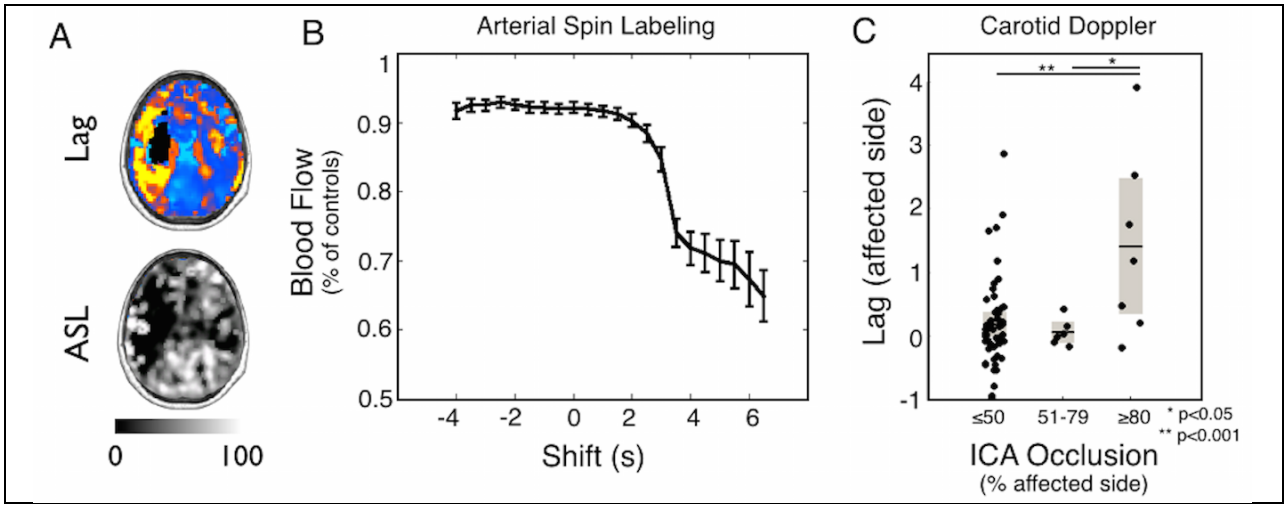

Figure 2-3 Areas of lag show reduced blood flow.
(a) A sample patient showing left hemisphere lag and corresponding areas of hypoperfusion on ASL. (b) The average blood flow as a percent of healthy controls is measured for ROIs and plotted as a function of lag in all 107 sub-acute scans. Areas with greater than 2 s of lag show a significant decrement in rCBF (relative to zero lag) and hypoperfusion increases as lag magnitude increased. (c) Doppler imaging of the internal carotid artery (ICA) on the affected side is categorized as 50%, 51–79%, or 80% occlusion and compared lag in the affected hemisphere.

These results raise the question of whether hypo-perfusion in the acute post-stroke period recovers in parallel with lag. To address this question, we measured change in lag (1 year minus

2 weeks) versus change in rCBF for all ROIs showing lag >0 sub-acutely. Although a significant relationship was present between recovery of lag, and recovery of rCBF (Pearson's R = -0.12; P = 0.039), the variance explained by this relationship was small (r^2=0.015). This may be because overall, measures of perfusion did not change significantly between two weeks and one year post-stroke (2-week average = 85.7% of controls, 1-year average = 86.4% of controls; paired t-test p = 0.3719). Thus, while a strong relationship between lag and rCBF is present sub-acutely, areas in which lag recovers do not necessarily return to normal perfusion.

2.4.5 Lag and resting state functional connectivity

A second goal of this study was to determine how lag affects measurement of resting state functional connectivity (FC). To this end, we explored how lag affects 1) properties of the BOLD signal, 2) measurement of functional connectivity using R-fMRI, and 3) FC-behavior relationships.

2.4.6 Altered BOLD signal power

R-fMRI BOLD signal characteristics were fundamentally altered in areas of lag (Figure 4). The 169 ROIs were divided in to three categories: no lag, lag, and lesion. Signal power was evaluated in the range 0.009-0.09Hz. The blue, red, and black lines show BOLD signal power in normal tissue, regions with >2s lag, and lesion, respectively. Areas of lag showed significantly decreased power relative to no-lag tissue in the range 0.046-0.09Hz. In the lower resting state frequency range, power in areas of lag was similar to that of areas of lesion.

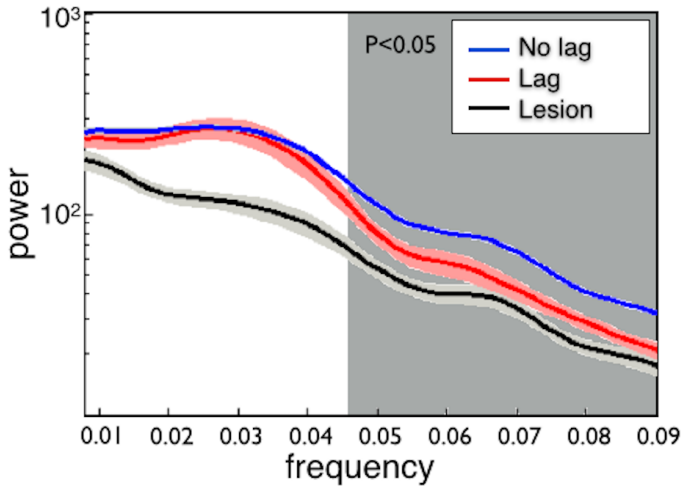

Figure 2-4 BOLD power spectra.
ROIs with lag show significantly decreased power relative to 'no lag' ROIs in the upper part of the resting state range (0.046–0.09 Hz). Power in this range is closer to that of infarcted regions. Transparent boundaries depict SEM in average power.

2.4.7 Lag disrupts functional connectivity but can be partially corrected

Analysis of functional connectivity (FC) revealed that hemodynamic lag considerably alters FC measures after stroke. Figure 5A shows seed-based correlation maps for four ROIs in different locations that showed >2s of lag. The leftmost column shows the four ROIs overlaid on the lag maps. The second column shows the correlation map for each ROI. The third column shows correlation maps after correction by shifting the timecourse by the measured lag. The rightmost column shows the group average correlation map for the same four ROIs in the controls. Correcting timecourses for lag normalized the correlation maps to a considerable extent.

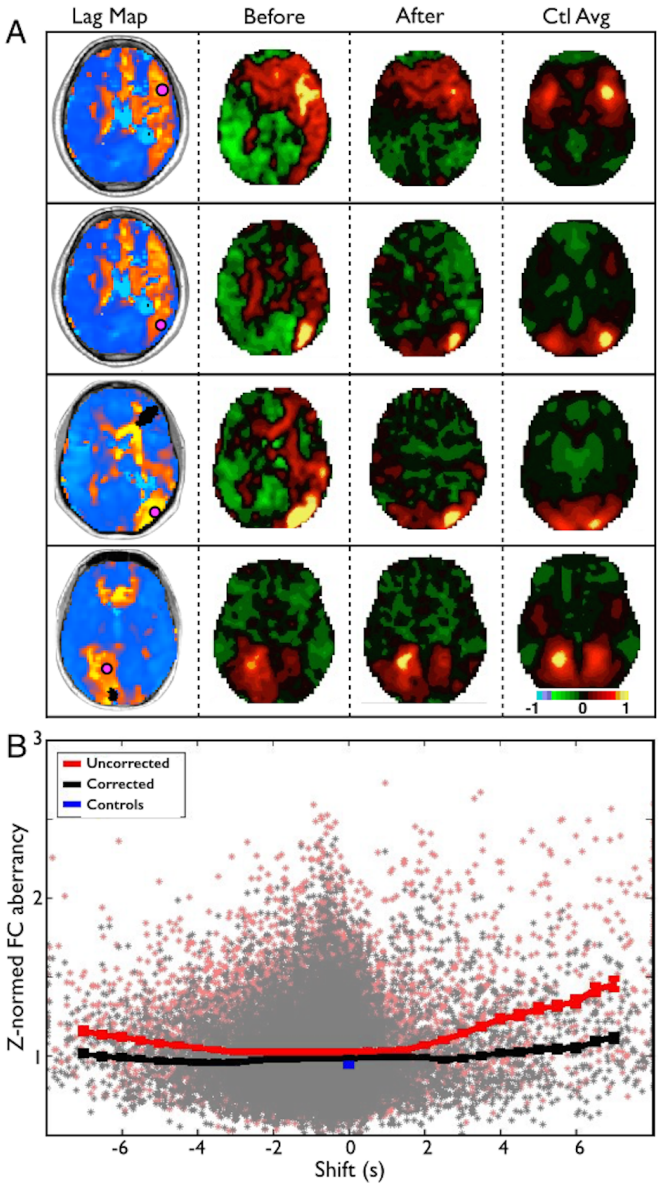

Figure 2-5. Lag disrupts functional connectivity but can be partially corrected.
(a) Seed-based correlation maps for four ROIs in different locations that showed >2 s of lag. The leftmost column show the four ROIs overlaid on the lag maps. The second column shows the correlation map for each ROI. The third column shows the correlation map for each ROI after the courses have been shifted to align optimally with the global signal. The rightmost column shows the average correlation map for the same four ROIs in the controls. Note improved similarity between patient correlation maps and controls following correction. (b) Relationship between lag and FC aberrancy (before and after correcting for lag) across all 169 ROIs and 107 subjects. The red line demonstrates the average aberrancy and SEM for ROIs at different shifts. Correcting timecourses for lag makes the functional connectivity in those regions less aberrant (black line).

Figure 5B shows the relationship between lag and FC aberrancy, before and after correcting for lag, across all 169 ROIs in 107 sub-acute patients. The red line demonstrates that the degree of FC aberrancy monotonically increases with lag above 2s. Shifting ROI timecourses to correct for lag makes the FC in those regions considerably less aberrant (black line). However, increased abnormality is still evident for lags > 2s even after correction. This result may reflect inherent changes in the frequency content of the BOLD signal in areas of lag (Figure 4).

2.4.8 Stroke FC-behavior relationships persist with lag correction

The observed relationship between lag and behavioral deficits raises important questions regarding previously observed FC-behavior relationships. To determine the effect of lag on previously established FC-behavior relationships, we measured FC-behavior correspondence in interhemispheric motor FC and motor function, and between interhemispheric dorsal attention network (DAN) FC and spatial neglect.

Figure 6A demonstrates that lag laterality measured in motor ROIs correlates with motor deficits. Thus, there exists a relationship between hemodynamic lag and behavior. Patients with motor lag laterality > 1s are shaded gray. Figure 6B shows that, as previously reported, motor network interhemispheric FC and motor function are highly correlated(Carter et al., 2010). We repeated the FC analysis using the lag-corrected timeseries and found that the FC-behavior relationship persists after correction (Figure 6C). Finally, we excluded all subjects with motor lag laterality greater than ±1 second (21/117 subjects) and recomputed the FC-behavior correlation. Figure 6E-H demonstrates the same results comparing lag and FC in the dorsal attention network with

spatial neglect. In both motor and attention networks, removal of subjects with severe lag eliminated the observation of interhemispheric anticorrelations. And in both cases, a robust FC-behavior relationship persisted (Figure 6D/H).

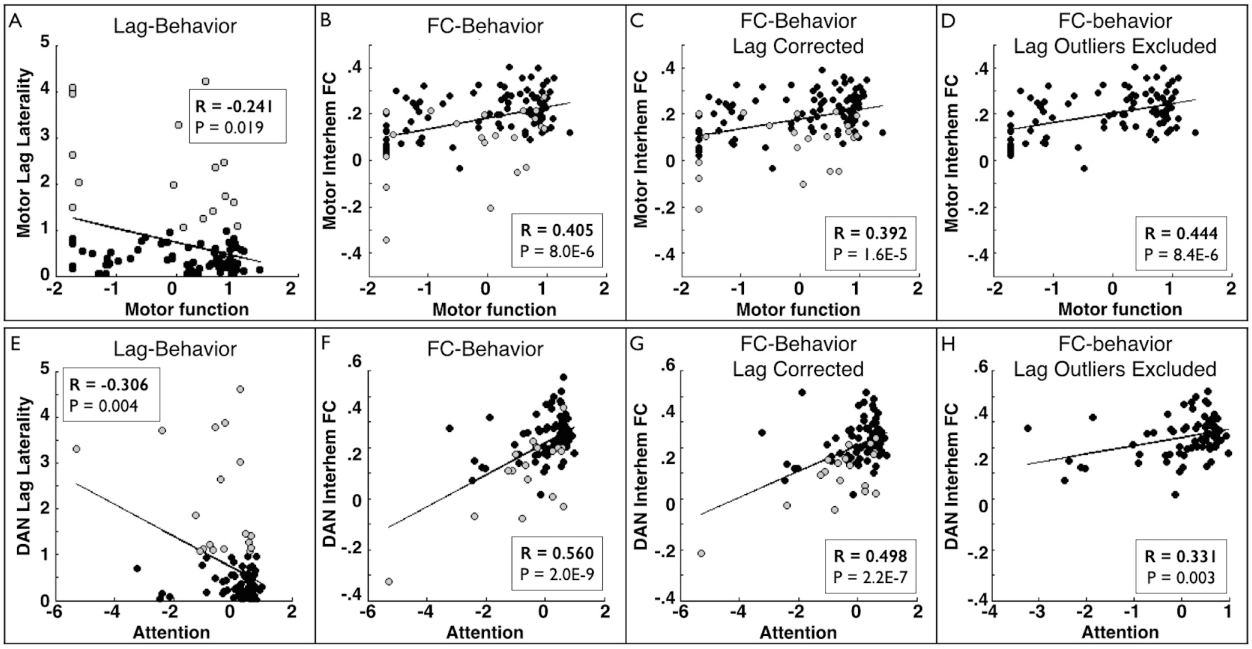

Figure 2-6. Stroke FC–behavior relationships persist after lag correction.
(a/e) Comparison of lag laterality measured within motor ROIs versus motor deficit or within dorsal attention network ROIs versus neglect reveal a significant relationship between lag and behavior. Patients with motor lag laterality > 1 s are shaded gray. (b/f) Interhemispheric connectivity and function are highly correlated (Pearson's correlation). (c/g) This relationship persists after lag has been corrected and (d/h) this relationship also persists when all subjects with within-network between-hemisphere lag > 1 s (21/107 for motor, 21/101 for dorsal attention) are excluded. Relationships in (a) and (e) were computed Spearman's nonparametric rank test; all other relationships were measured with Pearson's correlation.

2.5 Discussion

Our work builds on previous observations of hemodynamic lag in task-based and resting state fMRI (R-fMRI) in stroke as well as other conditions associated with vascular abnormalities. We extend previous observations by exploring the prevalence of lag in a representative stroke cohort,

examining the relationship of lag to rCBF, post-stroke motor deficits, lag changes over the course of recovery, and effects of hemodynamic lag on FC. Areas of hemodynamic lag can be identified in 20-30% of patients 2 weeks after stroke but this fraction drops to closer to one in ten by 1 year post-stroke. Hemodynamic lag preferentially occurs in the vascular distribution of the infarct, and positively correlates with the size of the lesion. We did not observe a relationship between severity of lag and etiology of the infarct (hemorrhagic, ischemic, or ischemic subtype). However, we did observe that lag severity predicts deficit in numerous behavioral domains and that lag recovery predicts improvement in visual field attention deficit (hemispatial neglect). Finally, hemodynamic lag alters measures of FC. Lag-related distortions in FC correlation values can be partially, but not entirely, corrected by temporally shifting timecourses.

Our primary measure of lag was regional delays relative to a gray matter reference signal. Prior studies of hemodynamic lag have used various reference signals including the whole brain signal(Amemiya et al., 2013; Lv et al., 2013), homotopic regions(Bauer et al., 2014), and superior sagittal sinus(Christen et al., 2015). We additionally measured lags between homotopic regions and found that lag laterality measured with a global gray matter references was correlated to lag laterality measured with homotopic reference ($R = 0.55, P < 10^{-9}$). The gray matter tissue compartment defines a time series representing the hemodynamic response to neural activity averaged over the whole brain. Previous work has shown that subregions within the gray matter compartment normally exhibit lags in the range of 1 sec relative to other gray matter regions, which most likely reflect neural rather than hemodynamic phenomenology(Mitra et al., 2014). Large lags not seen in healthy controls are reasonably attributed to hemodynamics.

2.5.1 Physiological Implications

Observed lag following stroke could be caused by 1) cell-level microvascular damage that disrupts neurovascular coupling, 2) rerouting of collateral blood flow, 3) altered neural activity, or some combination of these. Prior evidence together with our findings suggests that cell-level microvascular damage is the most likely cause for hemodynamic lag. Impaired astrocyte and pericyte reactivity (neurovascular coupling) occurs in tissue that is reperfused following ischemic stroke (Attwell et al., 2010; Petzold and Murthy, 2011). In fact, pericytes are more sensitive to ischemia than are neurons or astrocytes (Hall et al., 2014; Hauck et al., 2004; Yemisci et al., 2009). Damage to pericytes (Yemisci et al., 2009) or astrocytes (Schummers et al., 2008) can alter the HDR, suggesting that these cells likely play a role in perilesional hemodynamic changes. The higher rate of lag observed in patients that received tPA may occur because areas of transient ischemia that are reperfused as a results of the clinical intervention experience microvascular damage. Moreover, the observed decrease in BOLD signal power above 0.046 Hz (Figure 2C) may represent altered HDR kinetics. 0.046-0.09Hz is the range of frequencies in the normal hemodynamic response to task-induced neural activity (Hathout et al., 1999). Damage to pericytes or astrocytes could therefore reduce signal power in this range and could additionally lead to temporal delay by acting as a low-pass filter.

Blood flow after stroke may be rerouted through newly recruited collaterals(Shih et al., 2009) with consequent changes in arterial transit time. Mean arterial transit time can be thought of as the static component of cerebral perfusion while the HDR represents responses to neural activity. Therefore, a previously reported association between hemodynamic lag and mean arterial transit

time (Christen et al., 2015; Lv et al., 2013) could suggest that lag is attributable to static blood flow changes. However, static changes alone do not account for hemodynamic lag of the presently observes large magnitudes (> 2 sec) because changes in transit time typically are on the order of less than 1 second(MacIntosh et al., 2010).

Altered neural activity theoretically could contribute to observed hemodynamic lags. However, in our data, lags were observed in the white matter (Figs 1, 2, 3, 5), which reflect predominantly the static component of perfusion. Further evidence against a neuronal etiology has been obtained by prior studies of cerebrovascular disease patients with severely impaired BOLD fMRI responses to stimuli despite normal behavior (de Haan et al., 2013; Powers et al., 1988) and normal neuronal responses (measured with MEG)(Rossini et al., 2004).

Although hemodynamic lag is unlikely to reflect delayed neural responses, it is evident that neural function is affected in areas of hemodynamic compromise(Rosner et al., 1986). We observed a strong association between lag laterality (lag difference between hemispheres) and visual field bias (Table 1). This result is consistent with previous observations in cerebral microangiopathy patients linking delays in task evoked hemodynamic responses to performance deficits on a Stroop task(Schroeter et al., 2007). Similarly, focal right hemisphere perfusion deficits have been documented in stroke patients with hemispatial neglect(Hillis et al., 2005). Thus, the available evidence suggests that perfusion deficits can lead to abnormal brain function. However many questions remain regarding how hemodynamic disruption affects neural and cognitive function, both acutely and chronically.

2.5.2 Prognostic Implications

Although the pathophysiology of resting state hemodynamic lags is uncertain, our results suggest that lag indexes hemodynamic disruption and potentially reversible tissue compromise. Following stroke, lag occurs in the vascular distribution of the infarct, and correlates with measures of clinical deficits, mean transit time(Amemiya et al., 2013; Christen et al., 2015; Lv et al., 2013) and with hypoperfusion. Prior studies have linked hemodynamic failure to infarct extent(Lee et al., 2003; Olivot et al., 2009) and to risk of future ischemic stroke(Derdeyn, 2007). Measuring lag by R-fMRI is non-invasive and may have important prognostic utility. But, fully understanding the prognostic implications of resting state hemodynamic lag will require follow-up beyond our 1-year endpoint.

We acquired 30 minutes of resting state data. In future studies, it should be noted that analyzing 400 seconds of high quality resting state data is sufficient to identify the existence of lag (Fig S2). However, the reliability of lag maps continues to increase even after 20 minutes of resting state data acquisition.

2.5.3 Lag disrupts measurement of functional connectivity

Our results demonstrate that hemodynamic disruption following stroke produces artifactual R-fMRI effects. In addition to delay relative to the global signal, areas of lag showed significantly decreased BOLD signal power relative to no-lag tissue at frequencies above 0.046Hz. This observation implies that simply shifting timecourses to re-align with the global signal will not adequately correct quantitative measures of FC.

Recent studies have used FC analysis of R-fMRI data to study brain network reorganization following stroke (Baldassarre et al., 2014a; Carter et al., 2012a, 2012b, 2010; Ding et al., 2014; Grefkes and Fink, 2011; He et al., 2007; Jiang et al., 2013; Ovadia-Caro et al., 2013; Park et al., 2011; Siegel et al., 2014; van Meer et al., 2010a, 2010b; Várkuti et al., 2013; Wang et al., 2010; Zhang et al., 2014). Importantly, our data show that previously published post-stroke FC-behavior relationships persist even when subjects showing pathologic lag (delay of at least 1 second between affected and unaffected hemispheres) are removed from analyses. This observation confirms that post-stroke FC changes are not trivially caused by altered hemodynamics, but rather represent pathological alterations in neuronal communication and network structure. Excluding subjects with pathologic lag eliminated the observation of interhemispheric anticorrelations (while correcting lag often only decreases the magnitude of anticorrelations), suggesting that homotopic anticorrelation may be a useful indicator pathologic lag in other stroke FC data sets.

We observed that shifting timecourses to re-align with the global signal reduced FC changes caused by lag. However, we do not recommend this maneuver as a means of accounting for lag-related disruptions in future stroke FC-behavior studies. The observed decrease in resting BOLD signal power suggests that the signal in areas of lag is fundamentally altered, thus simply shifting timecourses will not adequately correct quantitative measures of functional connectivity.

2.5.4 Limitations

From the present study it is impossible to determine the relationship of stroke to lag, only that they co-occur in individual brains and in spatial distribution. Moreover, while we speculate on the pathophysiology underlying observed lags, the limitations of the present work obviate any conclusions.

Computation of hemodynamic lag undoubtedly includes measurement error. In particular, Figure 2B shows regions that lead the global gray matter signal by >2 seconds. This observation has been previously reported (Amemiya et al., 2013). However, we assign no particular pathological significance to this phenomenon. Conversely, lag is considerably more prevalent in the stroke group than controls, lawfully follows vascular distributions, and correlates with clinical deficits. All of these lines of evidence suggest that regional lags indicate hemodynamic compromise.

Lastly, it is possible that the correlation between hemodynamic lag and hypoperfusion is inflated by the pulsed arterial spin labeling method. In PASL, an excitation pulse labels arterial blood in the carotid artery and then tissue saturation is measured after a delay (bolus arrival time). We used a bolus arrival time of 1100ms. If areas of lag show elongated arterial arrival time, then the perfusion measurement may be occurring prior to the signal peak in those areas and thus appear artificially lowered (Donahue et al., 2012; MacIntosh et al., 2010). This phenomenon has been reported in stroke patients (Kimura et al., 2005) and multi-delay ASL sequences have been developed to measure and correct it (Wang et al., 2013).

2.5.5 Conclusion

Our results suggest that hemodynamic lag can be measured non-invasively using R-fMRI, occurs frequently following stroke, and considerably disrupts measurement of functional connectivity. FC-behavior relationships remain even when subjects showing lag have been removed from analyses. Resting state lag only provides a glimpse into the disruption that has occurred at a cellular and microvascular level. This work raises important questions regarding the mechanisms and physiological implications of hemodynamic lag that will require further work and better experimental models.

Supplementary information is available at the *Journal of Cerebral Blood Flow & Metabolism* website – www.nature.com/jcbfm.

2.6 Acknowledgment

This study was supported by, National Institute of Child Health and Human Development Health award (5R01HD061117 to M.C.), National Institute of Neurologic Disorders and Stroke (P30 NS048056 to A.Z.S.) National Institute of Health Medical Scientist training award, and American Heart Association Predoctoral Fellowship Award (5T32GM007200-39 & 14PRE19610010 to J.S.S.). Additional thanks to Lawrence Snyder, Anish Mitra, Tomer Livne, Adam Bauer, Beau Ances and Colin Derdeyn for conceptual guidance, to Nick Metcalf and Antonello Baldassarre for data processing, and to Sarah Krall and Tomer Livne for manuscript revision.

2.7 Supplementary Figures & Tables

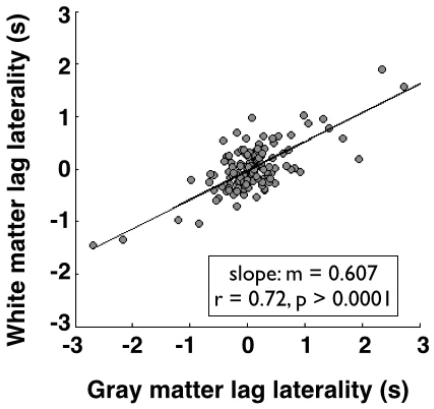

Supplementary Figure 2-1. Gray matter lag versus white matter lag.
The laterality measure is used to compare gray and white matter. Each circle represent a patient. A strong correlation is seen between the two measures although the slope of 0.607 suggests that gray matter lag is larger in magnitude.

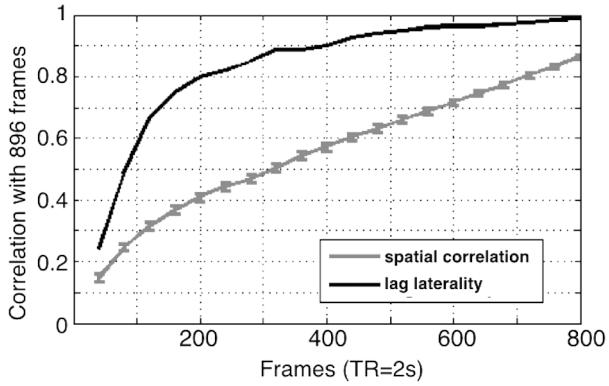

Supplementary Figure 2-2 Lag reliability as a function of acquisition length.
Summary statistics were computer on 93 acute subjects who had the full 896 frame (30 min) acquired. Lag laterality (black line) rises steeply until ~200 frames (6 minutes, 40seconds) and then gradually increases in reliability. Spatial correlation of the lag map increases steadily up to 800 frames.

	Source population	Study sample	Healthy controls
Age			
18-30	3%	4%	3%
31-50	23%	28%	23%
51 and over	78%	68%	68%
Gender			
Female	48%	47%	52%

Male	52%	53%	48%
Race			
Caucasian	62%**	34%	32%
African- American	35%**	64%	61%
Other	2%	2%	6%
Education			
Incomplete high school	22%	17%	16%
High school	40%	38%	29%
Incomplete college	23%	25%	35%
College	8%	8%	10%
Post-graduate	7%	12%	10%
Predisposing Factors			
Hypertension	73%	70%	26%**
Diabetes Mellitus	29%	31%	16%**
Coronary Artery Disease	22%**	8%	6%
Atrial fibrillation	11%*	5%	3%
Depression	11%*	5%	3%
Stroke Variables			
Ischemic Stroke	76%	82%	
Hemorrhagic Stroke	24%	18%	
tPA	10%	12%	
Thrombectomy	0%	0%	
NIHSS in hospital	8.3%	7.5%	

Supplementary Table 2-1 Statistical comparisons of demographic and risk factors for stroke. Asterisks represent significant differences from the study population and study sample based on chi-square test.

3 Resting fMRI in Stroke – approaches and considerations

The contents of this chapter are not published elsewhere

3.1 Abstract

Recent research has demonstrated the importance of global changes to the functional organization of brain network following stroke. Resting functional MRI (R-fMRI) is a non-invasive tool that enables the measurement of functional connectivity (FC) across the entire brain while placing minimal demands on the subject. For these reasons, it is a uniquely appealing tool for studying the distant effects of stroke. However, R-fMRI studies rely on a number of premises that cannot be assumed without careful validation in the context of stroke. Here, we describe strategies to identify and mitigate confounds specific to R-fMRI research in cerebrovascular disease. Four main topics are discussed: 1) achieving adequate co-registration of lesioned brains, 2) identifying and removing hemodynamic lags in resting BOLD, 3) identifying other vascular disruptions that effect the resting BOLD signal, 4) selecting an appropriate control cohort. For each topic, we provide evidence-based guidelines for steps to improve the interpretability and reproducibility of FC-stroke research. Our recommendations extend to any research using R-fMRI to study diseases that might alter cerebrovascular flow and dynamics or brain anatomy.

3.2 Intro

In stroke, a disruption to the brains vascular supply leads to infarction and structural damage (i.e. cell death) of gray/white matter. But stroke also produces remote changes in structurally normal brain areas – remote effects include metabolic, physiological, and connectional abnormalities (Carrera and Tononi, 2014), as well as shifting of brain tissue. It is becoming increasing apparent that understanding behavioral deficits post-stroke will require a complete description not only of lesion topography, but also of remote connectivity abnormalities (Baldassarre et al., 2014b; Carter et al., 2012a; He et al., 2007; Rehme et al., 2014; Siegel et al., 2016; van Meer et al., 2010b). Resting functional MRI (R-fMRI) presents a promising tool to examine network level changes in stroke and recovery (Carter et al., 2012b; Corbetta, 2012; Grefkes and Fink, 2014).

Interpretation of the correlation of BOLD fluctuations in healthy subjects frequently rests on numerous assumptions. For example, a critical assumption of most R-fMRI research is that neurovascular coupling is relatively consistent across brain areas, across time, and across individuals. Though imperfect even in a healthy population, such assumptions have enabled reliable mapping of spatial and temporal relationships between brain areas (Buckner et al., 2013). When studying cerebrovascular disease, a normal hemodynamic response cannot be assumed (D'Esposito et al., 2003). However, if certain additional steps are taken to empirically identify and control for relevant confounds, than measured FC-stroke relationships can be meaningfully interpreted.

The goal of this review is to provide evidence for the importance of these confounds, and explore best practices to manage them. We will first consider issues relating to inter-subject registration – focusing on volume-based registration errors caused by stroke and recommending surface-based methods to improve registration. We will then consider hemodynamic coupling – discussing evidence that vascular disease can produce changes in the magnitude and latency of the hemodynamic response, and recommending an approach to measure and remove this confound. Finally, we will consider selection of appropriate experimental controls and control subject selection.

Many of our recommendations are quite feasible in current FC-stroke datasets. However, these approaches are not implemented in the majority of FC-stroke studies. Moreover, many of our recommendations are not specific to stroke only, but extend to any research using R-fMRI to study diseases that might alter cerebrovascular dynamics or brain anatomy.

3.3 Registration of the cortical surface and subcortex

The majority of published FC-stroke research has relied on registration to a common atlas space using 6-parameter affine linear transformation (Ding et al., 2014; Ovadia-Caro et al., 2013; Park et al., 2011; Wang et al., 2013). The limitation with this approach is that a stroke, and pathophysiological processes associated with stroke can lead to substantial relative displacement of tissue (i.e. the central sulcus might move anterior or posterior relative to other brain landmarks). This phenomonen is illustrated in real stroke data after volume alignment in Fig. 1. An 8mm radius sphere is placed in the angular gyrus - defined based on anatomical landmarks -

in each individual linearly-aligned brain. A conjunction image shows good overlap in healthy individuals (with some voxels showing 100% overlap), but poor overlap in patients (with a maximum of 63% overlap). This was the case across the cortex. For 156 ROIs that span the cortex (Carl D. Hacker et al., 2013), ROI overlap was significantly lower in patients than controls ($t = 9.6$, $p < 0.001$). Non-linear alignment did not substantially improve seed co-localization in the angular gyrus. This is probably because it uses only tissue contrast and not cortical folding patterns. However, as discussed below, non-linear registration does substantially improve alignment of shifted subcortical structures.

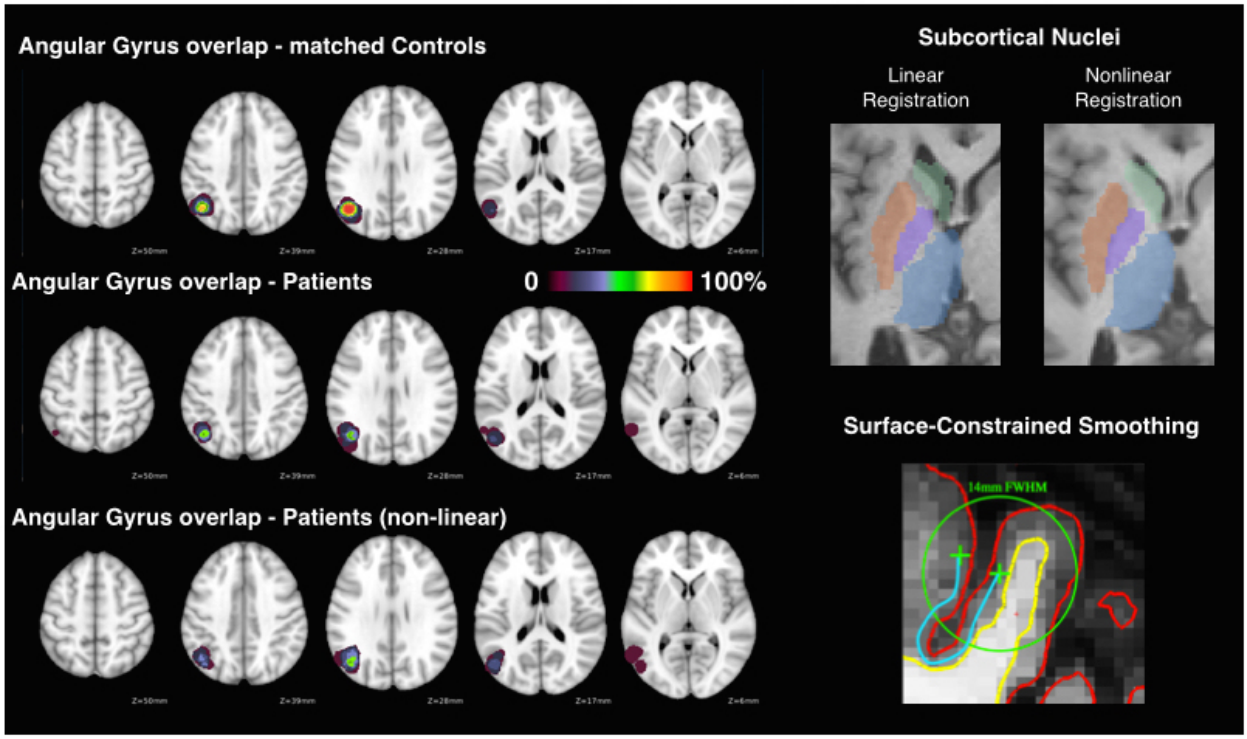

Figure 3-1 Nonlinear registration and surface-based tools improve stroke patient alignment. Quality of linear alignment is compared between 33 patients with large lesions (greater than 40 cm^3) on either hemisphere and 24 matched controls. A region in the right central sulcus was defined in each subject following surface folding-based registration. Separately, each brain was linearly aligned to a references atlas in talairach space. The landmark-defined angular gyrus region was then projected to the volume coordinates in the linearly aligned brains. **Top right:** An example of registration of subcortical nuclei with using linear versus nonlinear registration. Atlas-defined ROIs are shown for caudate, putamen, globus pallidus, and thalamus. Example patient (used in Figure

4) has a cortical lesions in the contralateral hemisphere. **Bottom Right**: A demonstration of surface smoothing enabled by Freesurfer (Image courtesy of Dr. Douglas N. Greve). The green line indicates the full-width half-max boundaries of a 14mm volume-smoothing kernel. Notice that the smoothing kernel would cause functional data to be smoothed across multiple gyral walls. This problem is mitigated with surface smoothing (blue line).

Surface-based registration offers a solution to variability in cortical shape and variability in shifting of tissue after stroke (Dale et al., 1999; Fischl, 2012; Fischl et al., 2002; Bruce Fischl et al., 1999; Glasser et al., 2013). Surface- and contour-based alignment approaches provide superior registration. The benefits of surface-based registration have been demonstrated in the healthy brain (B. Fischl et al., 1999; Ghosh et al., 2010) http://www.ncbi.nlm.nih.gov/pmc/articles/PMC4008670/) , and those benefits are magnified by the substantially increased heterogeneity resulting from stroke. However, to our knowledge, this is the first demonstration of the benefits of a surface-based approach in stroke FC analysis.

For analysis of subcortical nuclei and the cerebellum, nonlinear volume alignment (such as FSL FNIRT) may also provide registration that is superior to linear registration (Fig. 1, top right). This is because patient T1's often show anatomical shifts as well as enlarged ventricles. Even patients with more moderate lesions frequently show substantial enlargement of lateral ventricles, causing reduced quality of alignment of basal ganglia and thalamus.

Additional advantages exist to segmentation of tissue compartments beyond the important issue of registration. One is that surface segmentation enables surface-constrained smoothing, so that gray matter signal can be smoothed with minimal contamination by signal from CSF, white matter, or opposing gyral walls (Fig. 1, bottom right). Another advantage of segmentation is that it allows for high quality definition of tissue compartments in the individual that can then be used

as nuisance regressors (white matter, CSF) in data cleaning approaches such as aCompCor (Behzadi et al., 2007).

An important caveat of either nonlinear volume alignment or surface-based registration is that large lesions should be explicitly excluded or masked prior to alignment and the results should be carefully assessed for quality and feasibility. This is necessary in order to prevent the mislabeling of cortical structures.

Large lesions can cause distortion or failure of surface segmentation and registration. In such instances, we have found that painting over the lesion with voxel values from a T1 brain atlas can improve landmark and folding based surface alignment approaches. This is demonstrated in Figure 2. In the top middle panel, the high contrast lesion (blue arrow) has caused massive disruption of the surface segmentation (yellow arrows) .This causes errors in surface tessalation as well as parcellation (yellow dotted lines). But masking of the lesion enables Freesurfer to properly trace the remaining cortical surface. Surface within the masked area can then be removed from analysis. An important consideration is that, while this fix has enabled segmentation to complete in all cases, the resulting segmentation will require visual inspection and possible additional manual editing.

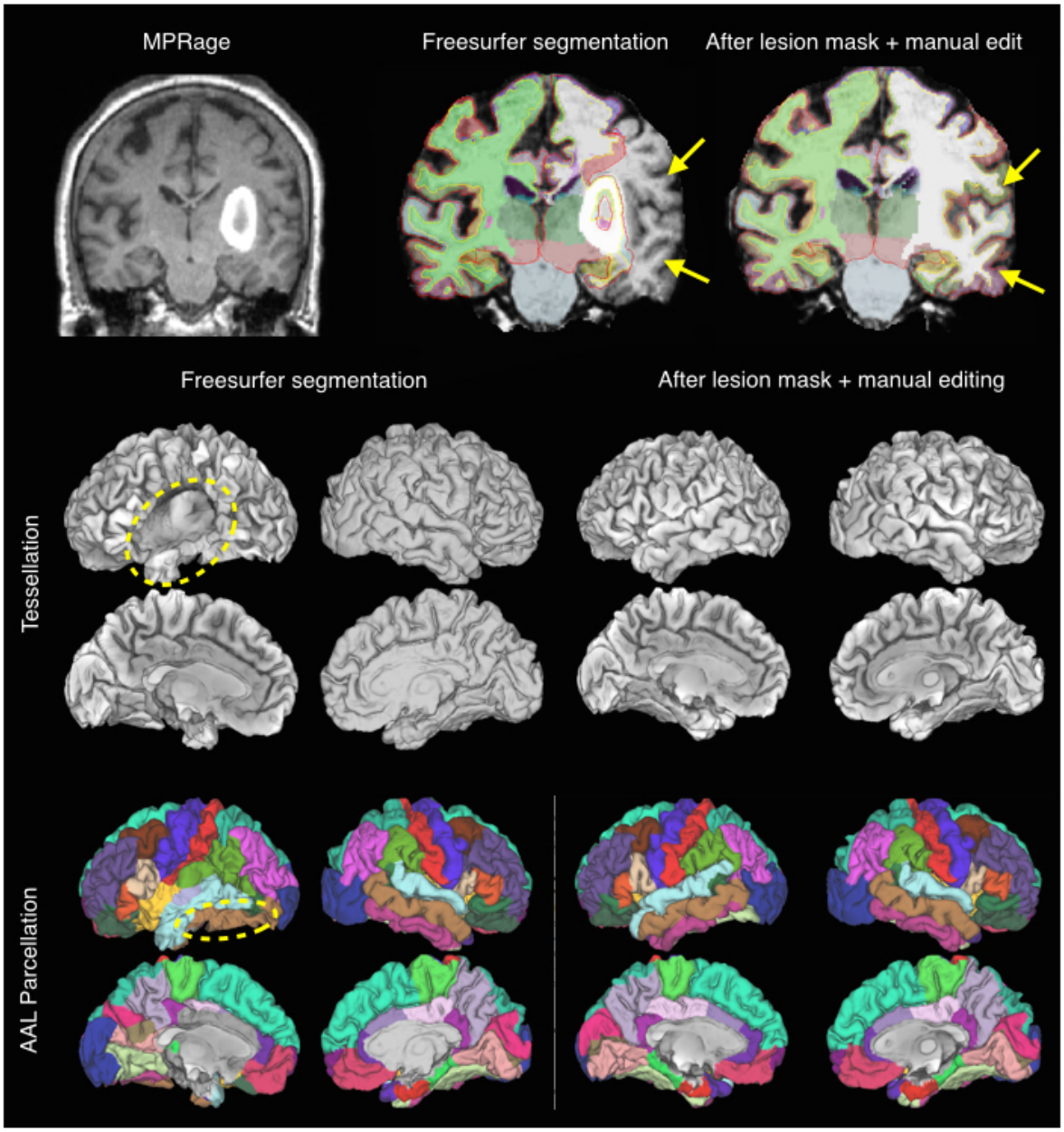

Figure 3-2. Free surfer segmentation error caused by a large lesion, and subsequent resolution after lesion-masking and manual editing.
Top: MPRage illustrating a hyper-intense hemorrhagic stroke. Unattended Freesurfer segmentation (middle) is unable to correctly identify the cortex lateral to the lesion. To resolve this, lesion masking with T1 atlas values and manual editing using control points is done. In the resulting segmentation (right), Freesurfer correctly identifies and segments the cortical surface. **Middle and bottom:** The surface and AAL parcellation generated by the post-freesurfer HCP pipeline show errors in tracing of the cortical surface as well as labeling errors (indicated by yellow dotted line). After lesion masking and manual editing, these errors are no longer present.

An approach we have found for easily identifying errors in pial surface segmentation is viewing the pial surface segmentation on top of the MPRage. In Connectome Workbench, the pial surface can be color-coded based on FC values to further assess accuracy. Displaying homotopic FC values (which should always be positive) can aid in identifying segmentation errors (Fig. 3).

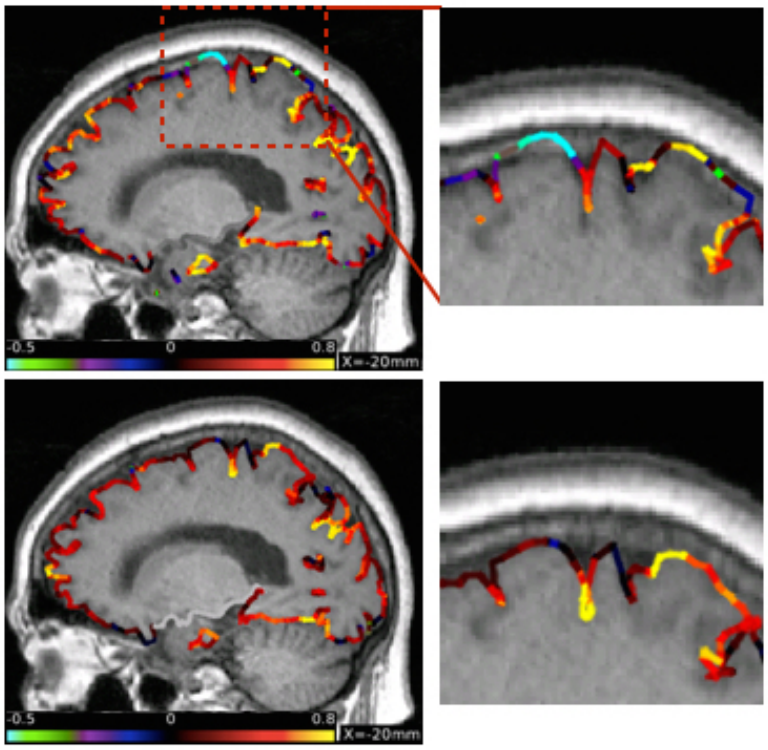

Figure 3-3. Identifying and correcting gray matter segmentation errors.
Top: The Freesurfer-defined pial surface is displayed as a ribbon over the subjects MPRage. The ribbon is color-coded based on Homotopic FC strength at each surface vertex. In locations in which errors of inclusion of dura mater have occurred, low or negative homotopic FC is found. **Bottom**: After manual editing of freesurfer segmentation pail ribbon accuracy is improved and homotopic FC values are higher.

Following proper segmentation and surface registration, we use post-freesurfer preprocessing pipelines from the Human Connectome Project (Glasser et al., 2013). Future improvements on the HCP pipeline should enable manual editing of FreeSurfer segmentation so that the entire

HCP preprocessing pipeline is compatible with the approach described above (correspondence with David Van Essen).

Misalignment has been a source of noise or confound in prior FC-stroke studies. However, this problem is avoidable. As we have quantitatively and qualitatively demonstrated, after curated surface segmentation, and nonlinear alignment of subcortical nuclei, improved functional alignment is possible.

3.4 Blood flow and hemodynamics

Stroke fMRI have shown reduced amplitude (D'Esposito et al., 2003; Krainik et al., 2005; Pineiro et al., 2002; Rossini et al., 2004) and increased latency (Altamura et al., 2009; Amemiya et al., 2012; Bonakdarpour et al., 2007; Carusone et al., 2002; Roc et al., 2006) - with BOLD responses sometimes peaking 15 seconds or more after transient neural activation. In task fMRI studies, changes in amplitude and latency have even been demonstrated in both affected and unaffected hemispheres and are most prominent during, though not limited to, the first three weeks after stroke (Krainik et al., 2005; Rossini et al., 2004). For a more extensive review of functional MRI studies in stroke, see (Lake et al., 2016). Importantly, changes in amplitude and latency often seem to co-occur, i.e. hemodynamically compromised vasculature shows a BOLD hemodynamic response function that is both reduced in amplitude and increased in latency (Amemiya et al., 2012; Bonakdarpour et al., 2007; Carusone et al., 2002).

Fortunately, it is possible to identify latency changes. The remainder of the articles discusses ways in which hemodynamic coupling is altered after stroke, means by which such alterations may be easily identified, and strategies to control for these confounds in FC-stroke analyses.

3.5 Hemodynamic lags

In the last 3 years, a handful of reports have been published identifying regional delays on the order of seconds in resting fMRI fluctuations in stroke and cerebrovascular disease patients (Amemiya et al., 2013; Bauer et al., 2014; Christen et al., 2015; Lv et al., 2013; Ovadia-Caro et al., 2014; Siegel et al., 2015). These delays are identified by cross-correlation (i.e. time shift analysis) of regional BOLD timecourses with some reference signal. This technique has been applied with different choices of reference signals including gray signal (Lv, 2015), homotopic signal from the non-lesioned hemisphere (Bauer, 2014), and a superior sagittal sinus seed (Christen 2015). Some benefits of this approach is that it is fairly robust to the choice of reference signal (Christen et al., 2015) and that a global measure of lag severity can be attained reliably from only six minutes of R-fMRI data (Siegel et al., 2015) – though spatial specificity requires longer scans.

Importantly, lag co-localized to areas of perfusion deficit as measured by contrast enhanced perfusion-weighted imaging (Amemiya et al., 2013; Lv et al., 2013) and arterial spin labeling (Siegel et al., 2015) and also seems to occur in areas with reduced amplitude of evoked BOLD response (Bauer et al., 2014). However, studies directly relating latency and amplitude of evoked response to lags in resting BOLD are still needed.

At two weeks post-stroke, the prevalence of patients showing substantial hemodynamic lags is above 30%. This number drops close to 15% by 3 year post-stroke and 10% by 1 year (Siegel et al., 2015). Interestingly, lag severity correlates with lesion size as well as severity of deficits (Siegel et al., 2015).

As would be expected, lags systematically alter measurements of FC from the affected node. This is easily illustrated by comparing homotopic lags to homotopic FC. In Fig. 4 each circle represents a pair of the ROIs on opposite hemispheres (homotopic) in one patient (red) or control (blue). The lag between homotopic ROIs is plotted on the x-axis while the functional connectivity (zero-lagged Pearson correlation) is plotted on the y-axis. This figure is generated using 107 sub-acutes stroke cohort and 24 age-matched controls described in (Siegel et al., 2015). This figure is particularly useful because one plot makes multiple important points – 1) hemodynamic lags produce a monotonic decrease in measured FC values, 2) even in areas with zero lag, homotopic FC is lower on average in patients than controls, 3) negative homotopic FC values observed in patients are likely (though not definitively) a symptom of lags, and 4) lags are common in patients and rare but reliably identified in a small minority of risk-matched controls (2/24 with consistent measures across scans 3 months apart).

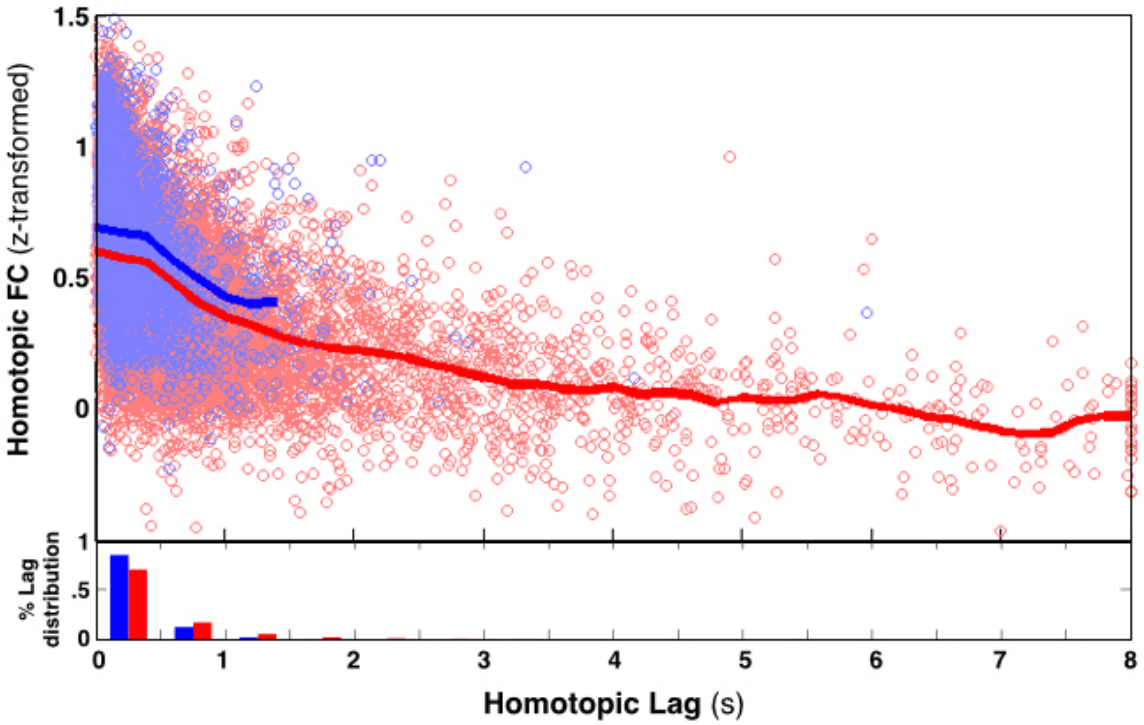

Figure 3-4. Hemodynamic lags systematically alter functional connectivity
Each circle represents a pair of the ROIs on opposite hemispheres (homotopic) in one patient (pale red) or control (pale blue). The lag between homotopic ROIs is plotted on the x-axis while the functional connectivity (zero-lagged Pearson correlation) is plotted on the y-axis. The LOWESS moving average is plotted in bright red and blue lines for patients and controls, respectively. This figure is generated using the 107 sub-acutes stroke cohort and 24 age-matched controls. A set of 78 left hemisphere ROIs (and their right hemisphere mirror image regions) were used for each subject. ROIs intersecting a lesion were excluded. Under, a histogram shows the proportion of homotopic ROI pairs showing lags. Even in sub-acute patients, the majority of regions show a lag of less than 0.5 seconds.

Interestingly, homotopic anti-correlations appear in many seminal FC-stroke studies (He et al., 2007; van Meer et al., 2010a), suggesting that the studies were likely affected by lag.

A few approaches have been proposed to correct for lags in FC analysis. Bauer et al., provided evidence that using the lesion timecourse as a nuisance regressor reduced aberrant observations attributable to lag in mice with transient MCA occlusions. Another approach that has been tested out is to shift timecourses in lagged tissue prior to FC analysis (Christen et al., 2015; Siegel et al., 2015). This approach is not recommended, and other sources of unwanted variance (head

motion, white matter, CSF signals) may or may not be shifted in these areas. Moreover, BOLD signal power is significantly reduced in areas showing lag, and neither approach describe above can correct fundamental changes to the BOLD signal.

In subjects with severe lags of greater than 1 second laterality (i.e. the entire lesioned hemisphere is delayed by greater than 1 second relative to contralesional) we recommend exclusion from FC analysis. The 1 second threshold is approximately four standard deviations outside of measures seen in unaffected subjects (which may reasonably be attributed to noise or neural latency). In patients with a constrained area of large magnitude lag (as is seen in the example patient in Fig. 3 – area of lag is highlighted with a green outline) it may be necessary to exclude the affected region from FC analysis. Since the effects of lags of 1-6 seconds are approximately linear (see Fig 5 of Siegel et al., 2015), more subtle lags can be co-varied out of any FC analysis (Baldassarre et al., 2016; Ramsey et al., 2016). Fortunately, this precaution is feasible because lags can be calculated using the same data used for canonical FC analysis. We would encourage any researcher investigating FC-stroke data to test for lags using publicly available software (nil.wustl.edu/Corbetta/resources/lagsuite.tar.gz).

3.6 Neurovascular Coupling

While identifying lags is important, it may not be a complete fix for the challenge of altered neurovascular coupling. In some patients, a decrease in amplitude (Krainik et al., 2005; Salinet et al., 2014), or a complete loss of the BOLD response (Blicher et al., 2012; Rossini et al., 2004) has been observed in the absence of lags. On it's own, it is difficult to interpret reduction/absence

of a evoked BOLD response – it might reflect a decrement in neural activity, loss of neurovascular coupling, or an inability of the vasculature itself to adequately increase local perfusion (Marshall, 2004; Pineiro et al., 2002; Rossini et al., 2004). Thus, approaches to better validate hemodynamic responsiveness to neural activity would be of value.

Carotid stenosis is perhaps a useful example of a vascular disease because it is relatively well characterized in its effects of neurovascular coupling, it is common in stroke patients, and it's effects on FC have been reported. Severe carotid stenosis (>70% occlusion) reduces both the static and dynamic components of cerebral blood flow (Powers et al., 1987). This results in uncoupling of the hemodynamic response from neural activity (Powers et al., 1988). Moderate stenosis (50-70% occlusion) may not alter coupling (Derdeyn et al., 1998), though this has not been carefully addressed. In a healthy asymptomatic population of adults over the age of 70, 4.8% exhibit moderate (>50% occlusion) and 1.6% exhibit severe (>70% occlusion) carotid stenosis (Weerd et al., 2010). In a stroke population, prevalence is substantially higher. Based on clinically acquired carotid doppler data from our stroke cohort, 20% of patients (13/66) show >50% occlusion with 11% (7/66) showing >80% occlusion on the affected side. Other studies have reported that as much as 33% of ischemic stroke patients exhibit moderate or severe intracranial stenosis, and 12% have stenosis on the hemisphere opposite the lesion (Wong et al., 1998). In most such cases, an embolic stroke produces an infarct in only a portion of the territory affected by the stenosis. Studies directly measuring FC changes in carotid stenosis patients relative to non-stenotic controls have explicitly shown large reduction in FC in the affected hemisphere (Chang et al., 2016; Cheng et al., 2012).

Though it is intuitive that changes in neurovascular coupling should alter FC measurement, the effects are not straightforward. Relatively small decreases in the magnitude of the HDR might have little effects because functional connectivity analysis typically relies on correlation (not covariance) of the r-fMRI signal. However, it is also possible that changes to neurovascular coupling can alter FC in profound ways. Further studies are required to understand the relationships between abnormalities of neurovascular coupling and FC. One goal of such studies would be to develop better techniques to identify and control for vascular changes in FC analysis. This is possible by employing a combination of R-fMRI with modalities for vascular imaging and electrophysiology. A challenge in such studies will be the fact that relationships between cerebral perfusion, cerebral autoregulation, and cerebrovascular coupling in the context of ischemia are exceptionally complex (for a review, see (Attwell et al., 2010)).

Some measures can be taken to identify pertinent vascular disruptions in FC-stroke analysis. These include assessment of internal carotid stenosis using carotid doppler, or assessment of local neurovascular coupling using CO_2 or hyperventilation fMRI paradigms (Krainik et al., 2005; Raichle and Plum, 1972). Other imaging techniques capable of identify clinically silent carotid stenosis include angiography (by MR and CT), transcranial doppler (which can be used in combination with arterial blood pressure to assess auto-regulatory impairment (Reinhard et al., 2005)), and possibly measures of static regional cerebral blood flow (though tissue at the edge of the autoregulatory range may show normal rCBF but no hemodynamic response).

Pulsed arterial spin labeling (ASL) techniques are frequently used as a non-invasive measure of perfusion, though decreased signal cannot be interpreted as rCBF change as it may also reflect

changes in mean transit time (Donahue et al., 2012; Kimura et al., 2005) and may not be effective at identifying perfusion deficit in stroke, (Bokkers, 2012 - Whole-brain arterial spin labeling perfusion MRI in patients with acute stroke). However, advanced in ASL are making it possible to classify multiple features of vascular flow using multi-delay sequences to more accurately model cerebra blood flow even in circumstances of altered transit time (Wang et al., 2013) (Koretsky 2012).

3.7 General Recommendations

Stroke patients as a population have significantly elevated prevalence of numerous medical problems. These include diabetes, hypertension, cardiovascular disease, cerebrovascular disease (such as carotid stenosis), white matter disease, and others (Sacco et al., 1997). For this reason, we emphasize two overarching recommendations for studies applying R-fMRI in stroke patients (or in using R-fMRI in stroke as a model to study brain networks).

The first recommendation is that an appropriate control population be used. While it may be difficult to perfectly match controls on all relevant health factors, an approach that can substantially reduce the influence of such factors is to use siblings of patients as controls (Corbetta et al., 2015). An alternative and equally valid approach is to compare performance measures between stroke patients (i.e. compare patient with and without deficit). This allays the challenge of substantial heterogeneity in any human stroke population.

The second recommendation is to carefully check MRI data in order to identify confounds and abnormalities. This should include separate assessment of segmentation, preprocessing, and

processing. As an example of how this can be done, we provide a set of images that we check in our patients to assess data quality (Fig. 5). Images on the left are primarily useful for checking surface segmentation. As shown in the right middle panel, we inspect a lag map for every subject. In some cases, a spatially constrained area in the vicinity of the lesion shows severe lags (green outline). This can by masked from FC analysis. As described previously, visualizing surface homotopic FC on top of an average volumes image can serve as an additional way to assess registration of functional and structural data.

We have mainly limited Figure 5 to images especially useful for identifying stroke- and comorbity-related problems. We also use approaches to asses head motion, artifact, and BOLD signal quality, that are commonly used in FC studies of normal populations, but discussion of those issues are beyond the focus of this paper (for a good discussion of those measures, we point the reader to Power et al., 2014).

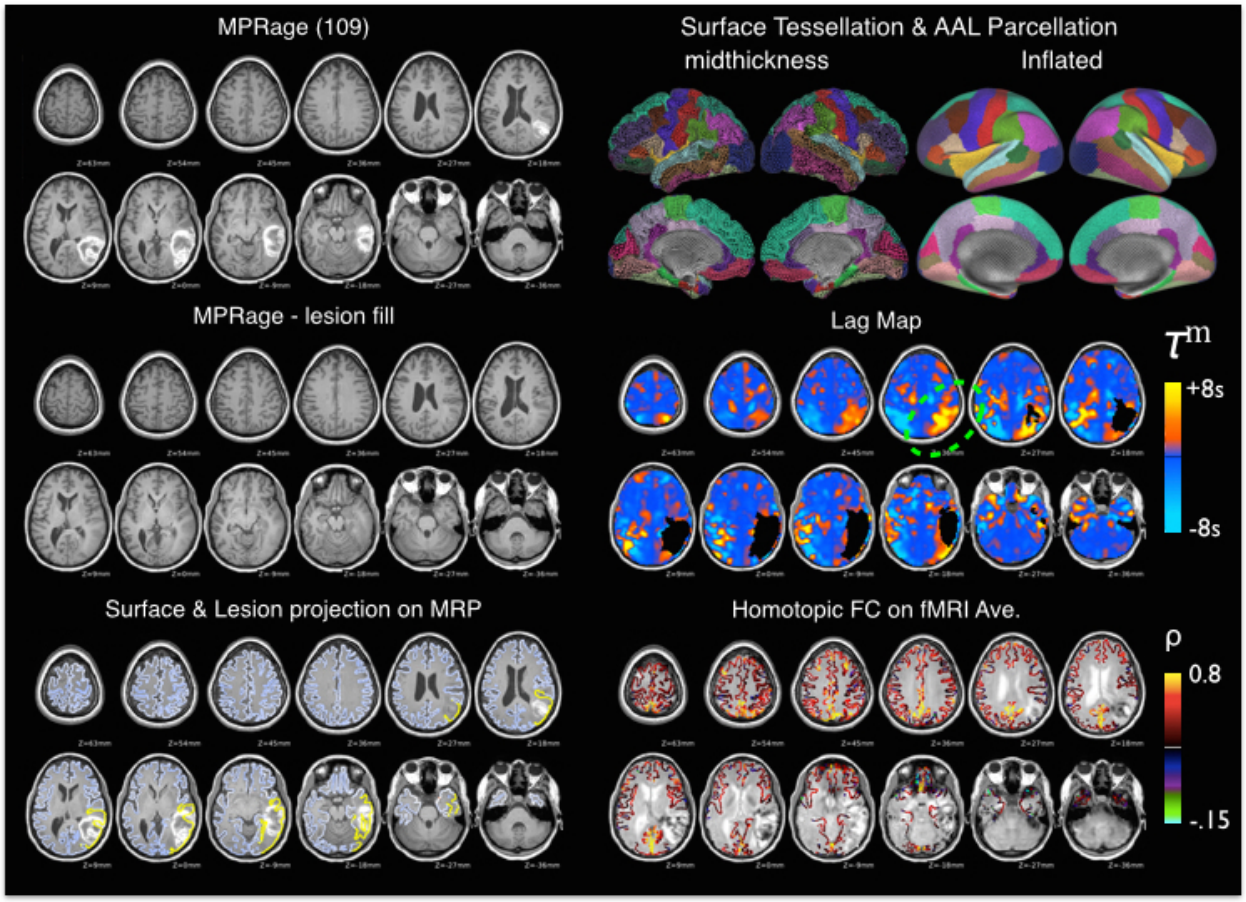

Figure 3-5. Quality assessment images for a sample subject
Top Left: MPRage. For this subject, FreeSurfer segmentation failed due to the large hyperintense hemorrhagic stroke. The manually identified lesion was temporarily painted over with atlas brain (**Middle Left**), allowing brain segmentation to run to completion. **Bottom Left:** cortical surface ribbon displayed on top of the MPRage. Yellow denotes vertices included in a surface lesion mask. **This is** particularly useful to determine proper labeling of lesion and exclusion of dura in brain segmentaiton. **Top Right**: results of FreeSurfer segmentation - this can be compared to reference AAL parcellation to ensure proper labeling of landmass such as superior temporal sulcus, superior frontal sulcus. **Middle Right:** Lag map using homotopic reference (code available at nil.wustl.edu/labs/corbetta/resources). Areas of substantial lags are identified dorsal to the lesion boundaries and will be corrected or excluded in FC analysis. **Bottom Right:** homotopic FC overlaid on an average of aligned functional MRI volumes. Useful for checking alignment of functional volumes with MPR and surface segmentation.

3.8 Asserting validity of FC based on prior findings

Having raised these important challenges and considerations, it is necessary to briefly comment on validity of prior FC-stroke research. There are numerous reasons why prior FC-stroke

findings represent promising translational advances, and why further FC-stroke research is merited. The reliability of correlations between FC and behavioral deficit in previous carefully executed studies give validity to FC-stroke research. For instance, multiple studies have identified common FC disruptions across a subset of patients that share a common deficit, even when lesion location is highly variable across that subset (Baldassarre et al., 2014b; Rehme et al., 2014; Siegel et al., 2016). Furthermore, there is a high degree of specificity in network-behavior relationships – for example, FC changes in attention areas predict hemispatial neglect while FC changes in motor areas predict hemiparesis (Baldassarre et al., 2016; Carter et al., 2010). Thirdly, investigations of parcel homogeneity suggests that, even 2 weeks after stroke, FC data is of sufficient quality to be homogenous within functional brain areas and heterogeneous across functional brain areas (Siegel, in submission; Gordon et al., 2016). We will avoid going further in to the interpretation of FC-stroke findings, as that is beyond the focus of this review.

We conclude that studies of functional connectivity in stroke have been and may continue to be a useful tool for understanding brain systems and for better characterizing the effects of stroke. But the most biologically valid and reproducible results will come when data are carefully assessed at each stage of acquisition and processing, with special attention to challenging issues such as registration and neurovascular coupling.

4 Disruptions of network connectivity predict impairment in multiple behavioral domains after stroke

This chapter has been published as a journal article. The citation is:

Siegel, J.S., Ramsey, L.E., Snyder, A.Z., Metcalf, N.V., Chacko, R.V., Weinberger, K., Baldassarre, A., Hacker, C.D., Shulman, G.L., Corbetta, M., 2016. Disruptions of network connectivity predict impairment in multiple behavioral domains after stroke. PNAS 201521083. doi:10.1073/pnas.1521083113.

4.1 Abstract

Deficits following stroke are classically attributed to focal damage, but recent evidence suggests a key role of distributed brain network disruption. We measured resting functional connectivity (FC), lesion topography, and behavior in multiple domains (attention, visual memory, verbal memory, language, motor, and visual) in a cohort of 132 stroke patients, and used machine-learning models to predict neurological impairment in individual subjects. We found that visual memory and verbal memory were better predicted by FC, whereas visual and motor impairments were better predicted by lesion topography. Attention and language deficits were well predicted by both. Next, we identified a general pattern of physiological network dysfunction consisting of decrease of interhemispheric integration and intrahemispheric segregation, which strongly related to behavioral impairment in multiple domains. Network-specific patterns of dysfunction predicted specific behavioral deficits, and loss of interhemispheric communication across a set of regions was associated with impairment across multiple behavioral domains. These results link key organizational features of brain networks to brain– behavior relationships in stroke.

4.2 Introduction

Although structural damage from stroke is focal, remote dysfunction can occur in regions of the brain distant from the area of damage (Carrera and Tononi, 2014; von Monakow, 1914). The set of regions that are directly damaged or indirectly affected is embedded within a larger functional network that is in dynamic balance with other networks in the brain. This framework posits that a lesion in a single location in the brain has the ability to disrupt brain functions far beyond the lesion boundaries (Alstott et al., 2009; Corbetta, 2012; Fornito et al., 2015).

Numerous correlates of remote physiological dysfunction have been proposed, including abnormal task recruitment of contralesional brain areas (Buckner et al., 1996; Chollet et al., 1991; Corbetta et al., 2005), disruption of metabolism (Feeney and Baron, 1986) or regional cerebral blood flow (Hillis et al., 2002; Perani et al., 1987), and more recently disruption of signal coherence (Carter et al., 2010; He et al., 2007; Nomura et al., 2010; Wang et al., 2010).

However, there is only a limited understanding of how remote physiological dysfunction is related to lesion topography (Boes et al., 2015; Nomura et al., 2010). Moreover, the behavioral relevance of reported physiological changes is unclear. While some studies have reported significant correlation with behavioral impairment, the total amount of behavioral variance explained is unknown. Finally, because mechanisms of remote dysfunction have typically been examined in relatively small groups of individuals, their generalization at the population level is unknown. As a result, physiological measures of brain function are not used in the evaluation and treatment of stroke victims.

More traditional lesion-symptom mapping studies have also used statistical methods to relate lesion topography to the severity of different behavioral deficits (Damasio et al., 1996; Karnath et al., 2001) . An implicit assumption of these studies is that the strength of association between structural damage and behavior is the same irrespective of the behavior that is measured. However, it is also possible that more integrative functions (attention, memory, executive) rely to a greater extent on distributed processing than sensory and motor functions. Surprisingly, the degree to which lesion topography accounts for the variability across different deficits is mostly unknown (for exceptions see (Corbetta et al., 2015; Phan et al., 2010; Smith et al., 2013)) As a result, lesion-behavior predictions also have not entered the main stream of clinical neuroscience.

In this study, we hypothesize that structural damage caused by stroke produces robust, physiological changes in network coherence that explain behavioral variance at the population level. We interpret the effects of these physiological changes in terms of the known functional organization of the brain. Regions subserving similar functions are grouped into networks, i.e. sets of regions that are highly connected (e.g. motor cortex and supplementary motor area for motor behavior). Dysfunction of these networks should underlie deficits in corresponding behavioral domains.

We use a similar framework to understand the weights of functional connections in accounting for behavior. Based on the normal organization of brain networks, we hypothesize that sensorimotor functions, which are more dependent on input/output pathways and tend to be associated with networks that sit peripherally in the brain's overall graph, will be more strongly dependent on structural variables (e.g. lesion topography), while integrative functions (e.g.

attention, memory) associated with more central networks will be more dependent on disrupted patterns of cortical coherence.

We evaluated these predictions within a clinically relevant sample, i.e. a large population of sub-acute stroke patients (n = 132) shown to be representative of a larger clinical population. Neurological impairments were described using behavioral measures that capture a large amount of inter-subject variance (Corbetta et al., 2015). Structural magnetic resonance imaging (MRI) and resting functional magnetic resonance imaging (R-fMRI) were used to measure lesion topography, and functional connectivity (FC) of brain networks, respectively. Structural, and functional data were then entered into a ridge regression machine-learning algorithm to predict deficits at the single subject level in six behavioral domains: attention, visual memory, verbal memory, language, motor and visual. Deficits were predicted using either a lesion-deficit model or a FC-deficit model, allowing us to compare the relative importance of lesion topography and network dysfunction in accounting for different behavioral deficits. Finally, FC-deficit models were used not only to identify the specific brain connections that were most predictive of deficits in each behavioral domain, but also to identify connections that predicted deficits across behavioral domains.

4.3 Methods

4.3.1 Subject Enrollment

Written informed consent was obtained from all participants in accordance with the Declaration of Helsinki ND procedures established by the Washington University in Saint Louis Institutional

Review Board. All participants were compensated for their time. All aspects of this study were approved by the Washington University School of Medicine (WUSM) Internal Review Board.

Subject enrollment and demographics are described in detail in Corbetta et al., 2015. First time stroke patients were recruited by a research coordinator through the in-patient service at Barnes-Jewish Hospital and the Rehabilitation Institute of St. Louis. Inclusion criteria were: 1) Age 18 or greater, 2) first symptomatic stroke, ischemic or intraparenchymal hemorrhagic etiology, 3) clinical evidence of motor, language, attention, visual, or memory deficits based on neurological examination, and 4) time of enrollment < 2 weeks post-stroke onset. Exclusion criteria were: 1) the inability to maintain wakefulness during testing, 2) the presence of other neurological, psychiatric or medical conditions that preclude active participation in research and/or may alter the interpretation of the behavioral/imaging studies (e.g., dementia, schizophrenia), or limit life expectancy to less than 1 year (e.g., cancer or congestive heart failure class IV), 3) evidence of clinically significant periventricular white matter disease (equal or > grade 5 of (Longstreth et al., 1996), and 4) contraindications for MRI including claustrophobia or scanner incompatible implants. In total, 6260 charts were screened; 132 patients met all inclusion criteria and completed the entire sub-acute protocol (mean age 52.8 years with range 22-77, 119 right handed, 63 female, 64 right hemisphere).

Demographically matched controls (n = 31) were recruited and underwent the same behavioral and imaging exams. Inclusion criteria for controls were: 1) healthy adult matched to stroke study population by age, gender, handedness, and level of education. Exclusion criteria were: 1) a positive history of neurological, psychiatric, or medical abnormalities preventing participation in

research activities, 2) a history of atherosclerotic (coronary, cerebral, peripheral) artery disease, 3) an abnormal neurological examination with signs of CNS dysfunction. In total, 31 controls completed the entire sub-acute protocol (mean age 55.7 years (SD =11.5) with a range 21-83).

4.3.2 Neuropsychological Assessment

All participants underwent a behavioral battery that included several assessments of motor, language, attention, memory, and visual function following each scanning session (Table S1). Imaging and behavioral testing session usually were performed on the same day. Scores were only recorded for tasks that subjects were able to complete. Therefore different domains have different numbers of subjects. Dimensionality reduction was performed on the performance data as described in detail in (Corbetta et al., 2015). First, tasks were categorized as attention, memory, language, motor, and vision. A principal components analysis (PCA) was run on each category. In attention, the first component described 26.1% of variance and was strongly related to measures of visual field bias (Posner task: left/right accuracy differences: $r = 0.83$; Mesulam: center of cancellation: $r = 0.75$) and general performance (accuracy, $r = -0.41$). In memory, the first two components accounted for 66.2% of variance in all measures of related to memory. The first component was highly related to measures of delayed recall of visual information (BVMT delayed recall: $r = 0.81$) and the second component was related to recall of verbal information (HVLT delayed recall $r = 0.93$). In language, the first component accounted for 77.3% of variance and was highly related to comprehension and production. In motor the first two components described left and right body deficit and explained 43.0% and 34.6% of variance, respectively.

Visual field deficits were measured in a computerized perimetry examination (Humphrey Field Analysis Model 750i). Each eye was tested using the central 24-2 threshold SITA-FAST protocol. PCA was not done because vision was assessed with a single functional test. Instead, the two vision domain scores used were the mean pattern deviation scores in the left and right hemifields. All tests included and correlation with the domain scores are shown in Table S1.

In total, eight domains were used for FC-deficit and lesion-deficit modeling. Scores in each domain were continuous and were normalized to have a mean of 0 and standard deviation of 1 in patients, and lower score indicating greater deficit. With deficit defined as at least 2 standard deviations below controls, we found the following: 1) Attention (31 with deficit / 88 total patients), 2) Visual Memory (27/88), 3) Verbal Memory (30/88), 4) Language (33/112), 5) Left Motor (37/106), 6) Right Motor (39/106), 7) Left Visual (13/58), and 8) Right Visual (10/58).

4.3.3 MRI and Lesion Analysis

Individual T1 MRI images were registered to the Montreal Neurological Institute brain using FSL FNIRT (FMRIB's Non-linear Image Registration Tool) (Andersson et al., 2007). Lesions were manually segmented on individual structural MRI images (T1-weighted MP-RAGE, T2-weighted spin echo images, and FLAIR images obtained 1-3 weeks post-stroke) using the Analyze biomedical imaging software system (www.mayo.edu; Robb and Hanson, 1991). Two board-certified neurologists (Maurizio Corbetta and Alexandre Carter) reviewed all segmentations. Special attention was given to distinguish lesion from CSF, hemorrhage from surrounding vasogenic edema, and to identify the degree of periventricular white matter damage

present. In hemorrhagic strokes, edema was included in the lesion. A neurologist (MC) reviewed all segmentations a second time paying special attention to the borders of the lesions and degree of white matter disease. The staff that was involved in segmenting or in reviewing the lesions was blind to the individual behavioral data. Atlas-registered segmented lesions ranged from 0.02cm^3 to 82.97cm^3 with a mean of 10.15cm^3 (SD=13.94cm^3). Lesions were summed to display the number of patients with structural damage for each voxel (Fig.S1).

4.3.4 R-fMRI Acquisition

Patients were studied 2 weeks (mean = 13.4 days, SD=4.8 days), 3 months (mean = 112.5 days, SD=18.4 days), and 1 year (mean = 393.5 days, SD=55.1 days) post-stroke onset. Controls were studied twice at an interval of 3-months. All imaging was performed using a Siemens 3T Tim-Trio scanner at the Washington University School of Medicine (WUSM) and the standard 12-channel head coil. The MRI protocol included structural, functional, pulsed arterial spin labeling (PASL) and diffusion tensor scans. Structural scans included: (1) a sagittal T1-weighted MP-RAGE (TR=1950 msec, TE=2.26 msec, flip angle=90°, voxel size=1.0×1.0×1.0 mm); (2) a transverse T2-weighted turbo spin-echo (TR=2500 msec, TE=435 msec, voxel-size=1.0×1.0×1.0mm); and (3) sagittal FLAIR (fluid attenuated inversion recovery) (TR=7500 msec, TE=326 msec, voxel-size=1.5×1.5×1.5mm). PASL acquisition parameters were: TR=2600 msec, TE=13 msec, flip angle=90°, bandwidth 2.232 kHz/Px, and FoV 220mm. 120 volumes were acquired (322 seconds total), each containing 15 slices with slice thickness 6 mm and 23.7mm gap. Resting state functional scans were acquired with a gradient echo EPI sequence

(TR = 2000 msec, TE = 27 msec, 32 contiguous 4 mm slices, 4×4mm in-plane resolution) during which participants were instructed to fixate on a small cross in a low luminance environment. Six to eight resting state fMRI runs, each including 128 volumes (30 min total), were acquired.

4.3.5 fMRI Data Preprocessing

Preprocessing of fMRI data included: 1) compensation for asynchronous slice acquisition using sinc interpolation; 2) elimination of odd/even slice intensity differences resulting from interleaved acquisition; 3) whole brain intensity normalization to achieve a mode value of 1000; 4) removal of distortion using synthetic field map estimation and spatial realignment within and across fMRI runs; 5) resampling to 3mm cubic voxels in atlas space including realignment and atlas transformation in one resampling step. Cross-modal (e.g., T2-weighted to T1-weighted) image registration was accomplished by aligning image gradients (Rowland et al., 2005). Cross-model image registration in patients was checked by comparing the optimized voxel similarity measure to the 97.5 percentile obtained in the control group. In some cases, structural images were substituted across sessions to improve the quality of registration.

4.3.6 Functional Connectivity Processing

FC processing was similar to previous work from the lab (Baldassarre et al., 2014c), with the addition of surface projection and processing steps developed by the Human Connectome Project (Glasser et al., 2013). First, data were passed through several additional preprocessing steps: (i) regressors were computed based on freesurfer segmentation; (ii) removal by regression of the following sources of spurious variance: (a) six parameters obtained by rigid body correction of

head motion, (b) the signal averaged over the whole brain, (c) signal from ventricles and CSF, and (d) signal from white matter; (ii) temporal filtering retaining frequencies in the 0.009–0.08Hz band; and (iii) frame censoring. The first 4 frames of each BOLD run were excluded. Frame censoring was computed using framewise displacement with a threshold of 0.5mm. This frame-censoring criterion was uniformly applied to all R-fMRI data (patients and controls) before functional connectivity computations. Subjects with less than 120 usable BOLD frames were excluded (13 patients, 3 controls).

4.3.7 Surface Processing

Surface generation and processing of functional data followed procedures similar to Glasser et al.,(Glasser et al., 2013), with additional consideration for cortical segmentation in stroke patients. First, anatomical surfaces were generated for each subject's T1 MRI using FreeSurfer automated segmentation (B. Fischl et al., 1999). This included brain extraction, segmentation, generation of white matter and pial surface, inflation of the surfaces to a sphere, and surface shape-based spherical registration to the subjects "native" surface to the fs_average surface. Segmentations were manually checked for accuracy. For patients in whom the stroke disrupted automated segmentation, or registration, values within lesioned voxels were filled with normal atlas values prior to segmentation, and then masked immediately after (7 patients). The left and right hemispheres were then resampled to 164,000 vertices and registered to eachother (Van Essen et al., 2001), and finally downsampled to 10,242 vertices each for projection of functional data.

Following preprocessing of BOLD data, volumes were sampled to each subject's individual surface (between white matter and pial surface) using a ribbon-constrained sampling available in Connectome Workbench. Voxels with a high coefficient of variation (0.5 standard deviations above the mean coefficient of variation of all voxels in a 5mm sigma Gaussian neighborhood) were excluded from volume to surface mapping (Glasser et al., 2013). Timecourses were then smoothed along the 10,242 vertex surface using a 6mm FWHM Gaussian kernel. Finally, timecourses of all vertices within a parcel are averaged to make a parcel-wise timeseries.

Functional connectivity (FC) was then computed between each parcel using Fisher z-transformed Pearson correlation. Connectivity for any parcel that fell within the boundaries of the lesion was removed from univariate analyses and set to zero for multivariate models.

Homotopic FC was computed for each region by measuring FC with the corresponding vertices on the opposite hemisphere. Subjects with severe hemodynamic lags (greater than 0.5 second inter-hemispheric difference) measured from R-fMRI (Siegel et al., 2015) were excluded from all further FC analyses. This criterion excluded 21 subjects leaving a total of n = 100 stroke patients and n = 27 controls with FC data that met all of our quality controls.

4.3.8 Parcellation (Regions of Interest) and Community Assignments

We used a cortical surface parcellation generated by Gordon & Laumann and colleagues (Gordon et al., 2016) (Figure S1). The parcellation is based on R-fMRI boundary mapping and achieves full cortical coverage and optimal region homogeneity. The parcellation includes 324 regions of interest (159 left hemisphere,165 right hemisphere). The original parcellation includes

333 regions, and all regions less than 20 vertices (approx. 50mm^2) were excluded. Notably, the parcellation was generated on young adults age 18-33 and is applied here to adults age 21-83. However, we know of no evidence to suggest that boundaries between cortical areas shift in the course of healthy aging.

To validate the community structure, we conducted modularity optimization on controls and patients (Figure S2). Consistent with larger investigations of aging (Chan et al., 2014), we found that optimal community structure was largely, but not completely, consistent with predefined assignments. The location of intermingled colors in the spring-embedded areal graphs on the right of Figure S2 suggest that regions that switch assignment are typically on the edge between communities. Note that community assignments have no bearing on FC-deficit models discussed below.

4.3.9 Univariate Network FC Analysis

Group-wide patient (n = 100) versus control (n = 27) FC differences were interrogated based on the resting state network described above. We compared distributions of homotopic, ipsi-lesion/contralesional (randomly assigned L/R in control), and inter/intranetwork FC for patients and controls. In each case, patient-control distributions were compared using a two-tailed Student t-test. Three types of within-network connectivity were compared at the whole brain level; homotopic, ipsilesional, and contralesional. FDR correction was conducted on these three statistical tests.

For nine individual RSNS, within and between network differences were assessed. Here, 99 stroke-control t-tests (45 ipsilesional, 45 contralesional, 9 homotopic) were computed, significance cutoffs were determined via 10,000 permutations of group assignment (stroke versus control). Finally, the relationship between homotopic connectivity and ipsi-lesional DMN connectivity was assessed for eight RSNs (the nine used previously, minus the DMN), and results were FDR corrected for eight statistical tests.

4.3.10 Multivariate Ridge Regression

Lesion-deficit and FC-deficit relationships were interrogated using leave-one-out ridge regression models (Fig.2). We chose to use a linear multivariate ridge regression function to minimize bias but retain the ability to plot predictive weights back to brain anatomy (Phan et al., 2010). Transductive PCA (Zhu et al., 2008) was performed prior to modeling for both lesion topography as well as vectorized FC matrices (Smith et al., 2014). This step was carried out independently for every model and components that explained 95% of variance were retained. For lesion location, the PCA was performed on voxel-wise lesion maps from 65,549 $3mm^3$ brain voxels and for functional connectivity, the PCA was performed on 324-choose-2 = 52,326 edges. The number of components retained for each model were as follows: 1) Attention (50 lesion components, 74 FC components), 2) Visual Memory: (43,72), 3) Verbal Memory (43,72), 4) Language (56,90), 5) Left Motor (50/84), 6) Right Motor (50/84), 7) Left Visual (28/49), and 8) Right Visual (28/49).

All ridge regression models were trained and tested using a leave-one-out cross validation (LOOCV) loop (Golland and Fischl, 2003). In each loop, the regularization coefficient lambda was optimized by identifying a lambda between λ=1 and 10^5 that minimized leave-one-out prediction error over the training set. Next, optimal weights were solved across the entire training set using gradient descent to minimize error for the ridge regression equation shown in figure 2. Optimal model weights were applied to the lesion/FC of the left-out subject to predict that subject's behavioral score. A prediction was generated for all subjects in this way. Model accuracy was assessed using the square of the Pearson correlation coefficient between measured and predicted behavior scores. To visualize feature weights, the weight matrix was averaged across all n leave-one-out loops to generate a single set of consensus weights. Thus, solving for all behavioral scores in each domain produced two outputs: 1) accuracy – % variance explained (r^2), and 2) a consensus weight map – a vector (ω) containing relative predictive weights for every voxel/connection. The weights (ω) from the model were back-projected to the brain to display the most predictive functional connections and displayed using Caret (Van Essen et al., 2001).

Two models were combined for the left and right motor domains and left and right visual hemifields to determine the percent of variance explained for motor and visual models. The combined models were later used to determine total within and between RSN contributions to FC-deficit models. Difference in prediction accuracy between lesion-deficit versus FC-deficit models were assessed by a two-tailed Wilcoxon signed rank test on the squared prediction error $((\vec{\omega})^T \vec{x}_i - \vec{y}_i)^2$, where i indexes participant.

FC-deficit network contribution was also quantified based on *a priori* assigned RSN membership (Carl D Hacker et al., 2013). Thus, weights of all connections within and between each RSN were averaged to generate a 7x7 RSN weight matrix for each FC-deficit model.

The top 1% of weights were also classified according to four weight types: inter-hemispheric positive, inter-hemispheric negative, intrahemispheric positive, and intrahemispheric negative. The number of weights in the top 1% belonging to each of the four types was counted in each model. An ANOVA was run across all seven models to test for a difference in contribution between the four weight types.

An additional post-hoc model was run to predict global homotopic connectivity (averaged across all parcels) based on lesion location. This lesion-homotopic FC model was set up in the same manner as the lesion-deficit prediction models.

4.3.11 Multi-task Learning

To separate features of functional connectivity change that predict shared deficit across multiple domains versus those that are domain-specific, we applied multi-task learning (Daumé III, 2009). Multi-task learning (MTL) is a way to combine the FC-deficit prediction models by learning them jointly. In the setting of brain network decoding, it is reasonable to assume that some shared features determine domain-general functionality. The MTL equation simultaneously optimizes prediction for every domain by combining a domain-specific set of weights with a second set of weight that are held constant across all domains. L1 regularization is used to apply

a equal cost function to each, such that the model is not biased towards using either shared or domain-specific weights.

The multitask optimization equation is:

$$\arg\min_{\omega} \lambda||\overrightarrow{\omega_0}||_2 + \sum_{k=0}^{K}\sum_{i=1}^{n}((\overrightarrow{\omega_0 + \omega_k})^T\vec{x}_i - \vec{y}_i)^2 + \lambda||\overrightarrow{\omega_k}||_2 \quad \text{(X-1)}$$

In equation 1, the x vector indicates FC (in PCA space). The y vector contains behavioral scores for these same patients. λ, a regularization coefficient, is determined empirically using a leave-one-out approach over a range of λ values. The vector ω is the weight vector that describes the relative importance of each feature in x to the prediction of y. n is the number of subjects, and K is the number of behavioral domains being combined in the MTL problem. The prediction for subject *i* in domain *k* is generated by combining a set of domain specific weights ω_k with domain general weights ω_0 in the expression: $y_i = (\overrightarrow{\omega_0 + \omega_k})^T\vec{x}_i$.

Nodal contribution to the across-domain weights (ω_0) for the 324 ROIs was determined by taking the root-mean-square weight of all connections for each node.

4.4 Results

4.4.1 Abnormal FC patterns in stroke

We recruited 132 first-time symptomatic stroke patients 1-2 weeks after stroke, and 31 demographically matched controls. Patients were assessed with a broad neuropsychological battery measuring performance across six behavioral domains (vision, motor, language, visual memory, verbal memory, and attention), lesions were manually identified with multi-modal segmentation, and 30 minutes of R-fMRI data were acquired. 21 patients were excluded for hemodynamic lags (Lv et al., 2013; Siegel et al., 2015) and 11 patients and 4 controls were excluded for excessive head motion(Power, n.d.). After exclusion, 100 stroke patients and 27 age-matched controls were studied. To investigate the general effects of stroke, we compared FC features in the entire stoke cohort to those of the age-matched control cohort. A cortical parcellation of 324 regions was divided into 13 networks based on Gordon & Laumann et al. 2014 (Gordon et al., 2016) (Figs.S1, S2). Within-network connections were further classified as inter-hemispheric homotopic, ipsilesional intra-hemispheric, and contralesional intra-hemispheric connections.

Figure 1 shows the distribution of FC values in patients (red) and controls (blue) for three types of within-network connections: homotopic, ipsilesional, and contralesional. Decreased homotopic FC was the most prominent difference between patients and controls (t-statistic = 4.26, $p= 10^{-4}$, FDR correction). This effect was also tested for individual networks and significant differences were observed in all networks except CON, VAN, and DMN (Fig.S3B). A three-

factor analysis of variance (ANOVA) on homotopic FC revealed a significant effect of group ($p = 3x10^{-22}$), a significant effect of RSN ($p = 4x10^{-7}$), no significant effect of subject head motion ($p = 0.26$), and no significant interaction. By contrast, within-network intra-hemispheric connectivity was not significantly changed in both the ipsilesional and contralesional hemispheres (Fig.1B-C).

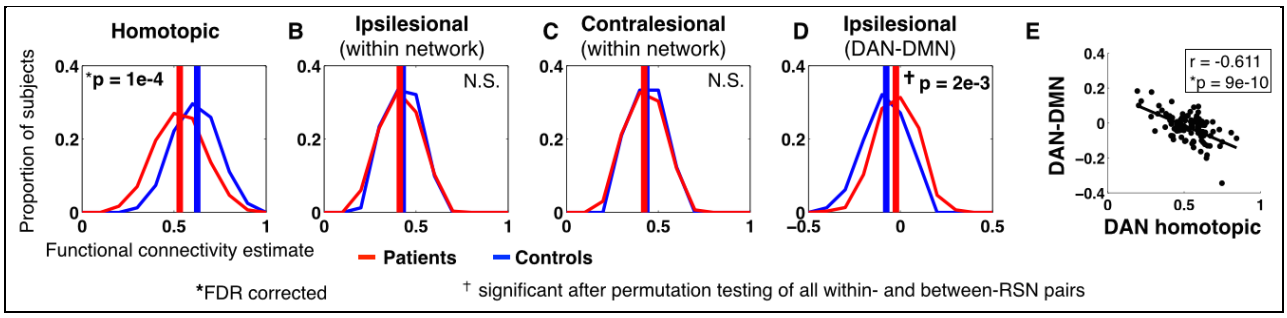

Figure 4-1. Stroke preferentially affects homotopic connections.
Red curves represent the distribution of within-RSN FC estimates over stroke patients (n = 100), blue curves represent the distribution of within-RSN FC over controls (n = 27). **A** FC between homotopic region pairs (the same location on opposite hemispheres) is averaged for each subject (pat: mean = 0.53, sd = 0.11; control: mean = 0.63, sd = 0.090; two-tailed t-test: $p = 4.0x10^{-3}$). **B** FC between all within-network ipsilesional region pairs is averaged for each subject. Intrahemispheric connections on a randomly chosen hemisphere are averaged in controls. (pat: mean = 0.41, sd = 0.064; control: mean = 0.43, sd = 0.046; two-tailed t-test: p = 0.26). **C** FC between all within-network contralesional region pairs is averaged for each subject. (pat: mean = 0.42, sd = 0.058; control: mean = 0.44, sd = 0.036; two-tailed t-test: p = 0.32). P-values for panels A-C are based on two-tailed t-test of overall within-network FC are corrected for three comparisons. **D** FC between all DAN-DMN between-network ipsilesional region pairs is averaged for each subject. (pat: mean = -0.024, sd = 0.077; control: mean = -0.078, sd = 0.075; two-tailed t-test: p = 0.0021). DAN-DMN was the only network pair that showed a significant ipsilesional connectivity difference after multiple comparison correction with permutations (see Fig.S3D) **E** Ipsilesional DAN-DMN FC is compared to homotopic FC between DAN nodes to show that within-hemisphere segregation of task positive and task negative RSNs relates to across-hemisphere integration. P-value is FDR corrected for eight comparisons.

To determine if differences observed between groups might result from differences in global neuronal fluctuations, R-fMRI data were additionally processed without global signal regression but instead using CompCor to remove non-neuronal sources of BOLD signal variance (Behzadi et al., 2007; Muschelli et al., 2014). We found that functional connectivity analyses conducted without global signal regression produced highly similar results (Fig.S3).

Next, we compared connectivity values between networks. Only a single RSN pair showed significant FC changes in the stroke group. Ipsilesional DAN-DMN FC connectivity was negative in controls but less negative in patients (Figs.1D & S3) (t-statistic = -3.15, p = 0.0021). Further, we found a strong relationship between decreased DAN homotopic FC and increased ipsilesional DAN-DMN FC (r = -0.61, p = 9e-10; Fig.1E), and no correlation in age-matched controls (r = 0.25, p = 0.19), with a significant difference between the two groups (Fisher r-to-z-transform; z = -4.24, p < 0.001). Other networks showed a similar relationship between ipsilesional network segregation (from the DMN) and homotopic integration, but to a lesser degree (SMD, r = -0.45, p = 5.2e-6 ; SMV, r = -0.28, p = 0.0103; CON, r = -0.56, p = 4.4e-7; VAN, r = -0.24, p = 0.0043; p-values are DFR corrected for eight comparisons).

We tested the relationship between damage and homotopic FC (averaged across the brain) using a univariate correlation with lesion size and a multivariate correlation with lesion topography. We found that lesion size predicted average homotopic connectivity ($r=-0.46$ $p=6x10^{-7}$), but the prediction was not improved by adding information about lesion topography (multivariate prediction: PVE=21% $r=0.46$ $p=7x10^{-7}$). This result shows that average homotopic FC is decreased by a similar amount following lesions of similar sizes, irrespective of the topography of the lesions. Therefore, a decrease in homotopic FC is a general consequence of stroke. However, the topography of the decrease in FC (i.e. which connections show a decreased as opposed to the overall magnitude of the decrease) likely depends on the topography of the lesion.

Potential sources of unwanted variance were compared to homotopic connectivity to determine effects on FC differences within or between groups. Group and individual differences in

homotopic FC were not significantly explained by head motion, % time with eyes open, or lag laterality (Fig.S4).

4.4.2 Prediction of behavioral deficits based on lesion and FC

Next, we investigated the extent to which structural data and functional data explained deficits in the stroke patients. Following manual lesion segmentation and R-fMRI processing (Fig.S1), lesion maps and vectorized FC matrices were used to generate Lesion-deficit and FC-deficit models using leave-one-out ridge regression (Fig.2).

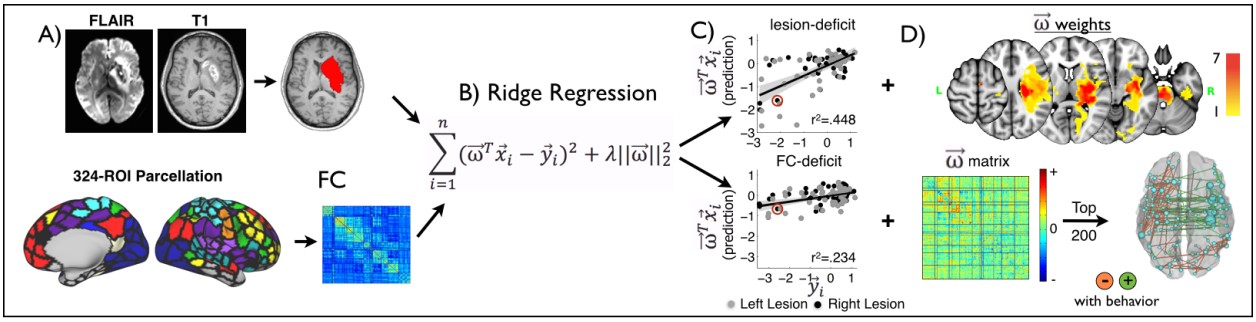

Figure 4-2. Prediction of behavioral deficits on the basis of structural and functional imaging.
A Experimental procedures for manual lesion segmentation (top), and for ROI-based functional connectivity estimation. **B** Ridge regression was applied using either lesion or functional connectivity to predict deficit for a left-out patient. A ridge regression function using lesion/FC to explain deficit is trained for n-1 subjects. For each patient, this function generates a prediction of deficit in each domain based on data, and a beta weight matrix that can be projected back on to the brain. **C** Predicted deficit scores were compared to measured scores for each patient to determine model accuracy. **D** Beta weights used to predict left motor deficit with either the lesion (top) or the FC matrix (bottom) are projected back on to the brain.
Abbreviations: R-fMRI = resting functional magnetic resonance imaging; FC = functional connectivity; ROI = region of interest; RSN = resting state network; MTL = multi-task learning; BVMT = brief visuospatial memory test; HVLT = hopkins verbal learning test;

Figure 3 shows the accuracy of lesion-deficit and FC-deficit model predictions in each domain. The bar graphs indicate percent of variance explained (r^2) by lesions (white bars) or by FC (black bars) in each model. The two rows of scatter plots show predicted and measured scores used to determine model accuracy for every subject. For simplicity, left and right motor and visual

predictions have been combined to only show contralesional prediction. The significance of each model was determined using permutation tests: attention (n = 80, lesion p = $4x10^{-4}$, FC p < $1x10^{-4}$), visual memory (n = 79, lesion p = $9x10^{-4}$, FC p < $1x10^{-4}$), verbal memory (n = 79, lesion p = $1.5x10^{-3}$, FC p < $1x10^{-4}$), language (n = 98, lesion p < $1x10^{-4}$, FC p < $1x10^{-4}$), left motor (n = 91, lesion p < $1x10^{-4}$, FC p = $1.1x10^{-3}$), right motor (n = 91, lesion p < $1x10^{-4}$, FC p < $1x10^{-4}$), left visual (n = 53, lesion p = $4x10^{-4}$, FC p = 0.0104), right visual (n = 53, lesion p = $1x10^{-4}$, FC p = 0.0902). See also figure S5. An additional control analysis confirmed that FC-deficit model accuracies surpassed chance when information from lesion location was included in null models (see supplemental data and Fig.S5).

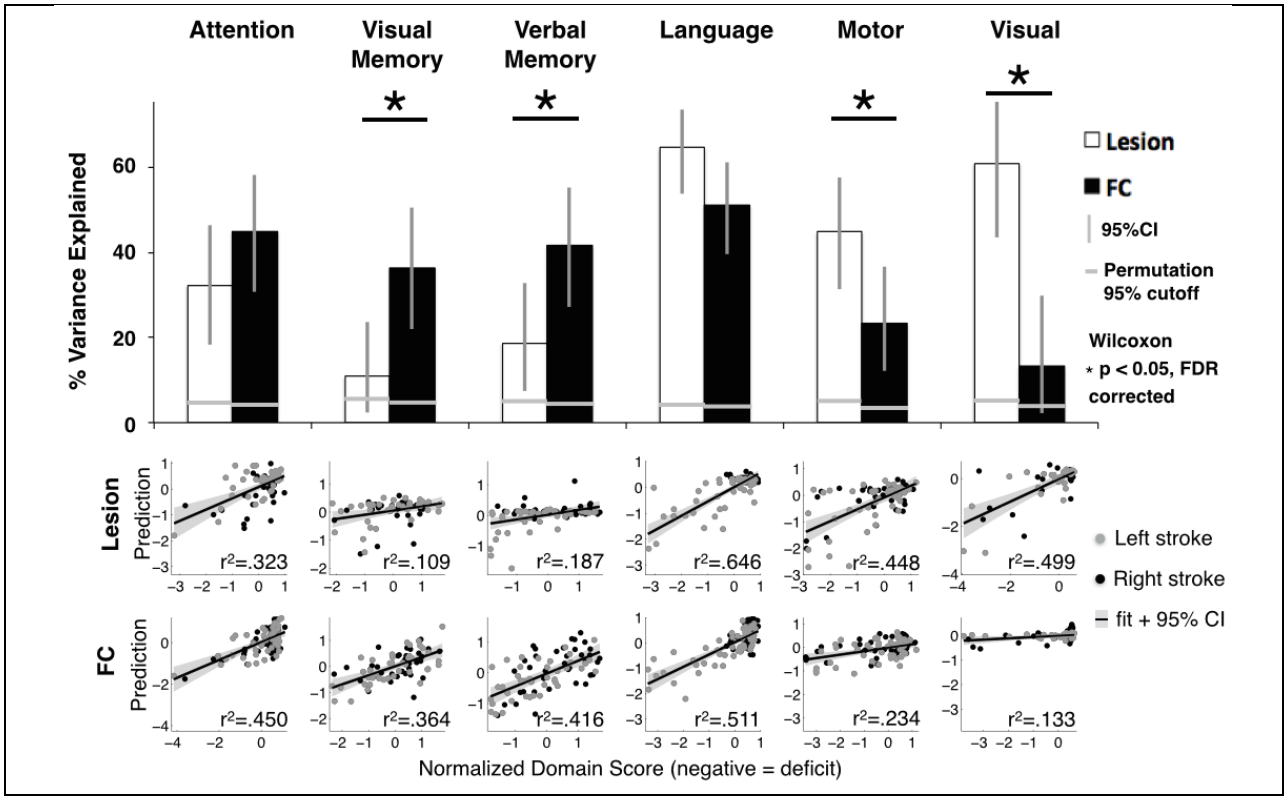

Figure 4-3. Lesion-deficit and FC-deficit model accuracies vary by domain.
The bar graph shows percent of variance explained across the six behavioral domains. White bars are lesion-deficit models, black bars are FC-deficit models. Lesion location predicts deficit significantly better in motor, and visual

domains. FC predicts deficit significantly better in the visual memory, and verbal memory domains. Statistical comparison between lesion-deficit and FC-deficit models (indicated by asterisks) were performed using a Wilcoxon signed rank test of prediction error and FDR corrected. Horizontal gray lines represent p = 0.05 cutoffs for the null model generated by permuting domain scores 10,000 times for each domain. All models perform significantly better than chance. The scatter plots below show the comparison between predicted and measured scores from lesion-deficit models (top row) and FC-deficit models (bottom row). Behavior scores are a composite of multiple tests in each domain and are on a z-normalized (mean = 0, sd = 1) scale. Motor and visual deficits were predicted separately for each hemisphere and the contralateral side but combined for visualization.

Prediction accuracy of the FC and lesion models was directly compared using a two-tailed Wilcoxon paired signed rank test of prediction errors. After false discovery rate correction, four domains showed significant differences between lesion-deficit and FC-deficit model accuracy. Visual memory (lesion = 10.9%, FC = 36.4%, p = 0.015), and verbal memory (lesion = 18.7%, FC = 41.6%, p = 0.007) were better predicted by FC than lesion location, whereas motor (lesion = 44.8%, FC = 23.4%, p = 0.009), and visual deficits (lesion = 49.9%, FC = 13.3%, p = 0.013) were better predicted by lesion location than FC. Attention showed a trend for higher prediction by FC, while language was equally predicted by both inputs (Attention - lesion = 32.3%, FC = 45.0%, p = 0.074; Language - lesion = 64.6%, FC = 51.1%, p = 0.21). For a complete description of permutation testing and control analyses, see supplement.

To determine if domain prediction results generalized to individual task performance scores, FC- and lesion-models were also generated for every performance measure included in the generation of domain scores. Some measures were predicted poorly. However, for measures that showed good prediction accuracy, the prediction differences observed in the domain scores frequently generalized to the raw scores (Fig.S6).

4.4.3 Topography of behaviorally predictive FC

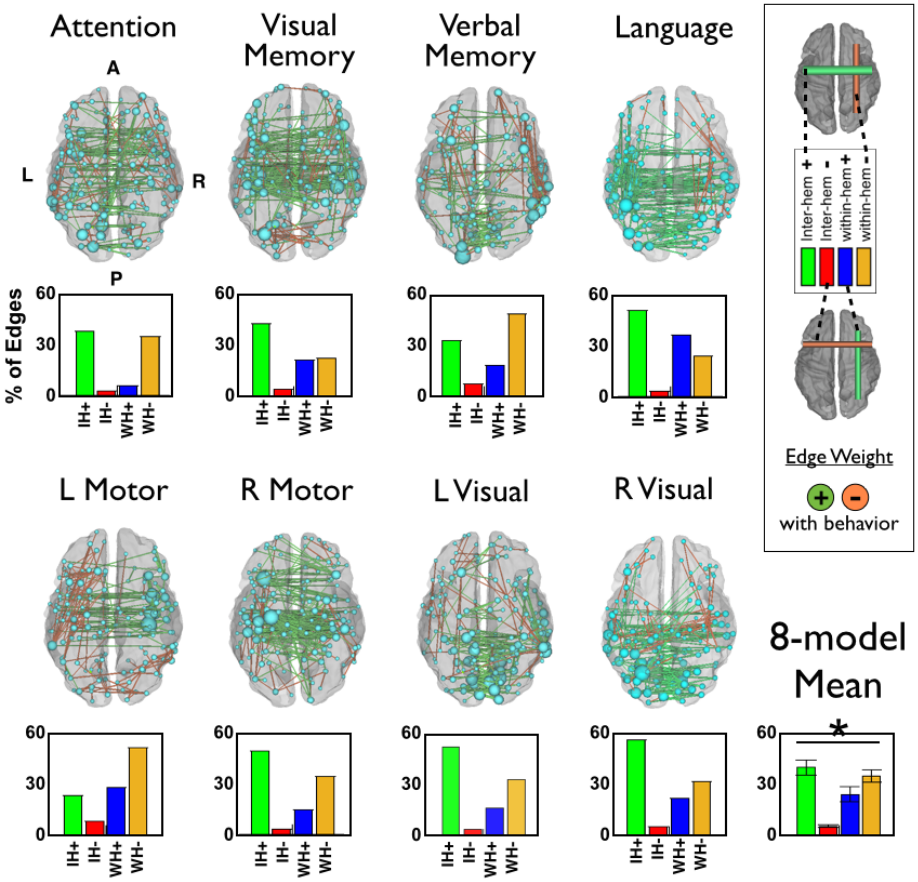

Figure 4-4. Most predictive connections and nodes for each FC-deficit model. Left: The top 200 connections driving each FC-behavior model are projected back on to a semi-transparent cerebrum (PALS atlas). Green connections indicate positive weights (increased FC predicts better performance), orange connections indicate negative weights (increased FC predicts worse performance). The subset of the 324 parcels included in the top 200 weights are displayed as spheres, sized according to their contribution to the model. Below, weights from each FC-behavior model are divided into 4 groups: inter-hemispheric positive, inter-hemispheric negative, intrahemispheric positive, and intrahemispheric negative. Bars indicate the average contribution of each of the four groups. The average across models is shown at the bottom right. An ANOVA indicates a significant difference in contribution of the four connection types ($p = 1.6x10^{-}$).

Weights from the FC and lesion prediction models were averaged across all leave-one-out models and projected back onto the brain (Fig.4; see also Fig.S7 for further visualization of FC-deficit and lesion-deficit weights). In figure 4, green edges indicate that increased FC predicted better behavior, and orange edges indicate that decreased FC predicted better behavior. It should

be noted that positive and negative weights do not imply positive or negative FC values, only a positive or negative relationship with the behavior of interest. The top 200 strongest weights are illustrated. The size of each node is relative to the total contribution of all of its connections to the model.

Considered side-by-side, common features of the FC-deficit maps are apparent (Fig.4). Specifically, the strongest weights tend to be positive inter-hemispheric, i.e. stronger FC correlates with better performance; and negative intra-hemispheric, i.e. stronger FC correlates with poorer performance. To compare the types of connections that were most heavily weighted in each domain, the top 1% of weights from each FC-deficit model were divided into four groups – inter-hemispheric positive, inter-hemispheric negative, within-hemisphere positive and within-hemisphere negative. The bar graphs in figure 4 show the average contribution of each of the four types of connections across all prediction models. An ANOVA confirmed a significant difference in the contribution of connection types ($p = 1.6x10^{-6}$) to deficit prediction, with positive inter-hemispheric weights showing the greatest contribution followed by negative within-hemisphere weights. Language is an exception since a significant prediction comes from positive intra-hemispheric weights in the left hemisphere, i.e. accurate language performance depends on communication between regions of the left hemisphere.

In figure 5, the average contribution of all positive connections within an RSN (circle radius) and between RSN pairs (line thickness) is illustrated for each FC-behavior prediction. In attention and memory domains, connections between RSNs are particularly prominent. By contrast, language weights are more limited to connections within the auditory network, motor weights to

connections within auditory and somatomotor networks, and visual weights to connections within visual and somatomotor networks, while connections between RSNs are not as prominent. To quantify this observation, we measured the ratio of positive weights within RSNs to positive weights between RSNs: attention: 1.431, visual memory: 1.526, verbal memory: 1.499, language = 1.768, motor = 1.605, visual = 1.624.

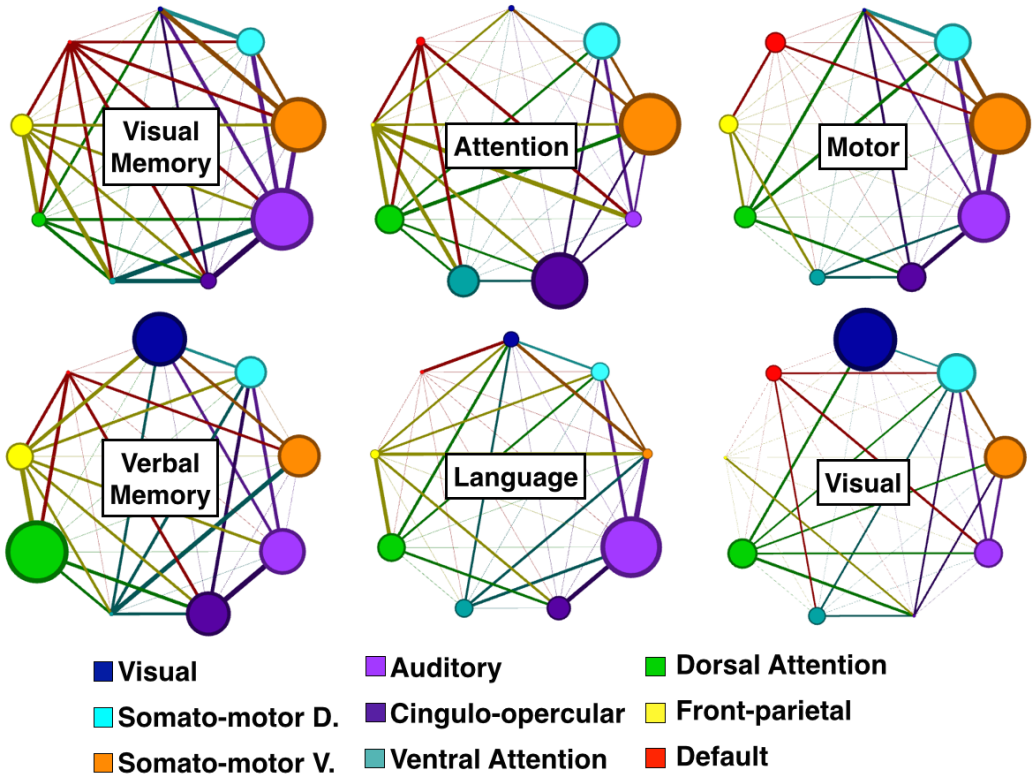

Figure 4-5. Network view of FC-deficit domain models.
Consensus positive weights (averaged across all leave-one-out cross validations) from each model are divided up by RSN to determine network influence. RSNs with at least 8 parcels are included (9 out of 13 RSNs). Node sizes are proportional to the average contribution of all within-network connections. Edge thicknesses are proportional to the average weighting of all between-network connections. Grayed edges (e.g. DMN-VIS in the Attention model) indicate no between-network weights. The key indicates RSN identities. Network diagrams are generated using Gephi (Bastian et al., 2009).

4.4.4 Prediction of common behavioral impairment

To further investigate shared features between models, we used multi-task learning. All domains were predicted by two sets of weights simultaneously. One set (ω_k) was optimized by domain while the other set (ω_o) was shared across all domains (Eq. 1). This procedure enabled us to differentiate domain-specific versus shared (across-domain) correlates of neurological deficit in these eight domains. The optimized multi-task learning model explained 28.7% of the variance across all patients and all five domains. The shared across-domain weights were explored to understand features of connectivity that predict common deficit across domains (Fig.6). The shared weights involved overwhelmingly inter-hemispheric connections (Fig.6b). Positive shared weights (green bars; reduced FC corresponds to worse deficit across domains) were distributed across RSNs, but weighed most heavily on dorsal attention network, cingulo-opercular network, auditory network, and somato-motor dorsal network (Fig.6d/e).

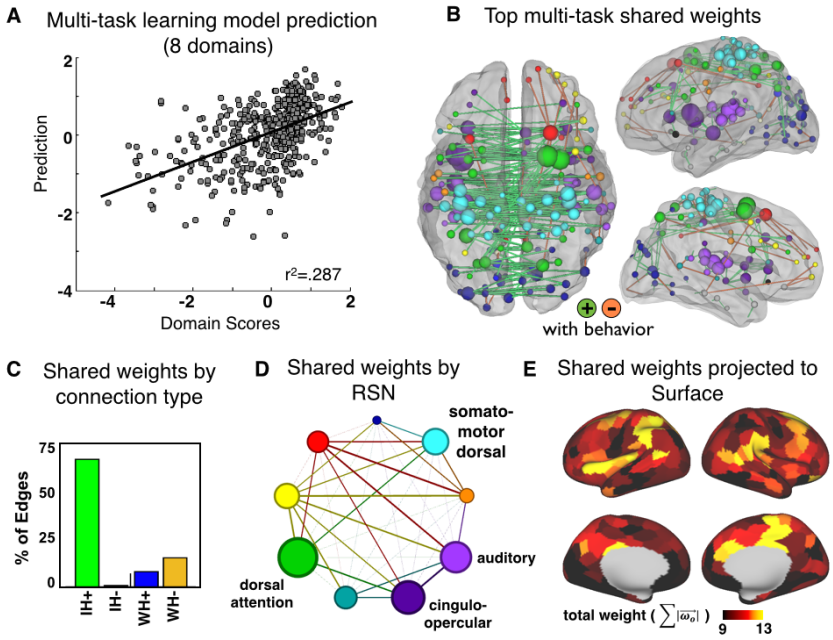

Figure 4-6. Multi-task learning shared weights.
A The multi-task learning (MTL) model explains 28.7% variance across all domains. **B** The top 200 weights for the MTL shared features are visualized in the brain. **C** Weights are divided in to 4 groups: inter-hemispheric positive, inter-hemispheric negative, intrahemispheric positive, and intrahemispheric negative. **D** Weights visualized by RSN. Node sizes are proportional to the average contribution of all within-network connections. Edge thicknesses are proportional to the average weighting of all between-network connections. **E** Shared weights are projected to the 324 surface parcels.

4.5 Discussion

We identified robust changes in network synchrony (measured with R-fMRI) after focal injury post-stroke, and determined their behavioral significance in six domains (attention, visual memory, verbal memory, language, motor, and visual). In addition, we compared the behavioral significance of network synchrony and lesion location across domains.

We found that changes in inter- and intra-hemispheric FC following stroke showed a consistent pattern across networks (Figs.1, S3). The largest changes in FC between patients and controls involved decreases in inter-hemispheric FC. Decreases in inter-hemispheric FC were

accompanied by increases in intra-hemispheric FC between networks that are normally segregated (e.g. DAN and DMN). Moreover, decreased inter-hemispheric FC was also the feature of FC that best predicted behavioral deficits within the patient sample. Decrement in specific RSNs predicted deficits in corresponding behavioral domains, consistent with the large-scale network organization of the brain (Figs.3-5). A multi-task model revealed that reduced inter-hemispheric FC in a set of nodes predicted shared deficits across domains (Fig.6). Jointly, the inter- and intra-hemispheric changes in FC constitute a general physiological network phenotype of stroke injury.

We also found a fundamental difference between behavioral domains. Memory deficits were better predicted by functional connectivity than by lesion location, while motor and visual deficits were better predicted by lesion location than by functional connectivity. Language deficits were well predicted by both and attention deficits showed a trend towards FC > lesion (Figs.3, S6). These results suggest that the behavioral significance of network synchrony was greater for associative domains whereas the behavioral significance of lesion topography was greater for sensorimotor domains. Below, we suggest that this division follows naturally from the greater dependence of associative functions on large-scale distributed interactions between brain systems, and of sensory-motor functions on input-output pathways.

4.5.1 Inter-hemispheric Connectivity and Stroke

Two lines of evidence from our study converge on the conclusion that disrupted communication between the hemispheres is a central feature of stroke. First, the largest and most consistent

change in FC from controls to patients involved a decrease in inter-hemispheric, homotopic FC. Second, alterations in inter-hemispheric connections showed the strongest association with behavioral impairment across nearly all domains. Reductions in inter-hemispheric coherence were predominant not only in the functional connectivity related to specific deficits (Baldassarre et al., 2014c; Carter et al., 2010; He et al., 2007; Rehme et al., 2014; van Meer et al., 2010b), but also in the multi-domain FC that generalized across deficits (Fig.6). This result reveals a key insight into how a stroke disrupts cognition: severe strokes not only cause local damage but produce a disruption of inter-hemispheric balance.

The physiology underlying reduced inter-hemispheric FC following a stroke remains unclear. One explanation is that the structural connections or mechanisms that mediate the transfer of signals between the hemispheres might be damaged or functioning abnormally. For example, reduced inter-hemispheric FC is accompanied by decreases in manganese transfer from the contralesional to the ipsilesional hemisphere (van Meer et al., 2010b), consistent with a reduction in callosal fibers. Alternatively, signals in the damaged and undamaged hemispheres might undergo hemisphere-specific changes that reduce their correlation. EEG signals (power, coherence) are abnormal both within and across hemispheres post-stroke, and correlate with behavioral impairment (Dubovik et al., 2012; Wu et al., 2015).

We find that the global average reduction in inter-hemispheric FC could be partly predicted by lesion load ($r = 0.46$), but could not be better predicted with additional information about lesion location. This is not to say that specific lesions do not disrupt inter-hemispheric FC in specific areas or networks. Prior studies have identified RSN-specific relationships between lesion

location and FC disruption (Baldassarre et al., n.d.; Nomura et al., 2010). But our results establish disrupted inter-hemispheric FC as a common effect of strokes, rather than a result of damage to specific structures such as the corpus callosum or thalamus. Further work is needed to better elucidate the cause of reduced inter-hemispheric coherence.

In our cohort, a decrease in inter-hemispheric FC was correlated with an increase in intra-hemispheric FC between DMN and DAN (Fig.1E). A similar phenomenon has been observed in monkeys following disconnection of the corpus callosum and anterior commissure (O'Reilly et al., 2013). This suggests that integration of RSNs across the hemispheres is linked to segregation of task-positive and task-negative RSNs within the hemispheres. The post-stroke reduction in integration and segregation can be thought of as resulting from a single disruptive process such as previously observed reductions in brain network modularity (Gratton et al., 2012) and information capacity (Deco et al., 2015).

4.5.2 Structure vs. Function - relative contribution to different behavioral deficits

In 1885, Karl Wernicke made the prescient observation that sensory and motor functions could be localized, but higher cognitive functions were instead dependent on communication across distributed brain networks.

> *"The acoustic images find their abode within the cortical terminals of the acoustic nerve, the visual images, within the cortical endings of the optic nerve, and the olfactory images in that of the olfactory nerve … Movement representation could be located in the cortical sites of the motor nerve origins… Any higher psychic process could not, I reasoned, be localized, but rested on the mutual interaction of these fundamental psychic elements*

mediated by means of their manifold connections via the association fibers" (Wernicke, 1885)

However, only recently have the tools been available to quantitatively test this hypothesis. Here, we found that associative domains were better predicted by FC than lesion topography while sensorimotor domains such as vision and motor were better predicted by lesion topography than FC.

Lesion-deficit mapping has been the cornerstone of functional localization since the early 19th century (Broca, 1861). The basic principle is that specific functions are performed in specific parts of the brain (Broca, 1861; Brodmann, 1909), and therefore careful anatomo-clinical correlations between behavioral impairment and structural damage can identify the part of the brain necessary for that function. One tacit assumption, however, is that sensory, motor, and cognitive functions are equally affected by structural damage. A second important set of results in our work instead emphasizes a fundamental distinction between cognitive and sensori-motor domains in relation to how well structural or functional connectivity damage explain behavioral variability. Below, we discuss the implication of our observations in understanding and comparing sensorimotor, memory, and language deficits.

Sensorimotor deficit

Behaviors that are directly dependent on the immediate interface with the environment can be localized with high fidelity in the cerebral cortex and depend on input/output white matter pathways. Accordingly, lesion location either in specialized cortex, underlying white matter, or connected subcortical regions, reliably predicted hemianopia (50% of variance) and hemiparesis

(45% of variance). By contrast, FC explained a significantly smaller amount of behavioral variance, and motor and visual FC-deficit models showed positive weights that were largely confined within the corresponding damaged RSN rather than reflecting between-network connections, i.e. the connectivity changes occurred mainly within the damaged network. These results are consistent with the peripheral location of the visual and sensorimotor networks in the overall brain graph (Power et al., 2011), and computational studies showing that damage to peripheral nodes do not cause widespread alterations in network structure (Alstott et al., 2009).

Visual and verbal memory deficit

Visual memory, and verbal memory deficit scores were better predicted by FC changes than lesion topography. The visual and verbal memory scores included measures of encoding and retrieval of visual shapes and words at short and long time intervals (Table S1). These functions require the coordination of an ensemble of mental operations and computations occurring in parallel across distributed networks (Corbetta and Shulman, 2002; Mesulam, 1990; Ullman, 1984). Correspondingly, weights in the memory FC-deficit models were distributed across many brain systems, in comparison with the more constrained distribution of motor and visual model weights.

Lesion-behavior studies have not clearly isolated a critical lesion site for visual or verbal memory. Likewise, a large literature on neglect indicates that a similar syndrome emerges for lesions at multiple cortical and subcortical sites (Corbetta and Shulman, 2011). Single unit studies have localized signals consistent with spatial working memory in multiple cortical and subcortical regions that are connected by reciprocal anatomical pathways, suggesting that

functions like memory and attention are distributed across many regions of the brain (Goldman-Rakic, 1988; Mesulam, 1990; Posner et al., 1988). This idea is also consistent with a large number of neuroimaging studies (Owen et al., 2005; Smith and Jonides, 1998).

Language deficit

Language impairments represent an interesting counterpoint to both sensorimotor and cognitive deficits. Both lesion topography and FC accounted for >40% of behavioral variance, with no significant difference in accuracy between the two models. FC regions predictive of language impairment involved canonical language regions, but also bilateral connections within and between other RSNs (Figures 4 & 5). Unlike other domains, language deficit showed substantial dependence on left intra-hemispheric connectivity. Language disorders can arise not only from pure disruption of language processing, but also from disruption of bilaterally distributed support processes including auditory processing, visual attention as in reading, and motor planning for speech (Connor et al., 2000; Gracco and Abbs, 1988; Tallal et al., 1996). That both lesion and FC predicted above 40% of variance supports the increasingly accepted theory that language function relies on highly localized brain regions as well as bilaterally distributed brain networks and connections (Fedorenko and Thompson-Schill, 2014). Damage to any of these structures can compromise the communication and function of the language system as a whole.

4.5.3 Caveats/Limitations

The accuracy of brain network models depends in part on the brain regions used in the models. Important considerations for FC analysis include 1) which the structures included, and 2) how

those structures are parcellated. We chose a cortical parcellation previously demonstrated to optimally separate FC data in healthy young adults (Gordon et al., 2016). However data from the cerebellum and basal ganglia were not included in this parcellation. Inclusion of these structures may improve FC-deficit models in future studies. Secondly, differences in connectivity between patients and age-matched controls could result from differences in parcellation fit (i.e. how well the parcellation matches real boundaries between functional brain areas) between groups. We assessed parcellation fit by measuring parcel homogeneity (Craddock et al., 2012). We found a small, but significant differences in parcel homogeneity (Fig.S2) with patients showing lower homogeneity than age-matched controls (paired t-test: t-stat = 8.0, $p < 0.0001$). Thus, some univariate FC differences reported between patients and controls may result from greater homogeneity in controls than patients. However, the small difference in homogeneity is unlikely to account for the large difference in FC reported in Figure 1.

Additionally, because our stroke cohort was chosen to represent the normal clinical population, lesions were not evenly distributed across the cortex. Lesion-deficit accuracy may be further improved in a more evenly sampled population.

As is the case with multivariate regression, a larger sample might also improve prediction accuracy. This is especially the case for the visual domain, in which only 58 subjects were included. Still, FC- and lesion-deficit models within each domain use identical subject, thus comparisons drawn between the two should be robust.

Homotopic FC is more stable across time and across conditions than other types of functional connections (Shen et al., 2015). It is possible that our FC-deficit models load most heavily on

inter-hemispheric FC because this stability enables greater fidelity in measurement of disruption. However, both the difference between patients and controls and the ability of inter-hemispheric FC to predict subtle deficits associated with disruption to the contralesional hemisphere suggests that this is not the only explanation for our observations.

4.5.4 Conclusions

The present work points to the fundamental importance of inter-hemispheric integration and intra-hemispheric segregation, and their disruption post-stroke. More generally, this study links major features of the pathophysiology of stroke to the normal organization of brain networks. Deficits in behavioral domains involve abnormal FC in corresponding networks, while deficits across domains emphasize homotopic FC in a small number of key brain regions. Similarly, abnormal connectivity best accounts for behavioral deficits involving associative functions such as memory that involve interactions between brain systems. Conversely, FC is less predictive in sensorimotor domains, and the predictive connections that are observed tend to be local and within-network.

4.6 Acknowledgement

We thank Nico Dosenbach and Brad Schlaggar for as- sistance with visualization software; Carl Hacker, Timothy Laumann, and Evan Gordon for data processing assistance; and Alexandre Carter for conceptual de- velopment. This study was supported by National Institute of Child Health and Human Development Health Award 5R01HD061117 (to M.C.), National Institute of Neurologic Disorders and Stroke (P30 NS048056 to A.Z.S.), National Institute of Health

Medical Scientist Training Award 5T32GM007200-39 and American Heart Association Predoctoral Fellowship Award 14PRE19610010 (to J.S.S.).

Supplemental methods can be accessed at www.pnas.org/content/113/30/E4367.full

4.7 Supplemental Figures and Tables

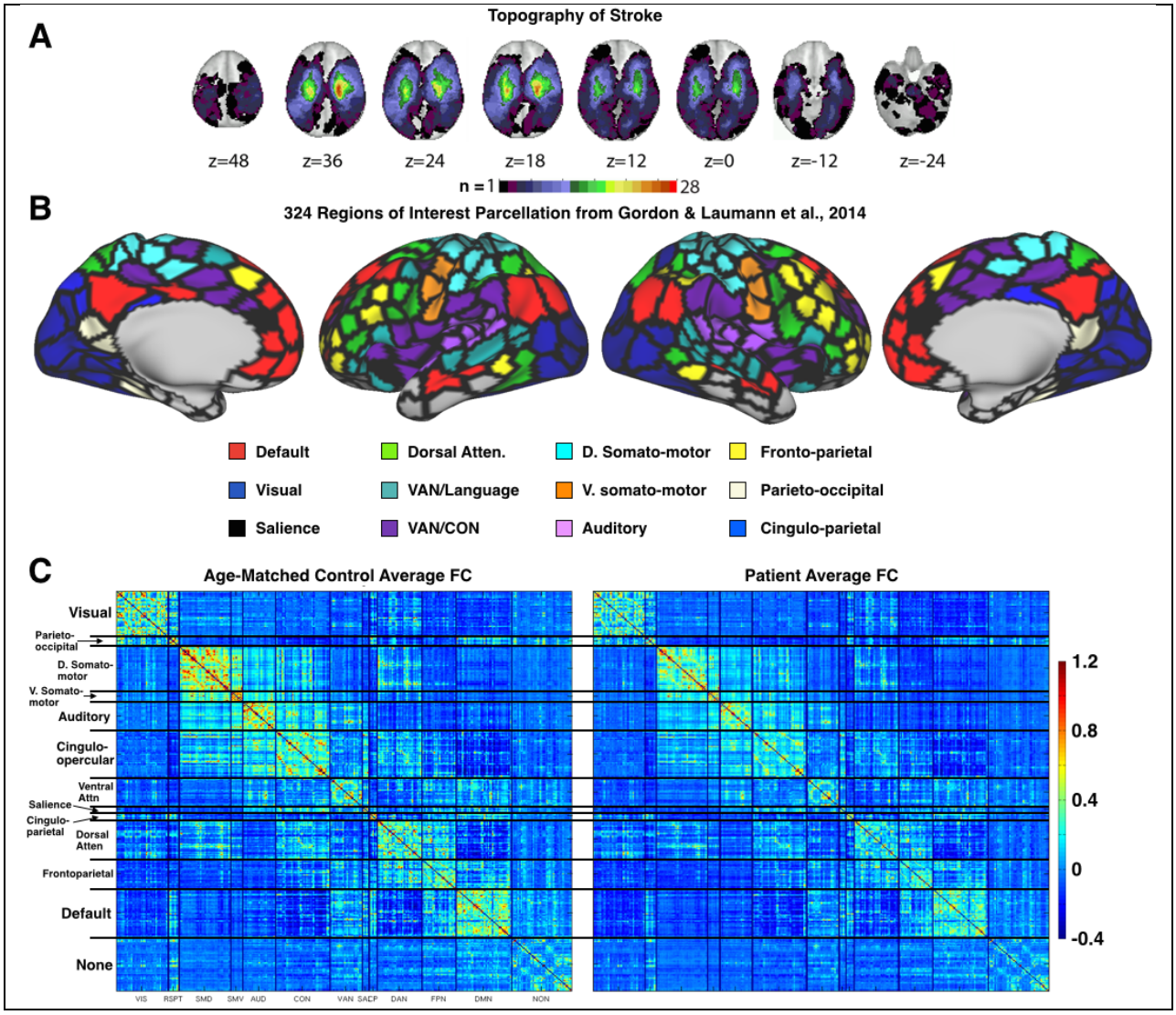

Figure S1: Lesion and FC visualization.
A: Topography of stroke. Lesion overlay map in atlas space for 132 stroke patients. Lesion distribution is representative of a larger source population. **B:** 324 region on interest parcellation from Gordon & Laumann et al.,

2014. Regions are color coded by RSN membership. **C:** Average Functional Connectivity. Average Fisher z-transformed FC matrices are shown for age-matched controls (n = 27) and stroke patients (n = 100) excluding regions that overlap lesions.

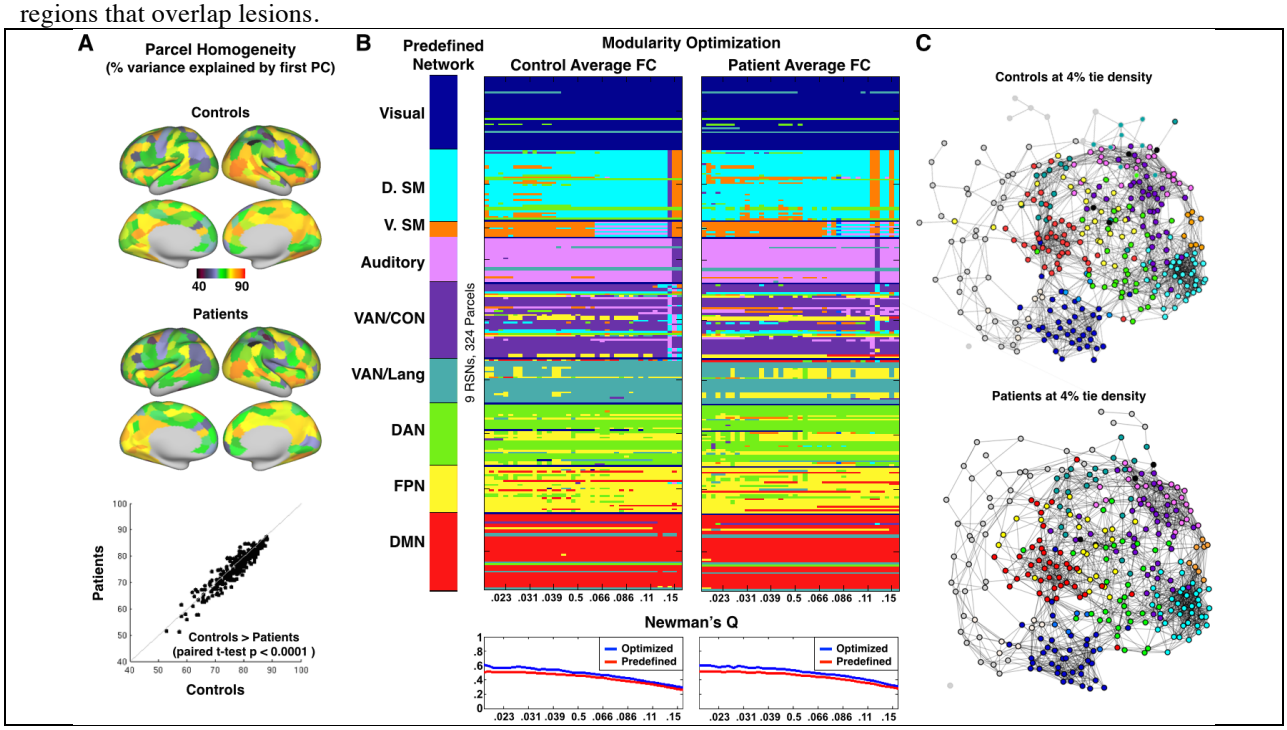

Figure S2: Parcel homogeneity and community (RSN) modularity of the Gordon & Laumann parcellation in controls and stroke patients.

A: Homogeneity of each parcel, calculated as the percent of the variance in RSFC patterns explained by the parcel's first PCA eigenvariate. Regional variability is highly consistent between patients and controls. Bottom: homogeneity is compared between controls and patients for every parcel. Patients show a small but consistent reduction in parcel homogeneity (control: mean = 0.70.8, sd = 8.3; pat: mean = 69.4, sd = 8.3; paired t-test: t-stat = 8.0, $p < 0.0001$). **B:** the leftmost column provides predefined community assignment based on Gordon et al. Here, as in later RSN-based analyses, RSNs with less than 7 regions are excluded. Modularity optimization was initialized with predefined community labels and run at a range of tie densities (0.02:0.15) in controls and patients. Below each visualization of modularity optimization is a plot of Newman's Q at every tie density for predefined community assignments (red) and optimized community assignments (blue). Optimal assignments show marginally greater modularity for the 9 major RSNs. **C**: Spring embedded graphs at 4% tie density. Areas are color-coded based on predefined community assignment.

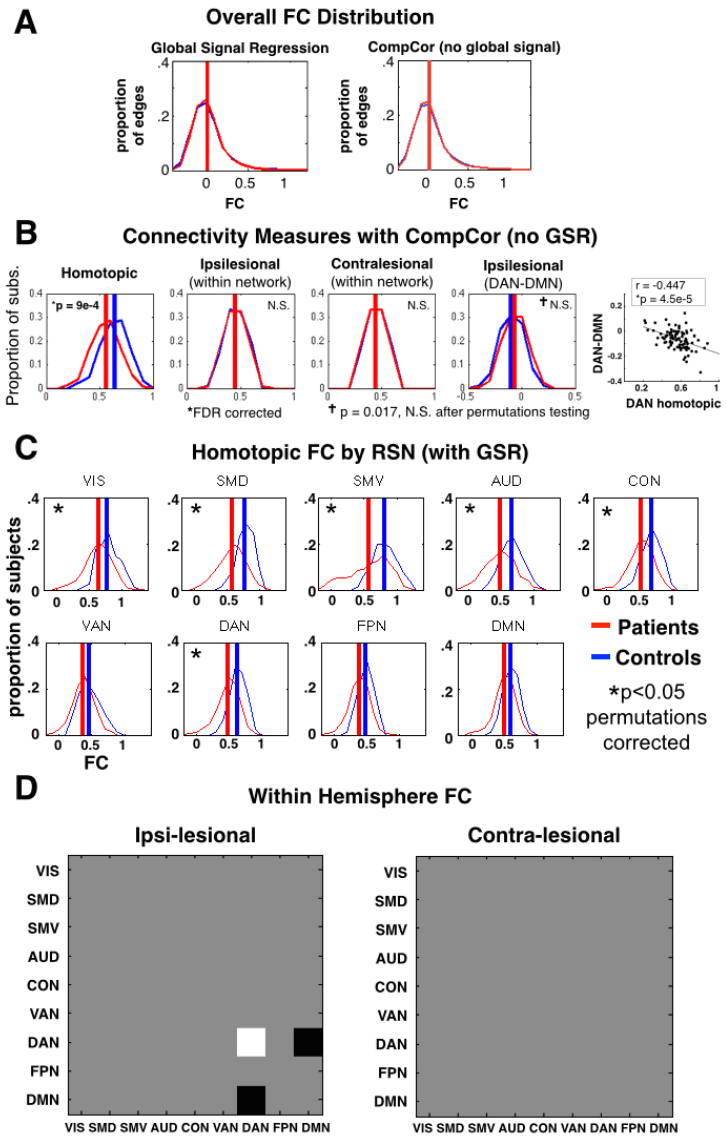

Figure S3: Stroke preferentially affects homotopic connections.
Functional connectivity changes are investigated without global signal regression, and within and between all RSN pairs. **A:** Red curves represent the distribution of FC estimates for all 324-choose-2 edges averaged over all patients (n=100), blue curves represent FC over all controls (n=27). **B**: Group FC comparisons using the same statistical analysis and multiple comparison correction as main Figure 1A-E, but with CompCor functional connectivity processing (see Supplemental Experimental Procedures). **C:** Homotopic FC distributions for patients and controls are shown for each RSN with at least 8 parcels (9 out of 13 RSNs). **D**: Intra-network and Inter-network FC differences were assessed within hemisphere. Black squares indicate patients > controls, white indicate patients < controls. C and D are jointly corrected for multiple comparisons using 10,000 permutations of group labels and 99 stroke-control t-tests (45 ipsilesional, 45 contralesional, 9 homotopic).VIS = Visual network (38 ROIs), SMD = dorsal somato-motor (37 ROIs); SMV = ventral somato-motor (8 ROIs); AUD = auditory (23 ROIs); CON = cingulo-opercular (39 ROIs); VAN = ventral attention (23 ROIs); DAN = dorsal attention network (32 ROIs); FPN = frontoparietal control network (24 ROIs); DMN = default mode network (40 ROIs).

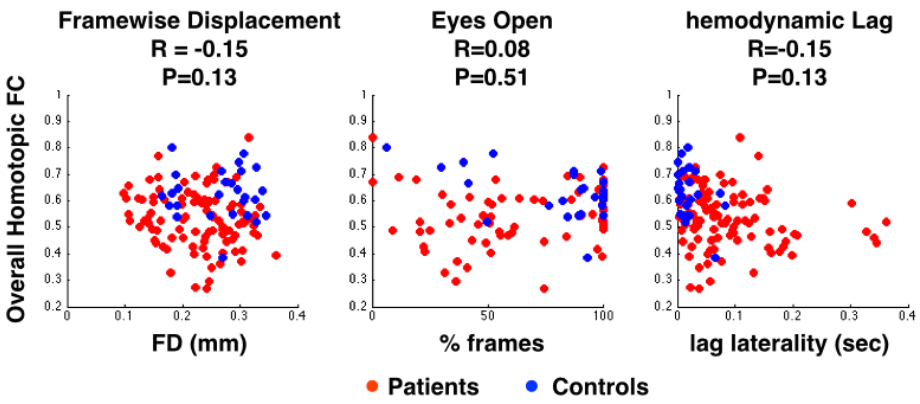

Figure S4: Group and individual homotopic FC differences are not explained by head motion, eyes open, or hemodynamic lag.
Left: Root mean square framewise displacement (FD) was not significantly different in patients (red dots) as compared to controls (blue dots) and shows no significant correlation with homotopic FC in the stroke patients. **Middle:** Percent of frames with eyes open was not significantly different in patients than controls, and shows no significant relationship to homotopic FC in the stroke patients. **Right:** After excluding 15 subjects with excessive hemodynamic lags, lag laterality was still significantly different in patients than controls (Wilcoxon rank sum test; P = 0.0021), however lag laterality showed no significant relationship with homotopic FC in the stroke patients.

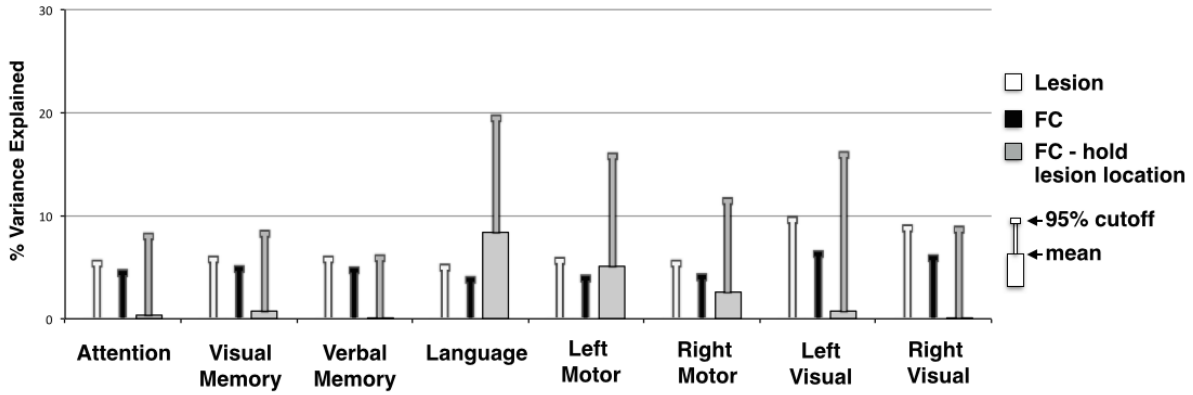

Figure S5: Permutation Testing.
Average variance explained and 95% cutoff from 10,000 permutations of each prediction model: lesion-deficit models (white), FC-deficit models (black), and FC-deficit models with lesion location retained (gray). Lesion-deficit and FC-deficit models were generated by randomly permuting behavioral scores. The 'FC – hold lesion location' models was generated by holding values within lesioned connections to zero, and then selecting all other FC values at random from the distribution of values for patients with no lesion. Note that with lesion information included, language and motor FC-deficit null models show substantial mean prediction, suggesting that FC models in these domains are picking up implicit structural information. Domains predicted by FC better than lesion (memory, attention) show very little influence.

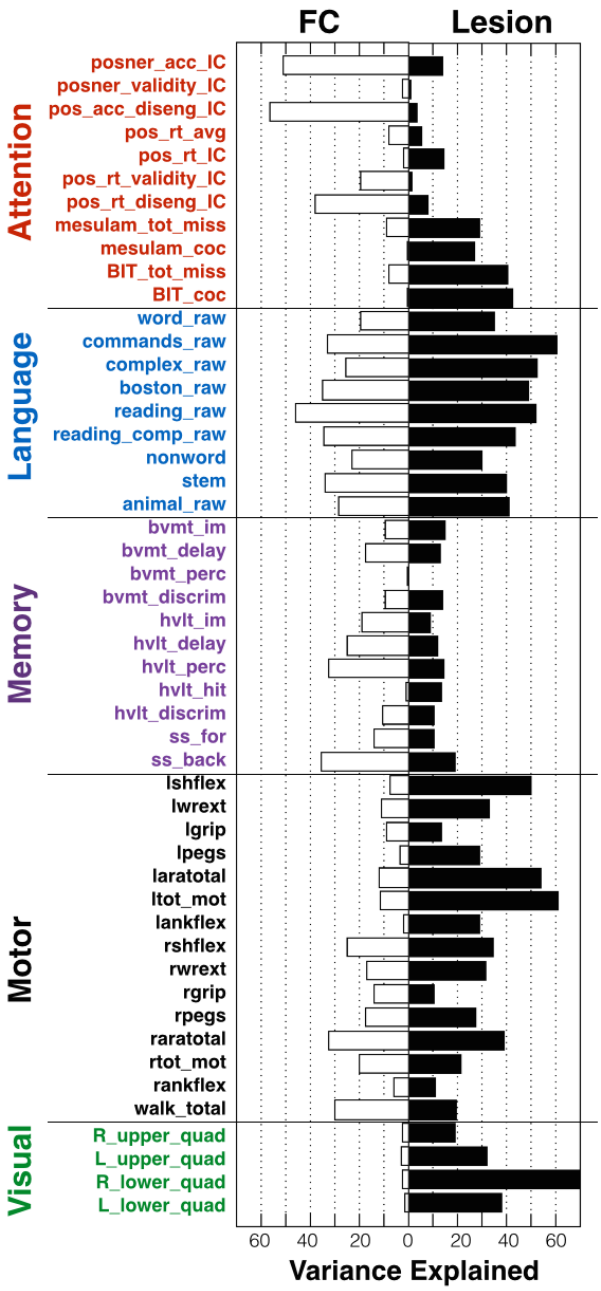

Figure S6. FC- and lesion-based prediction of individual performance measures.
To assess whether conclusions based on domain scores generalized to individual performance measures, we generated FC- and lesion-deficit prediction models for each measure. For some measures, the FC prediction was far worse than the domain score (e.g., bvmt_perc – brief visuospatial memory test percent correct). However, for measures that showed good prediction accuracy, the domain differences observed in the domain scores (e.g., that memory is better explained by FC and motor is better explained by lesion) appears to generalize to the raw scores. Full names of performance measures can be found in table S1.

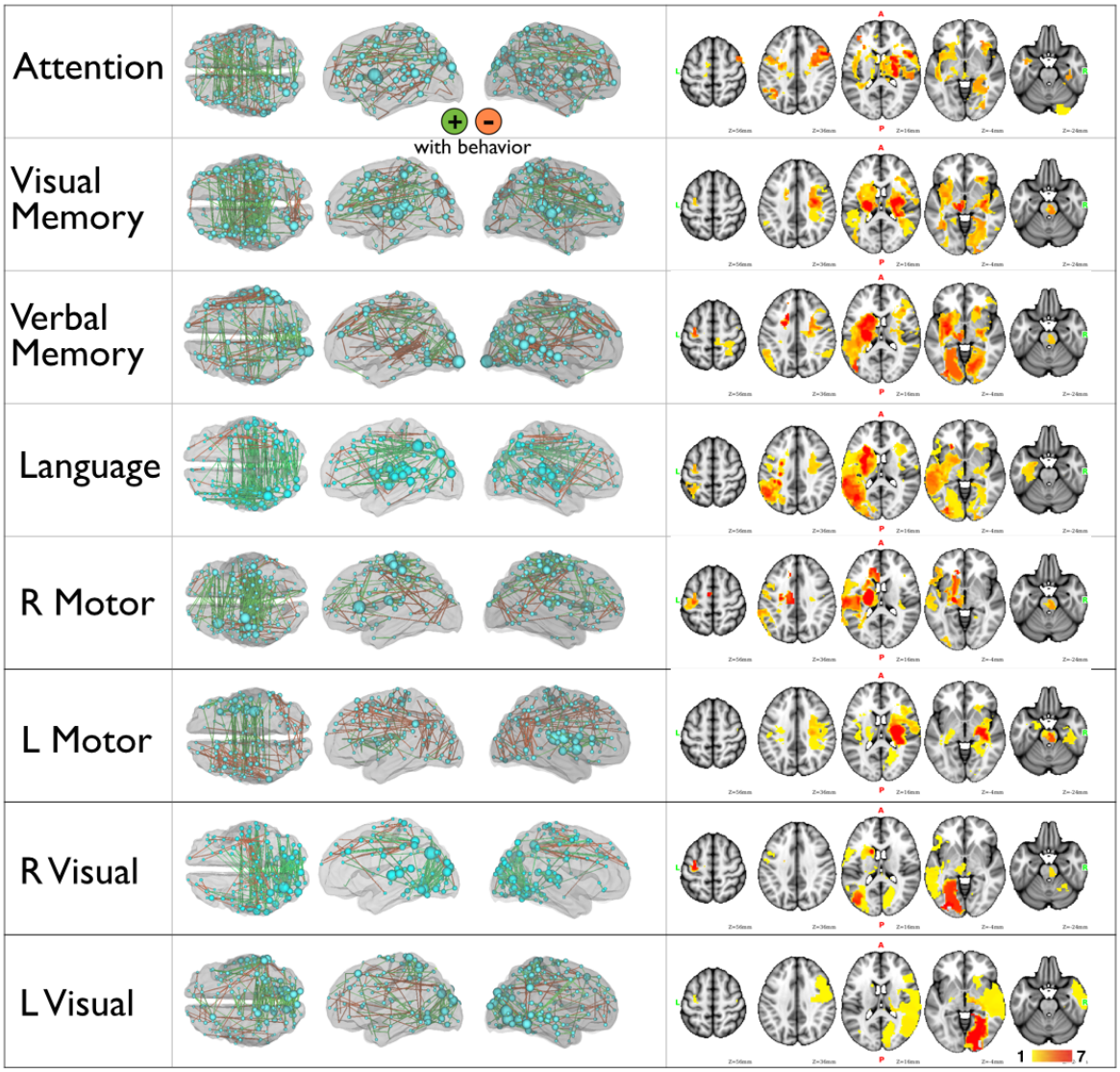

Figure S7: FC-deficit and Lesion-deficit maps.
Left: The top 200 connections driving each FC-behavior model are projected back on to a semi-transparent cerebrum (PALS atlas). Green connections indicate positive weights (increased FC predicts better performance); orange connections indicate negative weights (increased FC predicts worse performance). Also displayed are the 324 nodes, sized according to their contribution to the model. Right: lesion-deficit model weights projected on to a Montreal Neurological Institute brain atlas. Weights are normalized to have a mean of zero and standard deviation of 1.

A)

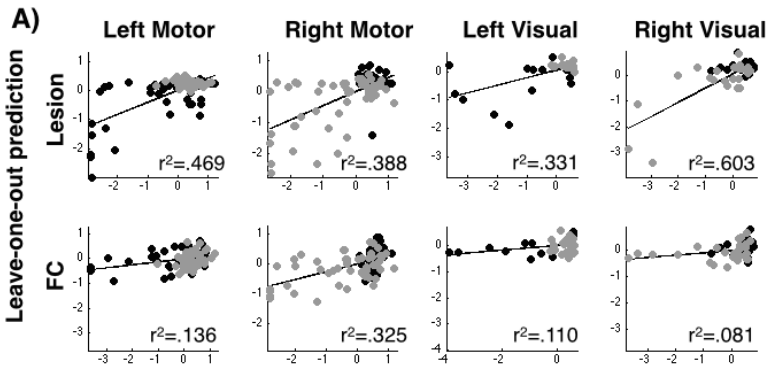

B)

	Left Motor function	Right Motor function	Left Visual function	Right Visual function
Left Lesion	lesion: NS **FC: .312**	lesion: .561 FC: .521	lesion: NS FC: NS	lesion: .786 FC: .278
Right Lesion	lesion: .650 FC: .421	lesion: NS **FC: .423**	lesion: .555 FC: .489	lesion: NS FC: NS

Figure S8. Motor and Visual pattern deviation results separated by lesioned hemisphere.
A) Motor and visual function were predicted separately for the left and right hemisphere lesion and then combined to determine prediction accuracy. B) Prediction accuracy is calculated separately for right lesion and left lesion patients. Note that left motor deficit is predicted for the ipsilesional hand, the FC-deficit significantly predicts ipsilesional function for both the left and right, but lesion-deficit model does not.

A) Cognitive Domains	Function tested	Test	Score Recorded	ATTN	VIS MEM	VER MEM	LAN
Visual Attention	Visual field	Posner orienting task, reaction time	Visual field effect [Left-Right], RT	.671			
	Shifting		Validity effect [Valid-Invalid], RT				
	Average		Overall performance, RT				
	Shifting		Disengage effect [(LI-LV)-(RI-RV)], RT				
	Visual field	Posner orienting task, accuracy	Visual field effect [Left-Right], accuracy	.828			
	Shifting		Validity effect [Valid-Invalid], accuracy				
	Average		Overall performance, accuracy	-.41			
	Shifting		Disengage effect [(LI-LV)-(RI-RV)], acc	.361			
	Visual Field	BIT star cancellation	Center-of-cancellation, Left vs. Right	.749			
		Mesulam symbol cancellation	Center-of-cancellation, Left vs. Right	.607			
Memory	Spatial, recall	**BVMT**	Immediate Total Recall T-score		.687		
			Delayed Recall T-score		.805		
			Delayed Recall percent retained		.766		
	Spatial, recognition		Delayed Recognition Discrimination Index		.699		
	Verbal, recall	**HVLT**	Immediate Total Recall T-score			.733	
			Delayed Recall T-score			.929	
	Verbal, recognition		Delayed Recall percent retained			.897	
	Verbal, recognition		Delayed Recognition Discrimination Index			.710	
	Spatial, recall	**Spatial Span**	Span Forward		.689		
			Span Backwards		.808		
Language	Comprehension	BDAE: Comprehension	Basic Word Discrimination				.858
			Commands				.885
			Complex Ideational Material				.855
	production, semantic	BDAE: Expression	Boston Naming Short Form				.925
	comprehension	BDAE: Reading	Oral Reading of Sentences				.910
			Comprehension of Oral Reading of Sentences				.890
	production, phonological	Experimental measures	Nonword Reading				.825
			Stem Completion				.914
	production, semantic	Verbal Fluency	Animal Naming test				.804

B) Sensori-motor Domains	Function tested	Test	Score Recorded	L MOT	R MOT	L VIS	R VIS
Motor	Range of Motion	AROM: Shoulder flexion	Left Shoulder flexion	.947			
			Right Shoulder flexion		.893		
			Left Wrist Extension	.874			
			Right Wrist Extension		.837		
	Strength	Jamar Dynamometer	Left Grip strength	.782			
			Right Grip Strength		.742		
	Dexterity	Nine-hole peg test	Left hand pegs/second	.850			
			Right hand pegs/second		.825		
	Dexterity and Range of motion	ARAT	Left total	.952			
			Right total		.913		
	Walking	Timed Walk	Index of Timed Walk + FIM Walk Item	.681	.558		
		FIM Walk Item					
	Strength	Motricity Index	Left Lower Extremity total	.917			
			Right Lower Extremity total		.896		
	Range of Motion	AROM: Lower extremity	Left Ankle dorsiflexion	.921			
			Right Ankle dorsiflexion		.845		
Vision	Acuity	Computerized Perimetry	Left Upper Q pattern dev			.940	
			Left Lower Q pattern dev			.955	
			Left Upper Q total deviation			.884	
			Left Lower Q total deviation			.922	
			Left average pattern deviation			1	
			Right Upper Q pattern dev				.878
			Right Lower Q pattern dev				.873
			Right Upper Q total deviation				.807
			Right Lower Q total deviation				.814
			Right average pattern deviation				1

Supplementary Table 4-1. Factor score correlation with raw behavioral measures.
Domains of function, function tested, list of tests, score recorded, and correlation with the 8 behavioral factors. The table is divided in to **(A)** sensorimotor domains and **(B)** cognitive domains. The behavioral factors are referred to in the text by the following labels: ATTN = attention, VIS MEM = visuospatial memory, VER MEM = verbal memory, LAN = language, L MOT = left motor, R MOT = right motor, L VIS = left visual, R VIS = right visual.

5 The circuitry of abulia: insights from functional connectivity MRI

This chapter has been published as a journal article. The citation is:

Siegel, J.S., Snyder, A.Z., Metcalf, N.V., Fucetola, R.P., Hacker, C.D., Shimony, J.S., Shulman, G.L., Corbetta, M., 2014. The circuitry of abulia: Insights from functional connectivity MRI. NeuroImage: Clinical. 6, 320–326.

5.1 Abstract

Background: Functional imaging and lesion studies have associated willed behavior with the anterior cingulate cortex (ACC). Abulia is a syndrome characterized by apathy and deficiency of motivated behavior. Abulia is most frequently associated with ACC damage, but also occurs following damage to subcortical nuclei (striatum, globus pallidus, thalamic nuclei). We present resting state functional connectivity MRI (fcMRI) data from an individual who suffered a stroke leading to abulia. We hypothesized that, although structural imaging revealed no damage to the patient3s ACC, fcMRI would uncover aberrant function in this region and in the relevant cortical networks.

Methods: Resting state correlations in the patient3s gray matter were compared to those of age-matched controls. Using a novel method to identify abnormal patterns of functional connectivity in single subjects, we identified areas and networks with aberrant connectivity.

Results: Networks associated with memory (default mode network) and executive function (cingulo-opercular network) were abnormal. The patient's anterior cingulate was among the areas showing aberrant functional connectivity. In a rescan 3 years later, deficits remained stable and fcMRI findings were replicated.

Conclusions: These findings suggest that the aberrant functional connectivity mapping approach described may be useful for linking stroke symptoms to disrupted network connectivity.

5.2 Introduction

Historically, neurologists have struggled to reconcile the principle of functional localization and the observation that the relationship between behavioral deficits and anatomical damage is only partial. A more modern view is that functionality is represented in distributed functional systems and their internal connections. And a growing body of evidence demonstrates that remote dysfunction can occur in regions functionally connected to – but outside of – the area of lesion. Resting state functional connectivity magnetic resonance imaging (fcMRI) can measure widely distributed brain networks and offers a promising avenue of investigation into ways in which injury and disease affect the connectivity of the brain. Numerous studies have found a correspondence between behavioral measures and brain connectivity.(Vaidya and Gordon, 2013) Moreover, previous stroke research has shown that deficits within attention networks are predictive of spatial neglect and that deficits in motor networks are predictive of motor deficits.(Carter et al., 2010; He et al., 2007; van Meer et al., 2010a) In the present case study of a patient with abulia following stroke, we employ fcMRI to map functional abnormalities by comparison with age-matched controls.

Abulia is characterized by the lack of spontaneous, goal-directed behavior. Clinically, it falls between apathy and akinetic mutism on a continuum of disorders of drive and motivation.(Barris and Schuman, 1953) Abulia is most commonly associated with lesions of the anterior cingulate cortex (ACC).(Cohen et al., 1999) This association is consistent with neuroimaging evidence linking the ACC to the initiation of goal-directed behavior.(Carter et al., 1999) However, abulia

or some degree of apathy is also caused by subcortical lesions of the anterior thalamus, caudate nucleus, globus pallidus, and internal capsule (for a review of Abulia see Vijayaraghavan et al., 2002).(Ghoshal et al., 2011; Jorge et al., 2010; Vijayaraghavan et al., 2002) It is therefore likely that a more accurate functional localization of abulia, and related deficits of willed behavior, involves a network-level dysfunction. A number of networks (fronto-parietal, cingulo-opercular, ventral attention network) have been recently described in relation to executive control.(Corbetta et al., 2008; Dosenbach et al., 2007; Seeley et al., 2007; Vincent et al., 2008)

This report describes findings in a patient who developed abulia, anterograde amnesia, and left-sided weakness following multiple small embolic infarcts. The patient sustained small infarcts in various brain regions, but not the ACC. We investigated the neural correlates of abulia in this patient using fcMRI and a novel analytic strategy designed to identify atypical functional connectivity both at specific locations and across brain networks. The method compares observed functional connectivity in individuals against an aged-matched reference group. We hypothesized that this tool would identify atypical functionality in abulia-associated cortical areas that were structurally intact.

5.3 Case History

A 38-year-old right-handed male lawyer (CS02) presented in the emergency room in December of 2005 with febrile illness and progressive unresponsiveness. The patient was hypoxemic and in septic shock secondary to infectious endocarditis of the aortic and mitral valves. CT and MRI revealed multiple small embolic strokes as well as a left subdural hematoma. CS02 remained in a

vegetative state for several weeks. He underwent aortic and mitral valve replacement six weeks post-onset, and acute inpatient rehabilitation at the Rehabilitation Institute of St. Louis for about 3 weeks. He continued to show improvements in cognitive function over the subsequent three months. FLAIR MRI images taken about 3 months post-onset (Fig 2A) showed areas of hyper-intensity in the left hippocampal formation, anterior thalamus, and inferior parietal lobe. Other lesions were present in the right occipital lobe, bilateral basal ganglia, right motor cortex, and right cerebellum.

Subsequent evaluations indicated that the patient's residual deficits included abulia, anterograde amnesia, left motor weakness and left homonymous upper quadrantanopia. This clinical picture was stable from May, 2006 through the dates of functional imaging and neuropsychological assessment in October, 2009 and again in December 2012.

Before the illness, CS02 was a highly intelligent, successful district attorney, with an active social life. He was passionate about history, baseball, and was an excellent golfer. After his illness, he was unable to return to the practice of law or live independently. He currently lives with his parents, manages his own finances, and spends his time reading and watching television. He still enjoys playing golf and remains a skilled golfer. He likes to exercise and will participate in cardio-vascular training if brought to a gymnasium. He is well groomed and socially appropriate, but rarely speaks spontaneously. When addressed, he answers tersely and concretely. His emotional range is restricted with absent or minimal positive or negative affect. He will engage in a game of catch as long as balls are thrown to him. He retains an excellent

memory for past events, facts, and pictures, but he has trouble learning new verbal information. He retains an interest in baseball statistics, which he continues to acquire.

For the last seven years (2006-2013), CS02 has been seen twice a year in the Cognitive Neurology Clinic (Dr. Corbetta). CSO2 has been tried on multiple medications in isolation or combination including dopaminergic agonists (L-Dopa; amantadine); stimulants (methylphenidate; nicotine); a cholinergic agent (donezepil); and, a nootropic agent (piracetam) with no significant change in his behavior.

		Patient Score
Self-Rating	Apathy	68
	Disinhibition	58
	Executive Dysfunction	67
	Total Score	67
Family Rating	Apathy	110
	Disinhibition	55
	Executive Dysfunction	75
	Total Score	85
Executive Function	Animal Naming	21,33
	WISC-III Mazes	48
	Iowa Gambling Test	41
	D-KEFS Word Context	47
	D-KEFS Tower Test	37
	D-KEFS Letter Fluency	33
	Category Fluency	20
	Category Switching	27
Memory	BVMT Total Immediate Recall	53,55
	BVMT Learning	60,47
	BVMT Delayed Recall	61,57
	HVLT Learning	33,46
	HVLT Total Immediate Recall	32,29
	HVLT Delayed Recall	13,18
	HVLT Recognition Hits	-14,17
	Spatial Span Forward	44,49
	Spatial Span Backward	65,45
Motor	Grip Strength L hand (kg)	40,41
	Grip Strength R hand (kg)	56,46
	9-Hole Peg L (pegs/second)	28,21
	9-Hole Peg R (pegs/second)	63,61
	Motricity Index LEFT leg	-88,-97
	Motricity Index RIGHT leg	53,53
	combined index FIM Walk + Timed Walk	15,15
Language	Word comprehension	59,48
	Commands	53,53
	Complex ideational material	60,2
	Boston Naming Test	53,53
	Oral Reading of Sentences	57,57
	Comprehension of oral reading of sentences	53,15
	Nonword reading	57,57
	Stem completion	60,60
Attention	Mesulam Total misses	59,45
	Posner RT	56,55
	Posner accuracy	55,55
	Posner RT VF Effect	56,57
	Posner RT Validity Effect	65,67
Social Cognition	Affect Naming	50
	Prosody Comprehension	57
	Pairs Comprehension	50
	Faces Immediate Recognition	33
	Faces Delayed Recognition	43

Table 5-1. Neuropsychological Data.
Normalized scores are based on an age and demographic adjusted population with a mean of 50 and a standard deviation of 10. In rows in which two scores are given, the first is performance at scan 1 (2009) and the second is performance at scan 2 (2012). In all other rows, data were only available from 2012. Indices for which the patient fell outside the confidence interval of healthy controls are highlighted. D-KEFS = Delis-Kaplan Executive Function System; BVMT = brief visuospatial memory test; HVLT = Hopkins Verbal Learning Test

5.4 Methods

5.4.1 Subjects and MRI Acquisition and Preprocessing

CS02, and 23 control subjects within 10 years of age of the patient and without any neurological or psychiatric history were studied. All participants provided informed consent in accordance with the Declaration of Helsinki. All study procedures were approved by the Washington University School of Medicine (WUSM) Institutional Review Board. CS02, as well as 14 of the 23 control subjects, underwent a comprehensive neuropsychological and behavioral evaluation in the domains of language, memory, attention, and motor function at the time of the fMRI. CS02 additionally underwent campimetry to identify visual field cuts. All structural and resting state scans were acquired on a Siemens Tim-Trio 3T Scanner. Scanning parameters were identical for both of the patient's visits and for all controls. Following atlas transformation of all fMRI data, functional connectivity was assessed in CS02 and all controls within a mask that included gray matter voxels and excluded areas of lesion (see Supplementary Methods).

5.4.2 Aberrant Functional Connectivity

Aberrant Functional Connectivity (AFC) mapping is a novel approach that compares an individual (i.e., the patient) to healthy controls (see Supplemental Methods and Figure 1 for a detailed description of this approach). Voxel-wise correlation matrices were computed by

correlating the time series within each gray-matter voxel (excluding those lesioned in the patient) against all other gray-matter voxels. For each voxel in the patient, the correlation map was compared to that of each control subject using spatial correlation. This comparison generated a t-statistic map representing the degree to which the patient differed from the reference population. To evaluate statistical significance, the same analysis was performed on the controls, treating each of the control subjects as a surrogate patient. The resulting AFC maps were explored using a 1) seed-based analysis and 2) a network-based analysis. In both cases, a t-score threshold (t=4.8) was chosen to define 'AFC+' voxels based on significance after multiple comparisons correction (p=1.3e-6).

The Yeo 2011 seven-network cortical map was used to define networks.(Yeo et al., 2011) Six sub-networks were included: the default mode network (DMN), cingulo-opercular network (CON), motor network, dorsal attention network (DAN), fronto-parietal network (FPN), and visual network. The seventh network was excluded as it is comprised of ventral areas affected by susceptibility inhomogeneity artifact.(Ojemann et al., 1997) The AFC map was thresholded and voxels were tallied according to network affiliation. In the region-based analysis, a peak finding algorithm was applied to the AFC map to define spherical regions of interest (ROIs) that showed significant difference from controls (high AFC scores). ROIs were then used to generate correlation maps. Seed-based correlation maps enabled qualitative inspection of FC abnormalities.

A number of follow-up experiments were run to validate the AFC results. CS02 was brought back for additional functional imaging and neuropsychological testing evaluation 3 years after

the initial scan. After masking out non-brain and lesioned voxels, spatial correlation between pairs of AFC maps was computed. Both fcMRI scans were split in half and within-scan correlation (between AFC maps generated with data from halves of the scan) and between-scan (between AFC maps generated 3 years apart) correlations were computed. Additionally, A 2-flourodeoxy-D-glucose (FDG) positron emission tomography (PET) scan of CS02 was obtained using a Siemens EXACT 962 HR+ scanner while the patient was resting with his eyes closed.

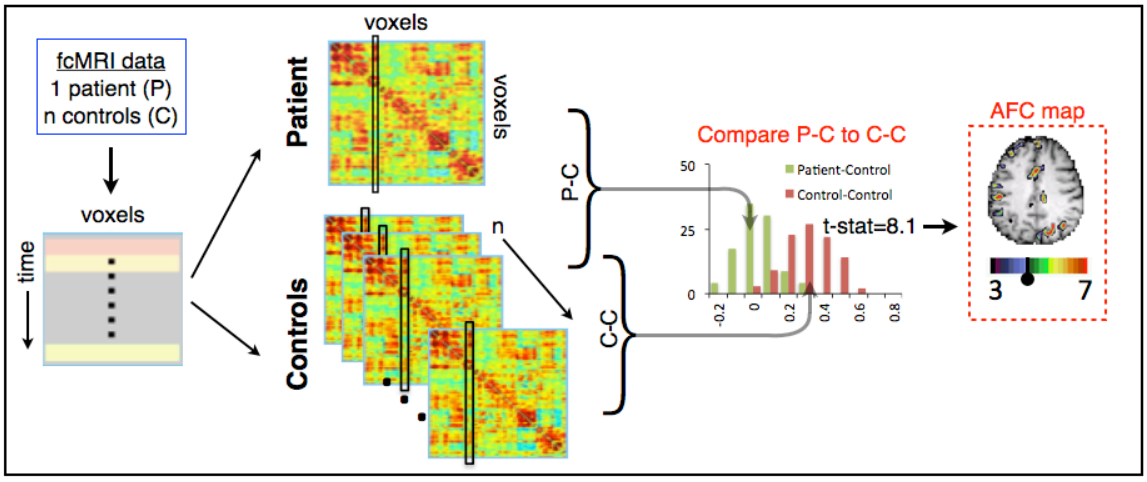

Figure 5-1. AFC Methodology Schematic.
fcMRI data are acquired, preprocessed, and registered to atlas space. For each subject, a correlation matrix is produced comparing every gray matter voxel to every other gray matter voxel . Each column of the matrix represents one voxel's full connectivity map. Next, every correlation matrix is compared to every other correlation matrix, column-by-column using spatial correlations, producing an (n+1)x(n+1) similarity matrix for each gray matter voxel. For each voxel, a Student t-test is computed to determine if 23 P-C similarity values (green) fell outside of the distribution of the n(n-1)/2 or 253 C-C similarity values (brown). Finally, the resultant image was overlaid on the patient's anatomical image, creating an Aberrant Functional Connectivity (AFC) map.

5.5 Results

5.5.1 Neuropsychological Evaluation identified Abulia and Anterograde Amnesia

The patient showed low scores on standardized measures of executive functions, as well as anterograde verbal memory and left-sided motor deficits (Table 1). The patient self-reported mild elevations in apathy and executive dysfunction, but collateral sources reported far more significant apathy. On the basis of these results and clinical evaluation, a diagnosis was made of abulia and moderate anterograde amnesia.

5.5.2 Aberrant Functional Connectivity (AFC)

Quality control metrics confirmed that atlas registration, fMRI signal properties, subject head motion, and brain-wide functional connectivity were within the range of the 23 controls (Table S1). The 'patient' correlation matrix was then compared to 'control' correlation matrices (Fig 1). The patient was individually compared to every control on a column-by-column basis using spatial correlation, thereby producing a patient-to-control (P-C) similarity image (1x34,428). The same comparison was computed between every pair of controls, producing $n \cdot (n-1)/2$ control-to-control C-C similarity images. For each of the 34,428 voxels, a Student t-test was computed comparing P-C values to C-C values. The t-test was chosen after both groups were shown to have normally distributed data (not shown). An image of t-scores throughout the brain could then be overlaid on the patient's anatomical image, creating an aberrant functional connectivity map

(AFC map). A t-score threshold (t=4.8) was chosen to define 'AFC+' voxels by calculating significance after multiple comparisons (p=1.3e-6).

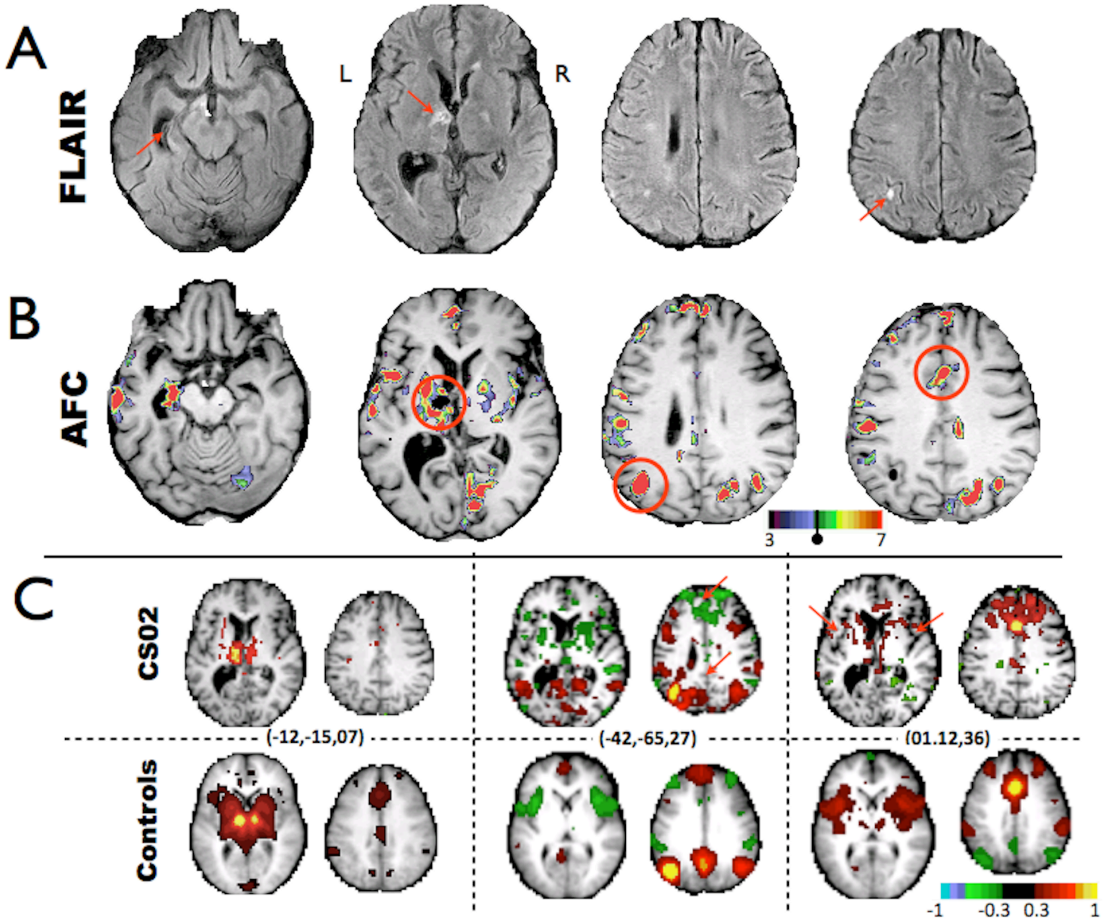

Figure 5-2. FLAIR, aberrant functional connectivity (AFC) map, and correlation maps demonstrate lesion-dysfunction relationship and functional connectivity changes.
A) FLAIR images with red arrows highlighting a lesion in the left anterior thalamus and micro-infarcts elsewhere. Atrophy of the left hippocampuis also evident. **B)** AFC map, produced using the aberrant functional connectivity method, demonstrates multiple foci of abnormality. Voxels masked out due to structural damage are shown in black (i.e. the left anterior thalamus). **C)** Correlations maps demonstrate aberrant functional connectivity. Peaks in the AFC map (circled in B) are used as seeds to generate whole-brain connectivity maps (no lesion mask) for the CS02 (top) and average connectivity maps for the 23 controls (bottom). Talairach coordinates for each correlation map are given in parenthesis. Left: a correlation map placed at the center of the lesion in controls illustrates ACC connectivity. CS02 demonstrates expected absence of functional connectivity. Middle and Right: Red arrows highlight areas of connectivity dropout in the patient.

Figure 2B shows the patient's AFC t-score map. Overall, the patient showed greater number of AFC+ voxels than 22 out of the 23 controls (Fig S1B). Areas of aberrant functional connectivity (AFC+) were observed near as well as distant to structural lesions. Regions showing aberrant functional connectivity included left hippocampus, left thalamus surrounding the thalamic lesion, left inferior parietal lobule, and anterior cingulate cortex.

5.5.3 Seed-based correlation mapping

A subset of AFC+ regions (red circles in Fig 2B) was selected to represent resting state networks that, in subsequent analyses, were shown to be especially aberrant in this patient. These regions were used to generate correlations maps to elucidate changes to functional connectivity patterns in AFC+ regions (Fig 2C). The left panel in figure 2C shows the correlation map corresponding to a seed in the lesioned left thalamus. The result obtained in the controls demonstrates functional connectivity with anterior cingulate cortex in addition to homotopic thalamus. By comparison, the result obtained in CS02 demonstrates expected absence of functional connectivity. The middle panel shows maps obtained with a seed in the inferior parietal lobule. Controls show a well-defined DMN including anticorrelations with the cingulo-opercular network (CON). CS02 shows a less well-defined DMN with abnormal anticorrelation between the IPL and the frontal pole. The right panel shows maps obtained with a seed in the ACC. Controls show a well-defined CON, with strong bilateral anterior insula functional connectivity with the dorsal ACC. None of these features are evident in CS02. Instead, CS02 shows diffuse connectivity with anterior portions of the frontal lobe. For comparison, some single control

subject correlation maps are shown in Figure S3. Figure S3 additionally shows connectivity from the AFC+ left anterior thalamus is disrupted for CS02 relative controls.

5.5.4 Network-based analysis

Distribution of AFC+ voxels across a seven network parcellations was assessed. Results were averaged between the patient's two visits and compared to averages across the 23 controls.(Yeo et al., 2011) When measured as percentage of network disrupted, the left default, bilateral cingulo-opercular, right motor network, and right visual network showed significant abnormality compared to controls (Fig 3). In controls, roughly 5% of voxels were above the AFC+ threshold. On average, these were evenly distributed across the resting state networks.

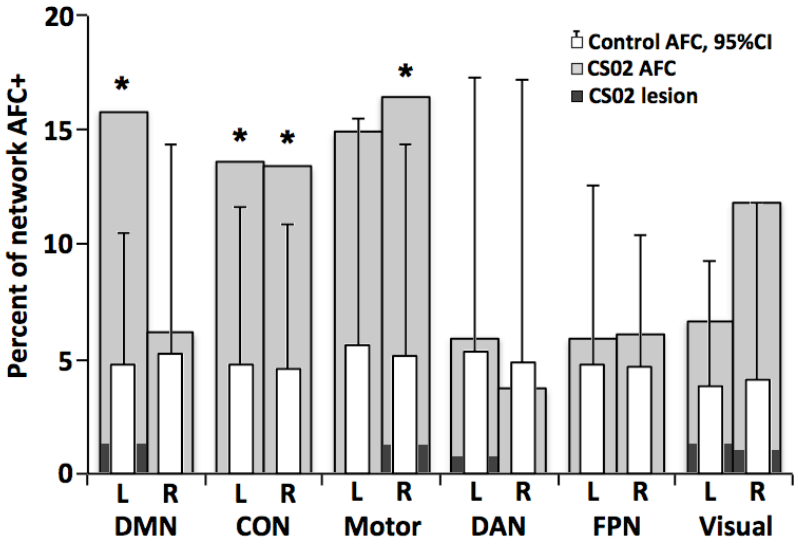

Figure 5-3. Left DMN, CON, and motor networks show the largest degree of disruption.
Voxels with significant AFC scores are classified based on the seven-network parcellation of Yeo *et al* 2011.(Yeo et al., 2011) Networks are additionally split by hemisphere (hemi-networks). In order to account for difference in network sizes, results are displayed as the percent of each network with AFC t-score greater than 4.8. Light gray bars display CS02 AFC results averaged over visits 1 and 2. White bars represent the network breakdown of aberrant functional connectivity in the 23 controls. Error lines represent upper 95% confidence intervals. Asterisks indicate hemi-networks in which CS02 shows disruption outside of the 95% CI of controls. The parcellation includes default mode network (DMN), cingulo-opercular network (CON), motor network, dorsal attention network

(DAN), fronto-parietal network (FPN), visual network. The total percent of AFC+ voxels in the patient and controls is shown in the far right.

5.5.5 Rescan and within-scan Validation

The within-scan spatial correlation was 0.81 and 0.80 for visits one and two respectively. The between-scan (3 years apart) spatial correlation was 0.60. Dominant patterns of aberrant functional connectivity remained qualitatively similar (Fig 4A). For comparison, spatial correlation between control subjects' AFC maps was measured. Spatial correlation between pairs of controls was 0.01 (s.d.=0.07), demonstrating that within-scan and between-scan correlation for CS02 is well above between-subject correlation (Fig 4B). These results show that AFC results in CS02 are consistent and reproducible.

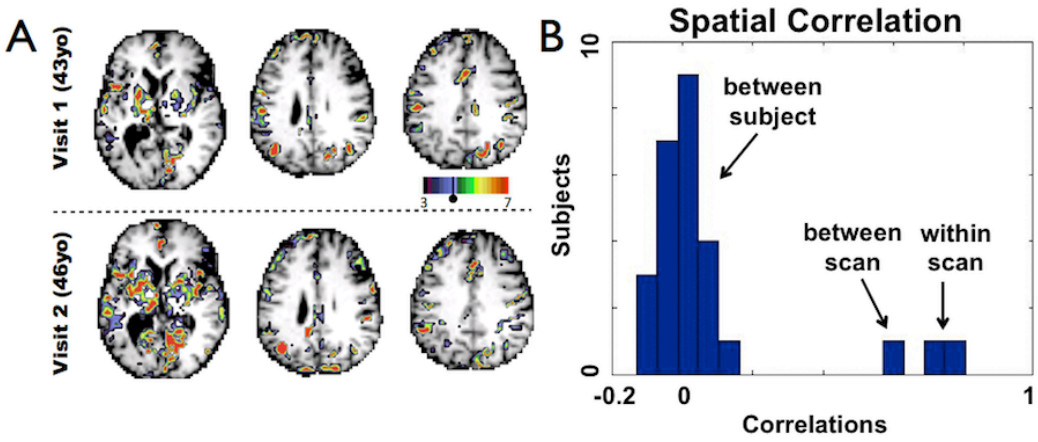

Figure 5-4. Reproducibility of AFC maps at 3 year follow up.
A) a visual comparison of AFC results from visit 1 and visit 2. The Pearson correlation between AFC maps is 0.5937. B) Pearson correlation for CS02 between AFC maps generated from half scans ('within scan') and AFC maps generated 3 years apart ('between scan') are shown and spatial correlation between different control subjects' AFC maps ('between subjects') is given as a control. Correlation between halves were 0.81 and 0.80 for visits 1 and 2 respectively.

AFC t-score distributions were generated for both scans of CS02 (Fig S1) and for controls. A t-test comparing rightward skewness between CS02 (both scans) and 23 controls yielded p=0.0565 (t=1.6579, df=23). This result means that the number of AFC+ voxels throughout the brain of CS02 was greater than that of controls, although the difference did not reach statistical significance.

5.5.6 Positron Emission Tomography

FDG PET scans were acquired to compare functional connectivity to metabolic activity (Fig. S2). No significant relationship between PET-FDG and AFC scores was observed (p-value=0.274).

5.6 Discussion

Abulia is most commonly associated with lesions of the anterior cingulate cortex (ACC), but has also been described in association with a variety of subcortical lesions.(Ghoshal et al., 2011; Jorge et al., 2010; Vijayaraghavan et al., 2002) These observations raise the question of whether common circuitry is disrupted by both types of lesion. It has been suggested that disconnections of limbic tracts projecting from the anterior thalamus to the cingulate might cause abulia.(Mega and Cohenour, 1997; Mega and Cummings, 1994) This is the first study to directly support this hypothesis. Our findings suggest that, even in the absence of cingulate damage, abulia with anterograde amnesia is associated with disruption of functional network organization including cingulate cortex. Furthermore, among the various recently proposed 'executive' networks(Corbetta et al., 2008; Dosenbach et al., 2007; Seeley et al., 2007; Vincent et al., 2008),

AFC identified the cingulo-opercular network as most closely affected in a case in which motivational behavior is severely disrupted.

5.6.1 Case summary – Links to behavior

CS02 sustained multiple embolic strokes that resulted in profound abulia, anterograde amnesia, left motor weakness, and left homonymous upper quadrantanopia. Some of these deficits could be explained in terms of focal damage (i.e., left hippocampal atrophy and anterograde amnesia). With respect to abulia the link was less clear . We speculate that the patient's neurologic status is better characterized by network-level disruption of functional organization, and not just for abulia. The association of right motor network AFC with left hemiparesis and of right visual network AFC with a left visual field cut seems apparent. The resting state network correlates of abulia and amnesia likely involve multiple networks and cannot be determined on the basis of a single case that is clinically complex. Possible implications of default mode network and cingulo-opercular network disruption are considered below.

Some AFC+ peaks were adjacent to structural lesions; but others, such as left Iateral posterior parietal cortex and dorsal ACC, were not. Elevated AFC scores could result from disconnection caused by damaged cortex or white matter tracts, but correlation maps from AFC peaks suggest that this is not the case. For example, functional connections between ACC and bilateral insula were disrupted despite absence of direct damage to ACC, insula, or the interconnecting white matter tracts. Similar considerations apply to inferior parietal lobule and ventromedial prefrontal cortex (Fig 2C).

5.6.2 Cingulo-opercular Network (CON)

The CON includes the anterior cingulate, bilateral anterior insula, and bilateral anterior thalami.(Corbetta et al., 2008; Dosenbach et al., 2007; Seeley et al., 2007; Vincent et al., 2008) This network is partially overlapping with other networks putatively related to executive control: fronto-parietal, ventral attention network, and salience network. The CON is implicated in task initiation, task switching, and conflict monitoring. FC strength between the ACC and the rest of the CON directly correlates with performance on a range of executive function tasks involving working memory, attention, inhibitory control, fluency, and task switching.(Onoda et al., 2012)

The anterior cingulate receives input from the anterior thalamus(PAPEZ JW, 1937) and has been associated with willed action across a variety of paradigms and a variety of imaging modalities.(Bush et al., 2000; Carter et al., 1999; Jahanshahi, 1998) Theoretical models of willed action have been formulated in terms of exploration of the environment(Swanson, 2000) and determining actions necessary to obtain desired goals.(Carter et al., 1999; Luu et al., 2003) A recent report in patients with implanted electrodes indicates that stimulation of dorsal ACC cortex leads to 'feelings of strong motivation and willingness'.(Parvizi et al., 2013) Our patient demonstrates the converse; functional disruption of the ACC has led to an amotivational state. Together, these findings highlight the critical role of the ACC, and CO network, in willed action.

5.6.3 Default Mode Network

The DMN is implicated in introspection, prospection, social cognition and memory (for a review see (Buckner et al., 2008). The hippocampus is functionally coupled within the DMN (Vincent et al., 2006), and DMN resting state functional connectivity has consistently shown association with memory encoding and recall (Sestieri et al., 2011). Changes to DMN functional connectivity have been observed in amnesic patients (Hayes et al., 2012) and reduced DMN connectivity has been reported in patients with memory-associated conditions such as Alzheimer's disease (Greicius et al., 2004). A prior study on a case of abulia and amnesia similarly found decreased ipsilateral default network connectivity (Jones et al., 2011). Interestingly, cases of left anterior thalamic lesions causing abulia appear to consistently show comorbid memory deficit (Nishio et al., 2011). Our interpretation is that disruption of DMN functional connectivity is related to the patient's anterograde amnesia. The patient's DMN AFC was lateralized to the left hemisphere. Correspondingly, CS02 exhibits a verbal memory deficit, but not a visuospatial memory deficit (Table 1) (Kelley et al., 1998).

5.6.4 Limitations and Conclusions

This paper demonstrates the use of fcMRI in an individual. Challenges to such an approach arise from normal individual variability in brain function and brain anatomy. But recent work has shown that reliable identification of resting state network topography within individuals is possible (Carl D Hacker et al., 2013; Mennes et al., 2010). To the extent that normality can be defined in resting state network terms, fcMRI can potentially offer a non-invasive tool for

identifying disruption to function and network structure. Not withstanding these advantages, a single case is insufficient to demonstrate a link between network dysfunction and clinical deficit.

Our approach was inspired by Stufflebeam *et al*.(Stufflebeam et al., 2011) who identified epileptogenic foci in individuals by comparing each voxel's local and global connectedness to that of controls. Although conceptually similar, our approach differs in that the spatial pattern of functional connectivity of a given region (functional connectivity 'fingerprint') is compared to controls. This strategy allows for the possibility that a region's functional connectivity fingerprint may be altered despite no change in sum connectedness. Further comparisons are needed to determine the extent to which 'aberrant' regions identified by these approaches differ.

The patient presented herein had multiple lesions and structural changes. Structural alterations make registration challenging. However, in our experience, adequate atlas transformation (misregistration < 2mm) is possible even in cases with large lesions provided that the lesion is segmented and masked out of the registration computations.(He et al., 2007) AFC+ regions (Fig. S2) had normal FDG PET scores, suggesting that these regions were in gray matter, and therefore, not identified as abnormal owing to misregistration.

Our patient's total AFC score fell within the tail of the control distribution (Fig S1B). However, we have not here demonstrated that this measure can reliably distinguish patients from controls. We attribute this limitation to the small sample size, limited signal to noise ratio of functional connectivity data, and natural variability within the population.(Mueller et al., 2013) A much larger subject sample would be needed to determine if the AFC approach can be used to differentiate affected individuals from the normal population. Future technical improvements in

resting state fMRI (Uğurbil et al., 2013) most likely will contribute to making the AFC approach more robust.

Nevertheless, our AFC technique reproducibly localized aberrant functional connectivity within an individual (Fig. 4). We believe that AFC has illuminated the pathophysiology of abulia in a patient without ACC structural damage. Moreover, our results illustrate the utility of functional imaging as a means of improving the understanding of neurologic deficits.

5.7 Acknowledgements

The authors disclose receipt of the following financial support for the research and/or authorship of this article: This study was supported by the National Institute of Health National Research Science Award 5T32GM007200-39, and National Institute of Mental Health 5R01HD061117-07 and the National Institute of Health Medical Scientist Training Award 5T32GM007200-40. Additional thanks to Lenny Ramsey, Jonathan Power, Gagan Wig, and Tim Laumann for guidance and code and Jennifer Rengachary for technical assistance (all in Washington University Department of Neurology).

Supplemental methods can be accessed at

www.sciencedirect.com/science/article/pii/S221315821400148X

5.8 Supplementary Figures and Tables

	Controls (SD)	Patient visit1, visit2
Age	44.8 (8.2)	43, 46
Atlas Registration	0.985(0.004)	0.984, 0.983
Framewise displacement	0.159 (0.036)	0.132, 0.126
DVAR (%)	2.14 (0.28)	2.26, 2.20
SD1	3.3(0.69)	3.0, 3.2
Frames	530(219)	603, 766
RMS Correlation	0.127(0.027)	0.089, 0.127

Table S1: Quality controls.
The Abulia patient falls within the normal range of controls for all quality control metrics tested. The atlas registration figure is the spatial correlation between the patients atlas-registered MP-RAGE and the atlas target image. Framewise displacement, DVAR, and SD1(Power et al., 2014) were calculated after high motion frames were removed.

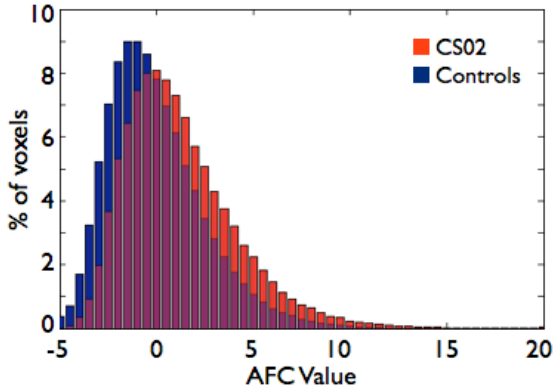

Figure S1: AFC t-value distribution in CS02 and in the 23 controls.
Both figure use CS02's AFC scores averaged between the initial scan and revisit. A) Negative values indicate the patient-control difference is less than the control-control difference and thus are essentially meaningless. Positive values above t=4.8 indicate voxels for which the patient-control difference is significantly greater than the control-control difference. As expected we see a skew to the right. A test that CS02's AFC distribution showed a greater degree of rightward skewness than controls trended towards significance (p=0.0565, df=23). B) Histogram of the total percent of voxels that surpass t=4.8 (indicated by the dashed line in A) in the 23 controls and in CS02 (red line). CS02 has a greater number of AFC+ voxels than 22 of the 23 controls.

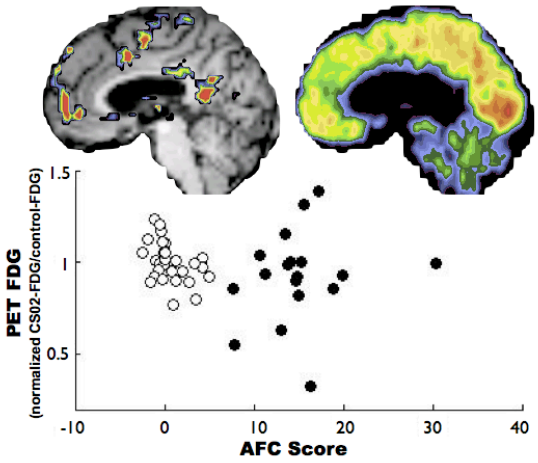

Figure S2. AFC scores did not correlate with regional glucose metabolism.
The open circles represent PET FDG values in CS02 in a set of canonical ROIs (Brier et al.,2012) excluding those overlapping structural lesions and positive AFC values. The PET FDG values have been normalized such that a value of 1 represents the mean in a separate cohort of 33 control subjects. The black circles represent 18 AFC peak ROIs. Note no correlation between increased AFC and glucose metabolism.

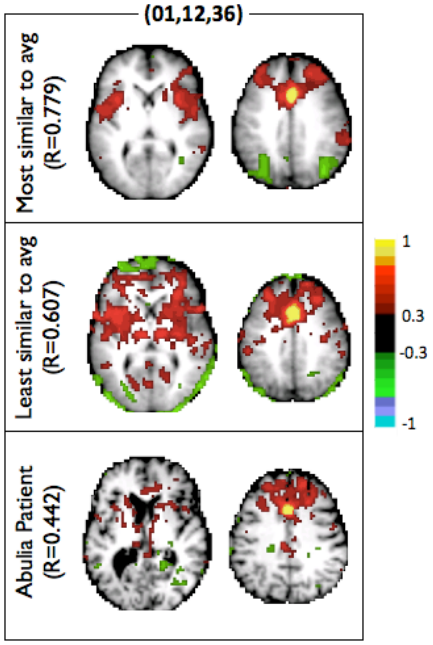

Figure S3: Individual correlation maps, obtained with the ACC seed used in the right panel of Figure 1C.
On top is the control subject closest to the mean, below is the control subject furthest from the mean, CS02 is on the bottom. CS02 falls outside the range defined by the control group.

6 Re-emergence of brain network modularity predicts stroke recovery

This chapter is currently under review as a journal article at Journal of Neuroscience.

Joshua S Siegel
Ben A. Seitzman
Lenny E. Ramsey
Evan M. Gordon
Mario Ortega
Nico U.F. Dosenbach
Steven E. Petersen
Gordon L. Shulman
Maurizio Corbetta

6.1 Abstract

Studies of stroke have identified local reorganization in perilesional tissue. However, because the brain is highly networked, strokes also broadly alter the brain's global network organization. Here, we assess network structure longitudinally in stroke patients, using resting state fMRI. The topology and boundaries of cortical regions remain unchanged across recovery. In contrast, the modularity of brain regions i.e. the degree of integration within and segregation between networks, was significantly reduced sub-acutely (n=107), but partially recovered by 3 months (n=85), and remains recovered by 1 year (n=67). Importantly, the return of modular network organization parallels recovery of language and attention, but not motor function. Finally, we explore individual subjects in depth using different tools for visualization of changes in brain connectivity over the course of recovery. This exploration provides more intuitive insights in to how changes in the brain's network organization can produce successful and unsuccessful recovery. In a patient with left temporo-parietal stroke and severe aphasia, acute loss of modularity reflected loss of association between frontal and temporo-parietal regions bi-hemispherically across multiple networks. These long distance connections then returned over time paralleling aphasia recovery. This work establishes the importance of normalization of large-scale modular brain systems in stroke recovery.

6.2 Introduction

The human brain is a collection of widely distributed cortical and sub-cortical systems that flexibly interact to enable cognitive function. The analysis of temporally correlated spontaneous activity, measured in the resting state with BOLD signal has emerged as a powerful tool for mapping brain network connectivity (Fox et al., 2005). R-fMRI studies have defined hierarchical and distributed brain networks (Power et al., 2011; Yeo et al., 2011) that correspond to the brain's functional domains (Bertolero et al., 2015; Smith et al., 2009). The spatial and temporal features of this organization appear to be optimized to support the segregation and integration of information (Petersen and Sporns, 2015).

A major goal in the study of stroke is to understand how stroke affects distributed brain networks. Although structural damage from stroke is focal, remote perturbations occur in regions of the brain distant from the area of damage (Carrera and Tononi, 2014). The set of regions that are directly damaged or indirectly affected is in turn embedded within a larger functional system that is in dynamic balance with other systems in the brain (Corbetta, 2012).

The healthy brain demonstrates integration within functional systems – measurable as highly correlated resting BOLD signal within systems – as well as segregation between systems – measurable as low correlation in resting BOLD signal across systems. This network property can be quantified with Modularity - a global network measure that compares the density of connections inside communities to the connections between communities (Newman, 2004).

Modular brain architecture is thought to enable efficient processing and flow of information (Bullmore and Sporns, 2009).

In contrast with the healthy brain, a common phenotype of stroke is a reduction of inter-hemispheric homotopic integration, and a reduction of within-hemisphere segregation between brain systems (Siegel et al., 2016). Both of these changes are consistent with a reduction in network modularity, which has been observed in stroke patients, even in the unaffected hemisphere (Gratton et al., 2012).

In the months following stroke, patients typically recover between 40-70% of initial clinical deficit (Lazar and Antoniello, 2008; Prabhakaran et al., 2007; Ramsey et al., n.d.). Evidence for functional remapping has been observed within a few millimeters of lesion boundaries (Murphy and Corbett, 2009; Nudo and Milliken, 1996). Normalization of connectivity with sites distant from the lesion has been observed in parallel with recovery (He et al., 2007; Lim et al., 2014; Ramsey et al., 2016; van Meer et al., 2010a). Little is known about how brain networks change on a larger spatial and temporal scale after stroke, and the behavioral relevance of both local and global changes remains unclear.

In the present work, we relate deficit and recovery following stroke to disruptions of the modular organization of brain systems. Specifically, we hypothesize that brain systems become less modular following stroke and that recovery of deficit can be predicted by the return of modularity. To test this, we follow a large prospective cohort of stroke patients over the course of deficit and chronic recovery – acquiring R-fMRI, and neuropsychological assessment at two weeks, three months, and one-year post-stroke.

6.3 Materials & Methods

6.3.1 Subject Enrollment

Written informed consent was obtained from all participants in accordance with the Declaration of Helsinki ND procedures established by the Washington University in Saint Louis Institutional Review Board. All participants were compensated for their time. All aspects of this study were approved by the Washington University School of Medicine (WUSM) Internal Review Board.

Subject enrollment and demographics are described in detail in (Corbetta et al., 2015). First time stroke patients with clinical evidence of motor, language, attention, visual, or memory deficits based on neurological examination were included. 132 patients met all inclusion criteria and completed the entire sub-acute protocol (mean age 52.8 years with range 22-77, 119 right handed, 63 female, 64 right hemisphere). Of those, 107 were included after all image processing and data quality exclusion criteria (Table 1).

Patients returned for a second timepoint at 3 months. At three month, 85 patients were included after all image processing and data quality exclusion criteria. Patients returned for a final timpeoint timepoint at 1 year. At one year, 67 patients were included after all image processing and data quality exclusion criteria. There was no difference in behavioral scores in any domains reported between those patients that returned for follow up at 1 year and those that did were lost to follow-up or data exclusion criteria (Language: $t_{(122)} = 1.18, p = 0.24$; Left Motor: $t_{(115)} = 1.00, p = 0.32$; Right Motor: $t_{(115)} = 0.40, p = 0.69$; Attention $t_{(99)} = –0.50, p = 0.62$)

Demographically matched controls (n = 31) were recruited and underwent the same behavioral and imaging exams. Controls were healthy adult matched to stroke study population by age, gender, handedness, and level of education. In total, 31 controls completed the entire sub-acute protocol (mean age 55.7 years (SD =11.5) with a range 21-83). Of those, 26 were included after all image processing and data quality exclusion criteria (Table 1).

6.3.2 Neuropsychological evaluation

All participants underwent a behavioral battery that included several assessments of motor, language, and attention following each scanning session. Imaging and behavioral testing session usually were performed on the same day. Scores were only recorded for tasks that subjects were able to complete. Dimensionality reduction was performed on the performance data using a factor analysis described in detail in Corbetta *et al*., 2015. As a results, the behavior measures used here represent multiple neuropsychological tests combined to generate more stable composite scores. For example, the language score was well aligned with measures of word comprehension (r = 0.858), complex ideational material (r = 0.885), and object naming (r = 0.925). The spatial attention score was well aligned with Mesulam center of cancellation (r = 0.749) and Posner task visual field effect (r = 0.828). The left motor score was well aligned with let shoulder flexion (r = 0.947), left hand 9-hole peg test (r = 0.850), and left lower extremity motricity index (r = .917). The right motor score was well aligned with right shoulder flexion (r = 0.893), right hand 9-hole peg test (r = 0.825), and right lower extremity motricity index (r = 0.896). For the complete list of tests used and correlations with the factor scores, see Corbetta et al., 2015.

Behavioral scores at chronic timepoints were calculated using the factors defined at the sub-acute timepoint. Recovery scores were calculated by first z-scoring behavioral factor scores relative to controls, and then determining the difference in z-normalized score between one year and two weeks. For example, patient 108 began with a language score 11.7SD below controls and had a language score 1.2SD below controls at one year, thus the recovery Δlanguage = 10.5.

6.3.3 Imaging

Patients were studied two weeks (mean = 13.4 days, SD=4.8 days), three months (mean = 112.5 days, SD=18.4 days), and one year (mean = 393.5 days, SD=55.1 days) after stroke onset. Controls were studied twice at an interval of 3-months. All imaging was performed using a Siemens 3T Tim-Trio scanner at the Washington University School of Medicine (WUSM) and the standard 12-channel head coil. The MRI protocol included structural, functional, pulsed arterial spin labeling (PASL) and diffusion tensor scans. Structural scans included: (1) a sagittal T1-weighted MP-RAGE (TR=1950 msec, TE=2.26 msec, flip angle=90°, voxel size=1.0×1.0×1.0 mm); (2) a transverse T2-weighted turbo spin-echo (TR=2500 msec, TE=435 msec, voxel-size=1.0×1.0×1.0mm); and (3) sagittal FLAIR (fluid attenuated inversion recovery) (TR=7500 msec, TE=326 msec, voxel-size=1.5×1.5×1.5mm). Resting state functional scans were acquired with a gradient echo EPI sequence (TR = 2000 msec, TE = 27 msec, 32 contiguous 4 mm slices, 4×4mm in-plane resolution) during which participants were instructed to fixate on a small cross in a low luminance environment. Six to eight resting state fMRI runs, each including 128 volumes (30 min total), were acquired. A camera fixated on the eyes was

used to determine when a subject's eyes were open or closed during scans. Patients had eyes open on 65.6+-31.9% of frames, and controls had eyes open on 76.8+-30.2% of frames ($t(114)=-1.7$, $p = 0.091$).

6.3.4 Lesion Masking

Lesions were manually segmented on individual structural MRI images (T1-weighted MP-RAGE, T2-weighted spin echo images, and FLAIR images obtained 1-3 weeks post-stroke) using the Analyze biomedical imaging software system (www.mayo.edu; Robb and Hanson, 1991). Two board-certified neurologists (Maurizio Corbetta and Alexandre Carter) reviewed all segmentations. In hemorrhagic strokes, edema was included in the lesion. A neurologist (MC) reviewed all segmentations a second time paying special attention to the borders of the lesions and degree of white matter disease. Atlas-registered segmented lesions ranged from $0.02cm^3$ to $82.97cm^3$ with a mean of $10.15cm^3$ ($SD=13.94cm^3$). Lesions were summed to display the number of patients with structural damage for each voxel (Fig 1A).

6.3.5 fMRI data preprocessing

Preprocessing of fMRI data included: 1) compensation for asynchronous slice acquisition using sinc interpolation; 2) elimination of odd/even slice intensity differences resulting from interleaved acquisition; 3) whole brain intensity normalization to achieve a mode value of 1000; 4) removal of distortion using synthetic field map estimation and spatial realignment within and across fMRI runs; 5) resampling to 3mm cubic voxels in atlas space including realignment and atlas transformation in one resampling step. Cross-modal (e.g., T2-weighted to T1-weighted)

image registration was accomplished by aligning image gradients. Cross-model image registration in patients was checked by comparing the optimized voxel similarity measure to the 97.5 percentile obtained in the control group. In some cases, structural images were substituted across sessions to improve the quality of registration.

6.3.6 Functional Connectivity Processing

Following cross-modal registration, data were passed through several additional preprocessing steps: (i) tissue-based regressors were computed based on freesurfer segmentation; (ii) removal by regression of the following sources of spurious variance: (a) six parameters obtained by rigid body correction of head motion, (b) the signal averaged over the whole brain, (c) signal from ventricles and CSF, and (d) signal from white matter; (ii) temporal filtering retaining frequencies in the 0.009–0.08-Hz band; and (iii) frame censoring. The first four frames of each BOLD run were excluded. Frame censoring was computed using framewise displacement with a threshold of 0.5 mm. This frame-censoring criterion was uniformly applied to all R-fMRI data (patients and controls) before functional connectivity computations.

FC quality-based exclusion criteria included 1) less than 180 usable frames after motion scrubbing, and 2) severe hemodynamic lags (greater than 1 second inter-hemispheric difference) measured from R-fMRI (Siegel et al., 2015). After motion and lag exclusion, 107 patients were included at two weeks, 85 patients at three months, 67 patients at 1 year, 26 controls at timepoint one, and 25 at timepoint two (Table 1).

6.3.7 Surface Processing

Surface generation and processing of functional data followed procedures similar to Glasser et al. (Glasser et al., 2013), with additional consideration for cortical segmentation in stroke patients. First, anatomical surfaces were generated for each subject's T1 MRI using FreeSurfer automated segmentation (B. Fischl et al., 1999). This included brain extraction, segmentation, generation of white matter and pial surface, inflation of the surfaces to a sphere, and surface shape-based spherical registration to the subjects "native" surface to the fs_average surface. Segmentations were manually checked for accuracy. For patients in whom the stroke disrupted automated segmentation, or registration, values within lesioned voxels were filled with normal atlas values prior to segmentation, and then masked immediately after (7 patients). The left and right hemispheres were then resampled to 164,000 vertices and registered to each other (Van Essen et al., 2001), and finally down-sampled to 10,242 vertices each (a combined total of 18,722 vertices after exclusion of medial wall) for projection of functional data.

Following preprocessing, BOLD data was sampled to each subject's individual surface (between white matter and pial surface) using a ribbon-constrained sampling available in Connectome Workbench. Voxels with a high coefficient of variation (0.5 standard deviations above the mean coefficient of variation of all voxels in a 5mm sigma Gaussian neighborhood) were excluded from volume to surface mapping (Glasser et al., 2013). Timecourses were then smoothed along the 10,242 vertex surface using a 3mm FWHM Gaussian kernel.

All brain surface visualizations were generated using Connectome Workbench (Marcus et al., 2013).

6.3.8 Gordon & Laumann Parcellation

We used a cortical surface parcellation generated by Gordon & Laumann and colleagues (Gordon et al., 2016) (Figure 1). The parcellation is based on R-fMRI boundary mapping and achieves full cortical coverage and optimal region homogeneity. The parcellation includes 324 regions of interest (159 left hemisphere,165 right hemisphere). The original parcellation includes 333 regions, and all regions less than 20 vertices (approx. 50mm^2) were excluded. Notably, the parcellation was generated on 120 young adults age 18-33 and is applied here to adults age 21-83.

To generate parcel-wise FC, timecourses of all vertices within a parcel were averaged. Functional connectivity (FC) was then computed between each parcel timeseries using Fisher z-transformed Pearson correlation. All vertices that fell within the lesion were masked out, and parcels with greater than 50% lesion overlap excluded from all analyses.

6.3.9 Parcel Homogeneity

Prior to homogeneity analysis, whole-brain connectivity was computed between every pair of vertices (18722x18722). Next, the following steps were taken to measure parcellation homogeneity. 1) for each parcel, a principal component analysis was run across the connectivity maps of all vertices belonging to that parcel. Parcels contained between 23 and 233 vertices -

each first principal component is a connectivity map that explains X% of variance across those vertices. 2) The percent of variance explained by the first principal component was used as a measure of parcel homogeneity. 3) This measured was averaged across all 324 brain parcels to produce a brain-wide measure of parcel homogeneity. 4) To compare this measure to a null distribution (Gordon et al., 2016), the parcellation was rotated randomly around the cortical surface (1,000 times for the group average FC homogeneity, 100 times for each individual subject). 5) Parcel homogeneity was re-assessed in the same manner using the randomly rotated parcels.

For the group analysis, parcel homogeneity was expressed as a p-value based on the number of null rotations with greater homogeneity than the real parcellation. For the individual subject analyses, parcel homogeneity was turned in to a z-score (difference from the mean of the null rotations divided by the standard deviation of the null rotations). Parcels overlapping with the lesion were excluded from the real and null homogeneity. Values were imputed for parcels overlapping the lesion, medial wall, and high susceptibility areas (those colored gray in Fig. 1B) after null rotations.

6.3.10 Modularity

Modularity (Newman's Q) was calculated using the equation given in (Newman, 2004)

$$Q = \sum_{\mu \in M} \left[e_{uu} - \left(\sum_{v \in M} e_{uv} \right)^2 \right] \quad (1)$$

where the network (including nodes and binary undirected links) is fully subdivided into a set of nonoverlapping modules M, and e_{uv} is the proportion of all links that connect nodes in module μ with nodes in module ν. Modules assignments were chosen a priori based on infomap community detection in healthy young adults (Gordon et al., 2016). Parcels with greater than 50% damage due to stroke were removed completely from networks prior to calculating modularity. Modularity was calculated at edge densities ranging from 4%-20%. This is the range between which modularity was found to be reduced in prior stroke FC analyses (Gratton et al., 2012).

We chose to assess modularity using a priori systems rather than systems defined individually using community detection for a number of reasons: 1) we would be measuring modularity in a community structure that has been optimized to increase modularity, thereby making Q a biased statistic, 2) the number of communities found by modularity optimization can vary, and 3) highly localized clusters may appear modular, though they may in reality be attributed to absence of synchronized BOLD fluctuations across distributed brain systems (and thus, predominance of distance dependent influences on the BOLD signal).

Modularity was found to correlate with magnitude of hemodynamic lags ($r = 0.374$, $p = 7 \times 10^{-5}$), number of frames remaining after scrubbing ($r = 0.316$, $p = 9 \times 10^{-4}$), and RMS head motion after scrubbing ($r = 0.279$, $p = 0.0036$). At each edge density, Modularity estimates from all subjects

at all timepoints were concatenated in to a single vector, and the three confounds were simultaneously regressed out. After confound regression, no significant association remained between any group and any confound measure at any edge density threshold.

Modularity was also measured within each hemisphere. Brainstem stroke patients were excluded from this analysis, and cerebellar strokes were flipped (i.e. for a right cerebellar stroke, the left cerebral cortex is ipsilesional). For comparison, control subject hemispheres were randomly labeled ipsilesional or contralesional.

To compare modularity with behavior measures, we first attained a single summary measure of modularity (across edge densities). Modularity values were normalized to average values in controls at each edge density (to have a mean of 1 and sd of .15), and then averaged across edge densities. Next, we modeled change in behavior and change in modularity in each patient. Because more stroke recovery is nonlinear, behavioral recovery was model in each subject using a log function (Suzuki et al., 2013):

$$Y = m * \log(t) + b \quad (2)$$

where t is time post-stroke in days (14, 90, 365) and Y is any of the four behavior scores (language, attention, left motor, right motor) at those timepoints. The slope m and intercept b were then solved using a least squares fit. A slope of modularity change was estimated in the same way (replace Y with modularity scores). Finally, the slopes for behavioral recovery in each domain were compared to the slope for modularity change using Pearson correaltion to

determine of the two were related. P-values were corrected for four comparisons (Benjamini and Hochberg, 1995).

6.3.11 Community Detection, Assignment, and Visualization

Community detection was accomplished using an implementation of the Louvain community detection algorithm (Blondel et al., 2008) accessed from the Brain Connectivity Toolbox (Rubinov and Sporns, 2010). This is an iterative algorithm that identifies the subdivision of the network into non-overlapping groups of nodes, which maximizes the number of within-group edges, and minimizes the number of between-group edges. For visualization, individuals Louvain-defined communities were assigned network labels (and thus colors) based on maximum similarity with the a priori communities. System-to-system assignment was accomplished using the Hungarian algorithm (Munkres, 1957). Sping-embedded graphs were generated using the Social Network Image Animator (SoNIA) software package (Bender-deMoll and McFarland, 2006).

6.4 Results

6.4.1 Functional brain areas defined in healthy young adults remain present across stroke and recovery

In this study we recruited 132 stroke patients with heterogeneous lesions (Fig. 1A) using MRI, R-fMRI and neuropsychological evaluation. After careful censoring for motion and hemodynamic lags, data at two weeks (n=107), thee months (n=85), and one year (n=67) were

investigated and compared to controls at two timepoints (n=26 & n=25). We first asked whether brain areas, areal boundaries, and community structure remain constant in stroke patients. Of note, these questions were posed with respect to gross changes occurring throughout the cortex and should be thought of as complementary to studies of remapping that have focused with high resolution on perilesional cortex. We applied a cortical parcellation developed on an independent sample of 120 healthy young adults (mean age 25, range 19-31) (Fig. 1B: Gordon et al., 2014) to R-fMRI data from 107 stroke patients (mean age 53, range 22-77) and 26 age-matched controls (mean age 56, range 21-83). To determine if the cortical parcellation could accurately define functional brain areas and areal boundaries in our patients and controls, parcel homogeneity was assessed (Gordon et al., 2016). Briefly, for a parcel, the brain-wide connectivity pattern of all vertices was entered in to a principal component analysis (PCA). Parcel homogeneity was determined as the percent of variance in connectivity across all vertices explained by the first principal component. Mean parcel homogeneity was determined by averaging homogeneity values across all parcels. To determine parcellation fit, real mean parcel homogeneity was compared to the mean homogeneity values from 1,000 randomly rotated null model parcellations.

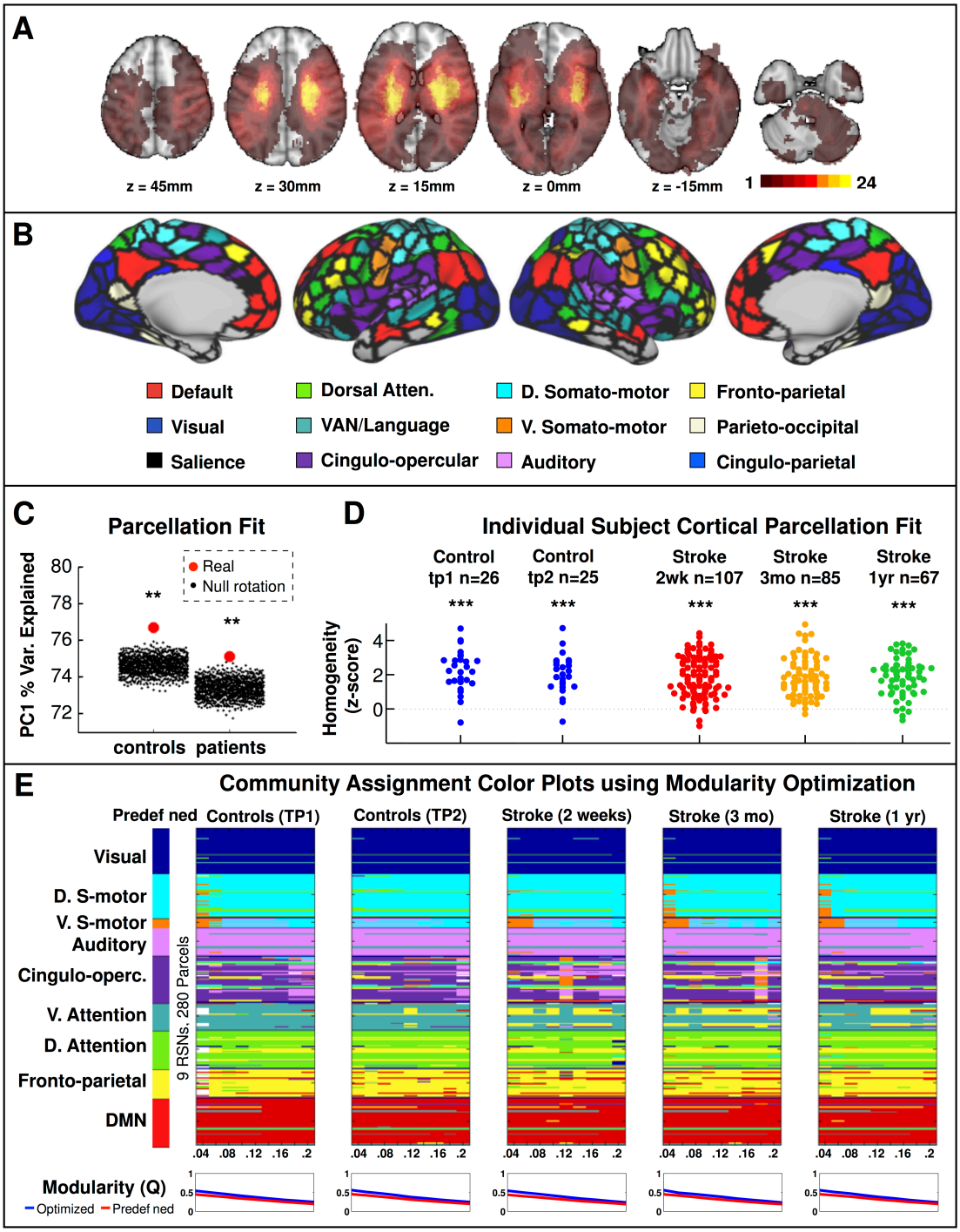

Figure 6-1. Functional brain areas and networks remain present across stages of stroke and recovery. A: Topography of stroke. Lesion overlay map in atlas space for 132 stroke patients. Lesion distribution is representative of a larger source population. B: 324 regions of interest parcellation from Gordon et al., 2016. Regions are color coded by RSN membership. C: Parcellation fit for group-averaged functional connectivity – average parcel homogeneity is shown in acute stroke patients and age-matched controls (red circles) compared to

1,000 null model iterations (black dots). In both groups the 324-region parcellation surpassed all 1,000 null models ($p<0.001$). A z-score can be generated by measuring the distance between real homogeneity and average null model in standard deviations. Group-averaged FC z-score is 4.86 in controls and 3.78 in patients. D: Z-scored parcellation homogeneity in individual subjects: patients (2 weeks, 3 months, 1 year) and controls (2 timepoints, 3 months apart). Difference between real homogeneity and 100 null model homogeneity is measured for each subject. E: Louvain modularity optimized community assignments. The leftmost column provides community assignment defined in healthy young adults with the Infomap algorithm by Gordon et al., 2016(Gordon et al., 2016). Here, unassigned parcels and communities with less than 7 parcels are excluded, resulting in 280 parcels. Louvain modularity optimization on group average FC matrices is shown for controls and patients in the community assignment color plots. In the community assignment color plots, each cell represents a specific parcel (280 parcels along the vertical dimension) at a specific tie density (2%-20% along the horizontal dimension). Parcels are ordered by predefined community membership, but colored by modularity-optimized community assignment (e.g. cells colored red have been assigned to the default mode network). The more similar that a color plot looks to the predefined network plot on the far left, the greater the consensus between predefined and optimized communities. Below each community assignment color plot is a plot of Newman's Q at every tie density for predefined (red) and optimized community assignments (blue).

Mean parcel homogeneity in age-matched controls was 76.7% and in sub-acute stroke patients was 75.1%. In both cohorts, the 324-region cortical parcellation yielded higher average parcel homogeneity than all 1,000 null rotations (Fig. 1C). These results indicate that cortical areas and the boundaries between areas remain largely constant in aging adults and even following stroke.

The same procedure was then conducted on individual subjects. Fig. 1D illustrates the relative homogeneity (average real homogeneity minus average null parcel homogeneity) for each subject at each timepoint. In all cohorts at all timepoints, parcel homogeneity was significantly greater than null. No significant difference was observed between groups or timepoints. Never-the-less, a correlation was observed lesion size and parcel homogeneity (Spearman's rho = -0.266, $p = 0.009$). Parcel homogeneity scores were similar between two weeks and three months in patients (Pearson's $r = 0.58$, $p = 2.9e\text{-}7$), and across timepoints in controls (Pearson's $r = 0.62$, $p = 0.002$).

From this set of analyses we concluded that the parcellation provides a reasonable representation of cortical areas in the majority of individual subjects, and that cortical areas remain largely stable over the course of stroke recovery.

Next, we assessed community structure (connectivity between parcels). The community structure described using the InfoMap algorithm in healthy young adults by (Gordon et al., 2016) is highly similar to structures defined here via unsupervised Louvain modularity optimization (Blondel et al., 2008) in patients and age-matched controls (Fig. 1E).

6.4.2 Modularity is reduced sub-acutely but returns in parallel with behavior

Having validated the use of the 324-region cortical parcellation, we next investigated our central question: how does network modularity change following stroke? Modularity is calculated on binary graphs (Fig. 2A), whereas functional connectivity values are continuous (z-transformed Pearson correlation coefficient). Thus, we thresholded each subject's connectivity matrix at a range of edge densities (between 4% and 20%), and calculated modularity (as defined in equation 1). Figure 2 B/C illustrates average modularity in controls and in stroke patients at 2 weeks, 3 months, and 1 year post-stroke (after controlling for subject motion and hemodynamic lags (Siegel et al., 2015)). As expected, we found that modularity in patients was significantly lower than controls two weeks after stroke (Fig. 2B), indicating a reduction in segregation of resting state networks. Over the course of stroke recovery, modularity increased towards the level of controls (Fig. 2C), with the majority of gains coming between two weeks and three

months (paired t-test; t(73) = -4.0, p = 6.3e-5) and no significant change between 3 months and one year (t(60) = -0.19, p = .43).

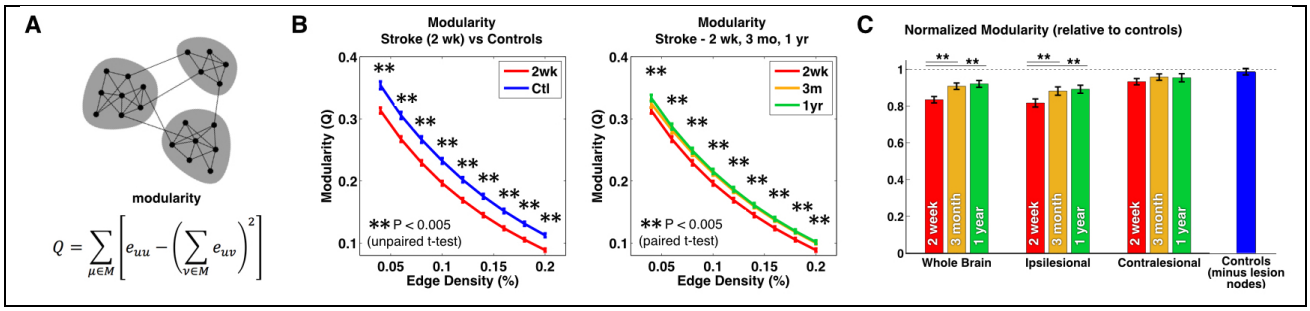

Figure 6-2. Behavior recovery following stroke is predicted by recovery of brain network modularity. **A:** Modularity measures the density of links inside communities compared to links between communities. Modularity is decreased in acute stroke patients **(B),** but returns to near control levels at 3 month and 1 year timepoints **(C). D:** Modularity, normalized to controls and averaged across densities (2-20%) is shown for the whole brain, ipsi-lesional, and contra-lesional hemisphere (compared to single hemisphere modularity in controls). ** indicates p < 0.005 (uncorrected) for an unpaired t-test between patients and controls in B and for a paired t-test between 2 weeks and 1 year for patients in C/D.

For all subsequent analyses, modularity values were normalized and then averaged across edge densities such that controls had a mean of 1 and standard deviation of 0.15.

We observed that ipsilesional and contralesional hemispheres showed an initial decrease in within-hemisphere modularity, but the decrease was larger in the ipsilesional hemisphere. Correspondingly, the ipsilesional hemisphere showed a significant increase by three months, while the contralesional hemisphere did not (Fig. 2D).

In patients, there was a significantly correlation between number of nodes damaged and modularity at two weeks (r = -.27, p = 0.0048), but not at three months (r = -.16, p = 0.15), or one year (r = -0.09, p = 0.47). To confirm that observed modularity decrease in stroke was not trivially caused by exclusion of lesioned nodes, we masked the same nodes in controls. Masking equivalent nodes did not significantly change modularity in controls (Fig. 2D). Neither did

number of nodes removed in controls correlate with modularity (r = 0.03, p = .73). Additionally, there was no significant correlation between percent of frames with eyes open and modularity in patients (r = 0.09, p = 0.42).Next, we hypothesized that return of modular network structure is related to recovery of function. To test this, we assessed function in four domains: 1) language – including both receptive and productive measures, 2) spatial attention – assessing visual attention to the contralesional hemifield, and 3/4) left/right motor – including a composite of upper and lower limb function. Consistent with prior reports (Lazar and Antoniello, 2008; Prabhakaran et al., 2007; Ramsey et al., n.d.), the majority of clinical recovery occurred in the first three months, with small additional improvement by 1 year (Fig. 2A).

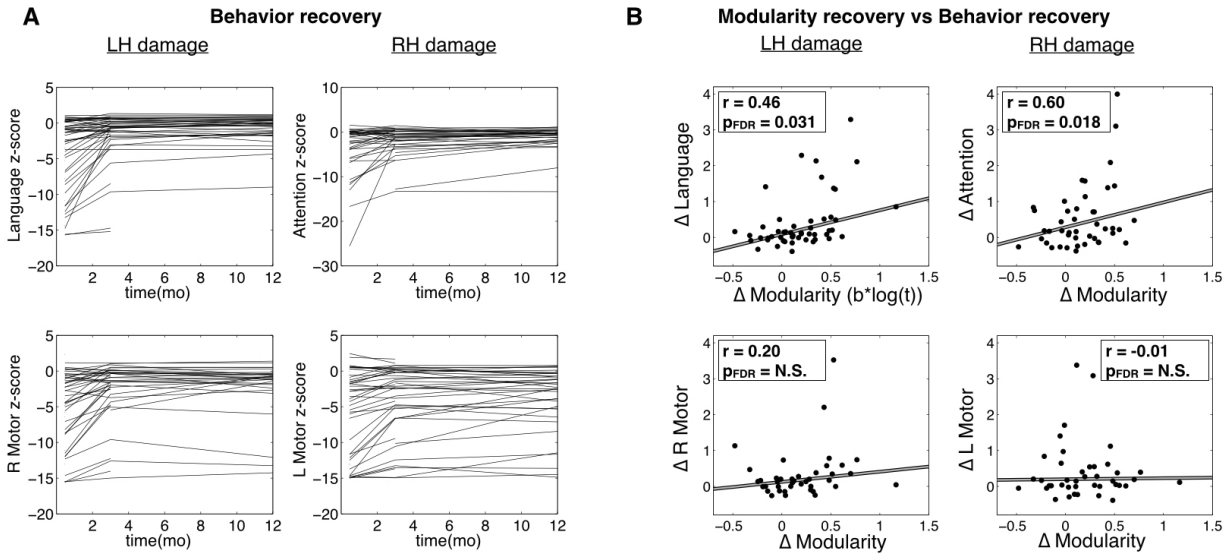

Figure 6-2. Recovery of modularity correlates with behavioral recovery by one year.
A: Behavioral scores (z-scored relative to age-matched controls) are plotted at 2 weeks, 3 months, and 1 year. For left hemisphere stroke patients, scores are shown for language and right (contralesional) motor function. For right hemisphere damage patients, scores are given for attention and left motor function. B: In left hemisphere stroke patients, recovery of network modularity in the first year predicts recovery of aphasia but not right motor function. In right hemisphere stroke patients, recovery of network modularity in the first year predicts recovery of spatial attention, but not left motor function.

To determine if a relationship was present between change in behavior and change in modularity, we first modeled each separately in each patient with a logarithm function (Eq. 2). We then compared the coefficients (i.e. rate of recovery) between modularity and behavior across subjects. Importantly, return of network modularity correlated with recovery of cognitive function by one year (Fig. 3B). In patients with right hemisphere lesions, change in modularity correlated with recovery of spatial attention ($r = 0.60$, $p_{corrected} = 0.018$, $n = 21$), but did not correlate with recovery of left motor deficit ($r = -0.01$, $p_{corrected} = 0.95$, $n = 24$). In patients with left hemisphere lesions, change in modularity correlated with recovery of aphasia ($r = 0.46$, $p_{corrected} = 0.031$, $n = 27$), but did not correlate with recovery of right motor deficit ($r = 0.20$, $p_{corrected} = 0.60$, $n = 19$). These results indicate that clinical recovery from stroke in adults parallels a return to the modular network structure of the healthy brain. Moreover, they suggest that higher cognitive functions such as attention and language are more dependent on segregation of processing across brain systems than is basic motor function.

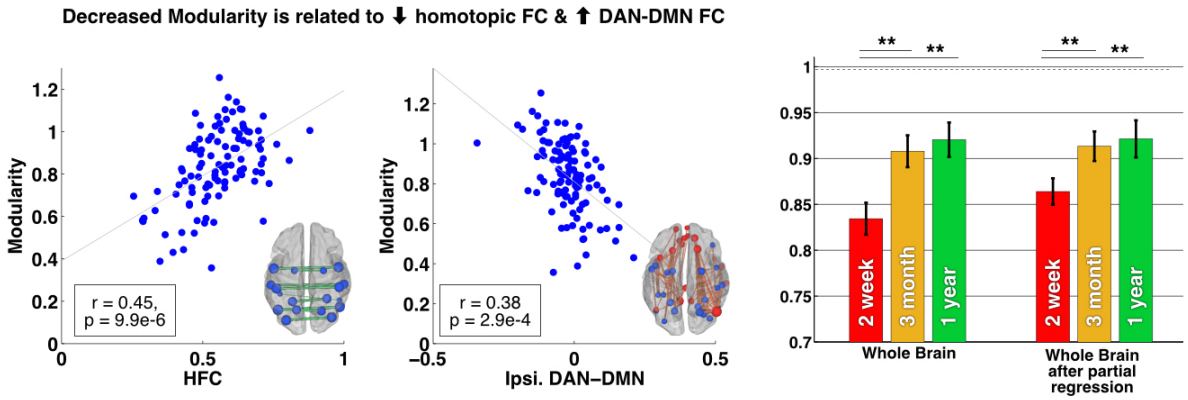

Figure 6-3. Modularity is related to interhemispheric integration and ipsilesional segregation.
A: The left scatter plot demonstrates the relationship between homotopic FC strength, averaged across the entire cerebral cortex, and modularity across all patients at 2 weeks ($r = 0.45$, $p - 9.9x10^{-6}$). The right scatter plot demonstrates the relationship ipsilesional DAN-DMN FC strength and modularity in all patients at 2 weeks ($r = -0.38$, $p = 2.9x10^{-4}$). The brain images next to each provide schematic visualizations of the type of connectivity tested.

B: A significant increase in modularity over time is still observed even after HFC and DAN-DMN FC are regressed from all data.

Previous work identified reduced homotopic integration and reduced within-hemisphere segregation as important and related phenotypes of stroke (Siegel et al., 2016). We conducted additional analyses to determine how the global measure of modularity relates to homotopic FC and ipsilesional DAN-DMN FC. We found that modularity in patients correlated with both homotopic connectivity ($r = 0.45$, $p - 9.9x10^{-6}$) and with ipsilesional DAN-DMN FC ($r = -0.38$, $p = 2.9x10^{-4}$) at 2 weeks. However, when both of these FC measures were regressed out from modularity in patients and controls, modularity still showed significant increase over time (Fig. 4).

6.4.3 Visualizing recovery of the brain graph in an aphasic case

Modularity is a brain-wide measure that cannot provide insight into what is happening at the level of individual brain areas or brain systems. Thus, to gain insight into how brain systems are changing as modularity returns, we investigated related measures in a series of three single case studies.

Patient 108 (P108) suffered a large stroke to the left parietal and temporal lobes (Fig. 5), resulting in severe acute aphasia, performing 11.7 standard deviations below control average. The patient recovered to 2.3 standard deviations below controls by 3 months, and showed a small additional improvement (to within 2 standard deviation) by 1 year post-stroke. The patient's modularity was 0.66 at 2 weeks (control mean=1, SD=0.15), and had returned to 1.00 by 3 months.

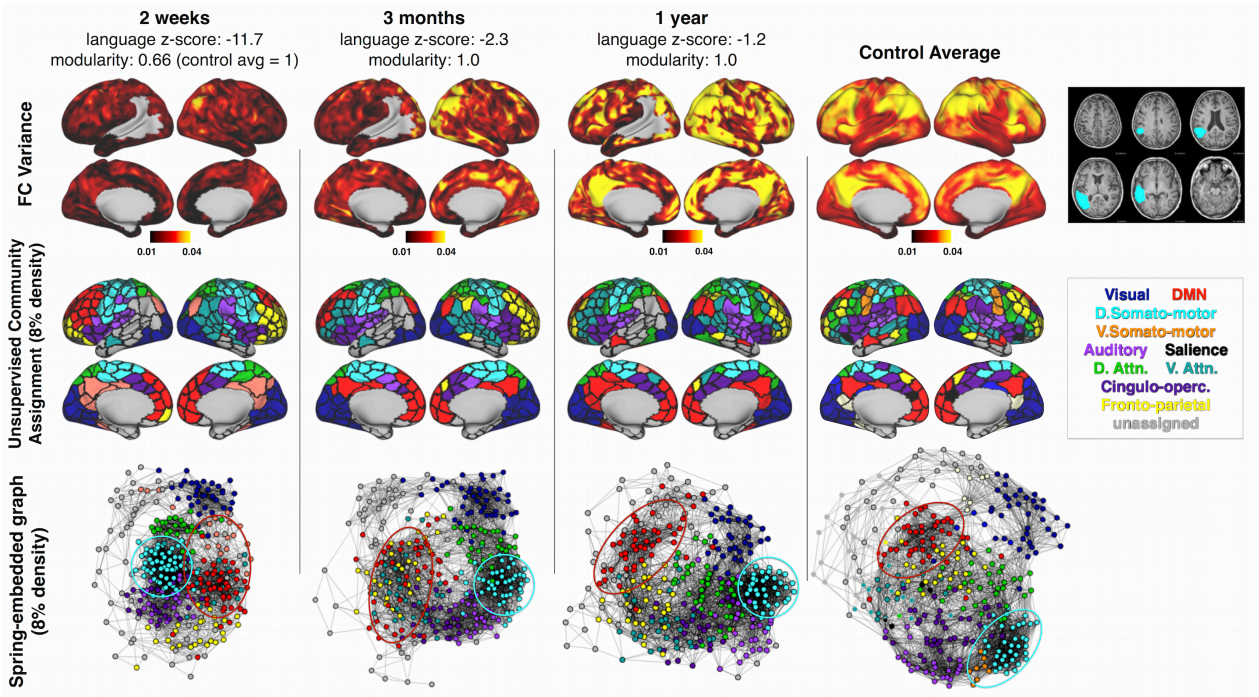

Figure 6-4. Case study of aphasic patient P108.
At two weeks post-stroke, language performance was 11.7 standard deviations below age-matched controls. This improved to 2.3 at 3 months and 1.2 at 1 year. Network visualizations are given at all three timepoints, with control averages shown in the right-most column for reference. **Top**: vertex-wise within hemisphere segregation, measured by FC variance across all within-hemisphere connections. **Middle**: unsupervised modularity-optimized community assignment for the 8% edge density threshold. The granularity of network communities increases with recovery. **Bottom**: Spring-embedded network representation at 8% edge density, based on modularity-defined communities (community colors are matched to figure 1). Note that the control average will look smoother than any individual subject. See Supplementary Fig. 9 for the same visualizations in a control with average modularity. Right: T1 and T2 MRIs. Red ovals highlight the stroke.

Figure 5 illustrates the re-emergence and re-segregation of functional brain systems over the course of recovery in P108 (relative to controls in the right column). The top row shows within-hemisphere variance in connectivity at each vertex (squared standard deviation of all within-hemisphere correlation coefficients greater than 20 mm from the seed). A normally functioning area will show strong positive FC within system and negative FC with other systems, resulting in higher FC variance (as is seen in the control average in the right column). Whereas, a

nonfunctional area should not show strong positive or negative correlations. Thus, FC variance reasonably assays segregation.

The middle row shows the results of unsupervised community detection using the Louvain algorithm. Community assignments are optimized for maximum modularity, and communities are colored based on maximal similarity with predefined communities (Munkres, 1957). At two weeks (Fig. 5, left column), brain systems appear highly localized. For example, the default mode system (red) is broken into an anterior and posterior component. Similarly, the fronto-parietal (yellow) and ventral attention networks are assigned to regions in temporal lobe and frontal lobe, respectively, but we do not see systems spanning lobes. By three months, the granularity of network communities in the intact cortex increases substantially, showing communication between frontal and parietal components restored in both the default mode network and control systems. The improvement is maintained at one year.

The bottom row shows the same community assignments, visualized as a spring-embedded graph. The spring-embedded graphs make it possible to visualize the 'distance' (in the graph-theoretical sense) between brain systems. At 2 weeks, systems that are normally highly segregated are clustered together (e.g. the somato-motor and default mode networks, indicated by cyan and red ovals, respectively). Over recovery, the somato-motor and default mode systems become more segregated (e.g. the distance between the cyan and red ovals increases over recovery, becoming more similar to controls). Together, the different visualizations in Figure 6 provide a picture of acute loss and chronic return of distributed and segregated brain systems in an individual brain.

In figures 6 and 7, the same visualizations are shown for two additional subjects. Patient P30 suffered a large MCA stroke to the insula, prefrontal cortex, and underlying white matter (Fig. 8). This patient showed severe left hemi-neglect, poor recovery by one year, and low modularity at all three timepoints (Fig. 6). Note that network assignments remain very similar to controls (Fig. 6, middle row), however, segregation between communities is substantially lower than controls (Fig. 6, bottom row), and remains low across timepoints, in parallel with the patients poor functional recovery.

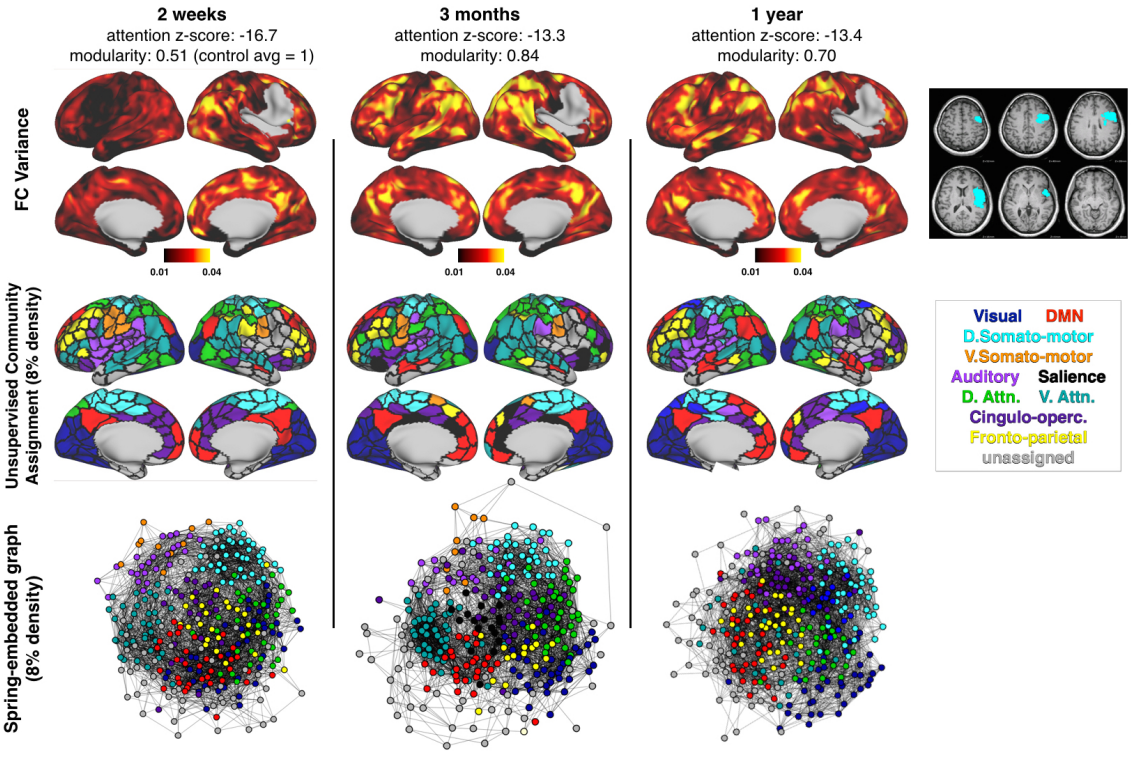

Figure 6-5 P30: Severe left hemi-neglect with poor recovery, low modularity throughout.
Results are generated and displayed as in Figure 6.

Patient P161 suffered a large MCA stroke in the caudate, putamen, and insula (Fig. 7). The patient exhibited severe left hemiparesis sub-acutely, but recovered substantially over time

(though remained 3.8SD below average). Despite this, the patient showed normal modularity at all timepoints. Modularity was not related to recovery in this patient because the deficits was in motor function rather than higher cognitive function.

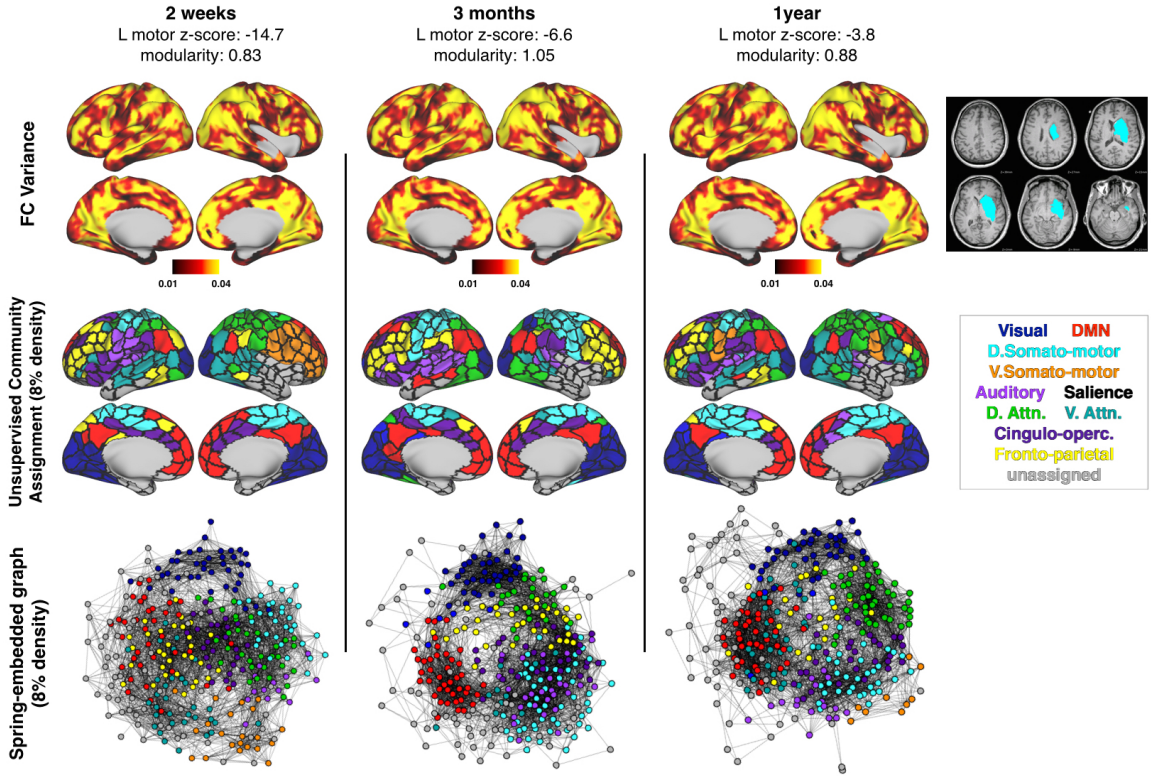

Figure 6-6. P161: Severe left hemiparesis with good recovery, minimal change in modularity by 1 year. Results are generated and displayed as in Figure 6.

6.5 Discussion

We assessed longitudinal changes in brain networks after stroke, using R-fMRI. We first established that the topology and boundaries of cortical regions remain unchanged across recovery. Next, we found that brain network modularity was significantly reduced sub-acutely,

but partially recovered over time. Reduced modularity reflects both reduced integration within functional brain systems, and reduced segregation between systems. Importantly, the return of modular network organization paralleled recovery of language and attention, but not motor function. This suggests that return of efficient processing and flow of information is critical to the return of higher cognitive function.

Remapping and reorganization have been demonstrated as a critical part of adult stroke recovery, but these processes are only observed within a few millimeters of lesion borders and the first month after stroke (Murphy and Corbett, 2009; Nudo and Milliken, 1996; Winship and Murphy, 2009). Our results argue that a normalization of balanced and modular brain systems is occurring over a much larger spatial and temporal scale. This is consistent with prior findings of acute decrease and chronic recovery of long-range interhemispheric connections in mice (van Meer et al., 2010a) and in humans (Ramsey et al., 2016) paralleling behavioral recovery. The principle of simultaneous local reorganization and global normalization is supported by mouse models of stroke in which neural activity was measured both globally and locally (1-2mm from the infarct) using optogenetic photostimulation (Lim et al., 2014). A global scaling (relative decrease) in connectivity occurred acutely, but recovered with time. Whereas, in perilesional tissue, non-uniform changes in connectivity were observed, consistent with remapping. These local and global observations likely reflect different processes occurring in the course of stroke recovery.

In the period following a stroke, molecular, cellular, and physiological changes occur not only in perilesional tissue, but throughout the brain (Carrera and Tononi, 2014; Feeney and Baron, 1986;

Murphy and Corbett, 2009). Thus, a variety of mechanisms (likely both neural and hemodynamic) converge to produce a disruption in the synchrony of infra-slow resting BOLD fluctuations across distributed brain systems. The more spatially constrained network structure shown sub-acutely in P108 may not reflect increased local communication (in the structural or informational sense), but rather an absence of synchronized BOLD fluctuations in distributed brain systems. A similar observation has been reported in correlation with data quality, so it is important to note that all data in this study was carefully censored for head motion (using both head motion and DVAR thresholds), tissue-based timecourse regression was applied, and potential confounds (FD, frames remaining, hemodynamic lag) were regressed from modularity at the group level. P108 showed low motion at all timepoints, but lowest sub-acutely (Table 1) – obviating head motion as an explanation for observed changes.

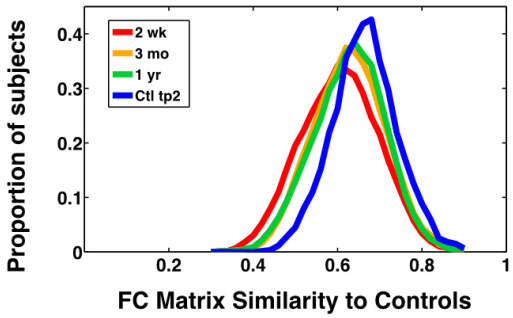

Figure 6-7. Group FC Similarity to controls.
Pearson correlation between all members of a given group and control at timepoint 1. The X-axis is correlation coefficient between pairs of FC matrices. This measure is computed by turning the 324-by-324 FC matrix in to a 52,326 vector for each subject. For a given group (i.e. patients at 2 weeks), a spatial correlation was computed between the FC vector of every subject and the FC vector of every subject in the control group. Each curve is a histogram of similarity values for one group. Similarity to controls increases between 2 weeks and 1 year post-stroke (paired t-test: $t = 3.9$, $p < 0.0001$).

In this work, we assess modularity relative to an *a priori* community structure defined in an independent group of young adults. An alternative approach would be to find community structure in each individual, and then measure modularity. However, such an approach would be less biologically valid and less interpretable for a number of reasons (see Methods: Modularity for a more lengthy consideration). Likewise, using an *a priori* community structure defined on our age-matched controls would bias controls towards greater modularity. An assumption of our approach is that community structure remains largely constant over the course of recovery. We validate this assumption by showing that, over recovery, patterns of brain connectivity become more similar to controls (Fig. 8).

A limitation of this work is that lesion and deficit were heterogeneous in our cohort. Thus, if multiple specific patterns of reorganization were present, these would have been overshadowed by the common trend of normalization. Animal models with controlled lesions (Watson et al., 1985) are better suited to studying reorganization, although specific interventions in commonly deficient human cohorts have also shown success (Liepert et al., 2000). An additional limitation is that the Newman's modularity is formulated for binary graphs. Thus, negative FC values are set to zero in binary matrices. The putative role that restoration of anti-correlations plays in recovery (Ramsey et al., 2016) may be downplayed by this approach.

Here, we followed a large cohort of stroke patients longitudinally over the course of deficit and recovery, measuring functional connectivity (using R-fMRI) and behavior. We observed that modular network structure was reduced after stroke, but recovered over time, in concert with behavioral recovery. Critically, our work suggests that the global normalization of network

structure predicts recovery of higher cognitive functions of language and attention, but not motor function. Future studies should therefore explore how rehabilitation strategies can target global brain systems. Moreover, further work will be needed to provide a more detailed picture of recovery within specific brain systems and cognitive domains.

6.6 Acknowledgment

We thank Timothy O. Laumann with assistance in implementation of the brain parcellation and surface analysis tools, Jonathan D. Power and Haoxin Sun for network visualization code, Alex Carter for advising and Nicholas V. Metcalf for data processing assistance.

6.7 Funding

This study was supported by, National Institute of Child Health and Human Development award (5R01HD061117 to M.C.), National Institute of Health Medical Scientist training award, and American Heart Association Predoctoral Fellowship Award (5T32GM007200-39 & 14PRE19610010 to J.S.S.).

		Timepoint 1	Timepoint 2
Controls	n	26	25
	Frames	571.4(210.0)	525.4(216.6)
	FD	.234(0.062)	.246(0.053)
	Lag	.191(0.046)	0.239(0.136)

Table 6-1A

		2 weeks	3 months	1 year
Patients	n	107	85	67
	Frames	596.0(209.6)	649.4(177.8)	632.9(177.8)
	FD	0.231(0.063)	0.224(0.057)	0.223(0.057)
	Lag	0.182(0.156)	0.291(0.156)	0.276(0.119)
Patient 108	Frames	737/896	644/896	637/896
	FD	0.2392	0.2495	0.2408
	Lag	0.1428	0.1448	0.1514

Table 6-1B

7 Further Discussion: Integrated hierarchical brain systems and human behavior

The contents of this chapter are not published elsewhere

7.1 Abstract

In this final chapter, we discuss how recent studies of brain-behavior relationships present new principles that can be incorporated in to the framework introduced at the end of chapter 1. Focal lesions, when examined at the population level, do not cause heterogeneous and unrelated symptoms, but instead produce clusters of correlated behavioral deficits that span neuropsychological tasks and behavioral domains. Correspondingly, the physiological disruption induced by stroke spans beyond the boundaries of the lesion, and even beyond the set of areas directly connected to the lesion, often producing global disruption to brain connectivity and network organization. These disruptions are low dimensional relative to the high variability of possible lesions. They frequently fall into canonical patterns of multi-nodal disruption – such as reduction in interhemispheric integration and brain network modularity. These observations are consistent with an integrated and hierarchical brain organization and these global disruptions appear to explain observed deficit. Here, we discuss principles of connectomics and information theory that unify recent observations on behavioral and connectivity deficits in stroke with advances in network models of the brain. We consider evidence linking brain function with behavior, and explore how connectomics principles can guide future studies.

7.2 Interdependent Behavior Deficits

Mounting evidence suggests that focal lesions, when examined at the population level do not cause isolated and heterogeneous symptoms, as suggested by traditional neurological models (see chapter 1), but instead produce a few clusters of correlated behavioral deficits both within and between domains of function. Importantly, these clusters account for the great majority (~70%) of variability across a large neuropsychological battery aimed at testing in depth multiple domains (motor, sensory, vision, language, attention, and memory). These clusters of deficits do not eliminate the possibility that pure behavioral syndromes may exist in a few selected cases, however, they indicate that behavioral impairment post-stroke is more accurately represented, certainly at the population level, by a few clusters of correlated deficits (Corbetta et al. 2015). These conclusions run counter to a long honored tradition in neuropsychology of double dissociations, but fit with more recent principles garnered from functional neuroimaging.

In the motor system, deficits of shoulder, arm, and hand functions are highly correlated across stroke patients with upper extremity impairment. A single component explains 85.7% of variance across 11 functional measures (Lang and Beebe, 2007). For instance, range of motion at the shoulder predicts hand function, even though these functions are supposedly mediated by different motor and premotor mechanisms. These findings are consistent with the emerging idea that cortex represent the most common components of natural movements, so called muscle synergies. Interesting synergies do not involve uniquely either proximal or distal upper extremity movements, but whatever combination of muscle activation that goes together during natural

movements. Interestingly, the space of muscle synergies is low dimensional, which solves a classic problem in motor control, i.e. how the brain independently control the high dimensional combination of torques, directions, and muscles that are necessary for any natural movement (Cheung et al., 2012, 2009; Howard et al., 2009; Ingram et al., 2008; Leo et al., 2016). Even though there are literally hundreds of possible hand finger combinations, it turns out that in natural conditions, two or three components explain nearly the entire variance of finger movements.

Clinical studies have adopted an easy to measure impairment scale to assess the effects of stroke. The NIH stroke scale (NIHSS) examines, at least at a cursory level, language, level of consciousness, and attention, even though it is heavily biased toward motor deficits that are the most common in stroke. Studies on the factor structure of the NIH Stroke Scale (NIHSS) (Lyden et al., 2004, 1999; Zandieh et al., 2012) indicate that with only two factors, one related to left hemisphere and one to right hemisphere damage, the majority of variability (~80-90%) in performance can be explained. This is surprising in relation to traditional neurological teaching about syndromes.

Our recent study shows that this simplified factor structure is not the result of poor sensitivity of the NIHSS in measuring cognitive impairment. We also found two mainly hemispheric factors, one loading on left motor/attention function, the other loading on right motor/attention function, but in addition identified a more cognitive factor which loaded on language and memory scores (Corbetta et al., 2015). Importantly, these clusters were similar in patients with cortical or

subcortical lesions, were largely independent of lesion size, and remained highly consistent across multiple timepoints (2 weeks, 3 months, 1 year) (Figure 1A-C).

It is our interpretation that this structure of behavioral impairment represents the abnormal output of a hierarchical brain organization, in which lesions in different locations lead to a simplified set of neural, hence behavioral, states. This idea is consistent with the demonstration of robust inter-dependencies between behavioral deficits. For instance, we have shown that in the course of recovery, deficits are not only consistently correlated between different domains, but that the degree of recovery can be predicted by specific across-domain relationships. Recovery from deficits of attention is worse in patients with acute deficits in motor, language, or spatial memory (Figure 1D). And conversely, patients with acute deficit in attention show worse recovery of language and spatial memory.

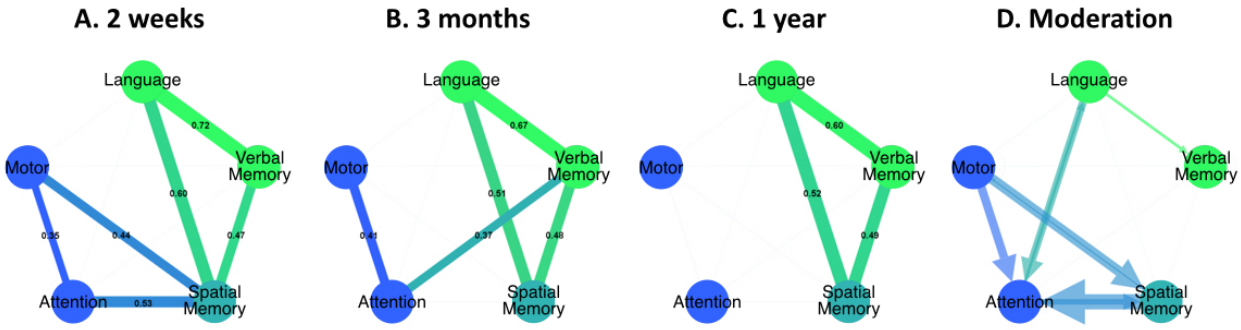

Figure 7-1. Behavioral clusters at 2 weeks, 3 months, 1 year, and moderation.
The correlations between the domains at 2 weeks (A), 3 months (B) and 1 year (C) and the moderation of 2 week deficit on recovery in a different domain (D). P<0.05, Bonferroni corrected.

These results are consistent with previous work showing inter-dependency of post-stroke deficits. In patients with unilateral spatial neglect, hence with visuospatial deficits, these deficits are made worse by deficits in sustained attention and working memory (Malhotra et al., 2005). Moreover, language problems in patients are increased when executive and working memory

deficits are present, which can disrupt a patient's ability to control lexical selection and to maintain phonological codes during sentence processing (Brownsett et al., 2014; Fillingham, Sage, & Lambon-Ralph, 2005; Francis, Clark, & Humphreys, 2003).

In a behavioral sense, correlation of performance between tasks can be explained by positing that many neuropsychological tests of behavior require the subject to perform a combination of cognitive operations. This can be thought of in two ways; first, that a cognitive component may be activated across a variety of mental operations (for example, the dorsal anterior cingulate from (Dosenbach et al., 2006)), and second, that a given task might activate numerous cognitive components (with the number of components varying depending on how simple or complex the task is). Work exploring intrinsic relationships between thousands of neuroimaging experiments has begun to model the complex relationships that exists between laboratory tasks and cognitive components (Yeo et al., 2015). It has been shown that a relatively small number of activation patterns are shared across many different behavioral conditions. We can think of this observation as 'cognitive synergies' akin to motor synergies in motor/premotor cortex.

The implications of this cognitive ontology for stroke is that damage to a single brain area will affect performance on numerous tasks. A study of 287 stroke patients modeled these complex relationships by studying performance on a broad range of cognitive tests (putatively targeting attention and executive functions, language, memory, praxis, motor function, affect, and number processing) from the Birmingham cognitive screen (Massa et al., 2015). When relationships between test scores were modeled, nominal assignment of specific tests to specific cognitive functions were largely invalid. For example, complex figure copying linked to tests of executive

function (such as rule finding and shifting), tests of attention (apple cancellation), tests of praxis (multi-step object use), language tests (sentence reading), and the Barthel index of activities of daily living and motor function. We argue that this interdependency of cognitive/behavioral deficits is not separable from the interdependent and hierarchical nature of brain systems.

To understand why some deficit are correlated, others localize to multiple locations, and still others cannot be localized at all, it is necessary to explore to network effects of stroke. We propose that such phenomena may best be understood as a consequence of focal injury to a hierarchically segregated and integrated brain network. In the next section, we explore this principle further with studies of brain connectivity after stroke.

7.3 Interdependent Functional Brain Systems

R-fMRI studies have defined spatially distributed brain systems (Doucet et al., 2011; Carl Hacker et al., 2013; Power et al., 2011; Yeo et al., 2011) that correspond to the brains functional domains (Bertolero et al., 2015; Smith et al., 2009). One key feature of functional brain system defined using R-fMRI is their modular but hierarchical organization (Doucet et al., 2011). At the highest level of brain organization, a division exists between the task-negative epi-system - primarily involved in memory of past events, visualization in future events, and conceptualization of the self – and the task-positive epi-system - primarily involved in the transient and sustained mental operations required to complete any external action or task. At a finer grain of detail, these epi-systems break in to specific brain systems – the task-negative epi-system containing the default mode network and fronto-parietal network, and the task-positive

epi-system containing sensory, motor, and attention systems. These systems break further in to sub-systems that exhibit repeating motifs of organization across the cortical surface (Power et al., 2011). These observations have cast prior studies localizing attention and hemispatial neglect in a new light (Fig. 2).

7.3.1 Lesions have widespread effects

A fundamental property of this organization is that a critical balance exists at each level of the hierarchy – disruption of one node has the potential not only to alter the function and the connection of distant nodes in that system but also to disrupt the balance between systems (Albert et al., 2000; Bullmore and Sporns, 2009). This has been illustrated by models of oscillatory cortical interactions derived from priors of structural connectivity (Alstott et al., 2009; Honey and Sporns, 2008). When lesions to different parts of the system were simulated, damage to central hubs produced widespread changes to network connectivity that extended beyond the functional system that was damaged and in some cases even to connections within the opposite hemisphere. The widespread effects of lesions on FC spanning numerous brain systems have since been borne out in real stroke data (Ovadia-Caro et al., 2013; Wang et al., 2014). And importantly, in controlled ablation experiments, modeled indirect network disruptions fit well with observed changes (Grayson et al., 2016).

A converse implication of these models is that damage to peripheral parts of the brain graph will have more constrained effects on the whole system. This bears out in a very interesting way when comparing damage and connectivity as correlates of behavior. Domain-general deficits and

deficits to higher associative functions such as learning and memory are predictable by large-scale distributed interactions between brain systems but only weakly related to damage in any particular location (Chapter 4, Figure 4-3). Whereas, sensory and motor deficits are strongly predicted by damage to a limited set of locations that are more peripheral in the overall brain graph (Power et al., 2011) and their associated input-output pathways in the white matter.

7.3.2 The relationships between FC and deficit

Evidence that the distributed network effects of lesions is relevant to behavioral deficits comes from recent studies comparing functional connectivity to behavior after stroke. Early stroke FC studies using small samples enabled the testing of more constrained hypotheses. For example, He and colleagues described how a relatively small cohort of 11 hemispatial neglect patients with heterogenous frontal/temporal/parietal lesions showed a common disruption in connectivity of the posterior inferior parietal sulcus that was predictive of acute severity and chronic recovery of neglect symptoms (He et al., 2007). When the study of FC-correlates of neglect expanded from n=11 to n=87 it became possible to examine the relationship between functional connectivity and neglect more broadly across the brain. This revealed a striking phenomenon – more than half of the cortical surface showed some alteration in it's pattern of connectivity that corresponded with severity of hemispatial neglect (Fig. 2F) (Baldassarre et al., 2014b). This included many brain areas and systems that are known to primarily support functions other than attention. Thus, the likely implication was that changes in attention systems were not functionally independent from changes in other brain systems. Concomitant changes occurred in attention networks, default

mode network and sensory-motor networks [as discussed previously, hemispatial neglect clusters with sustained attention, memory, and motor deficits].

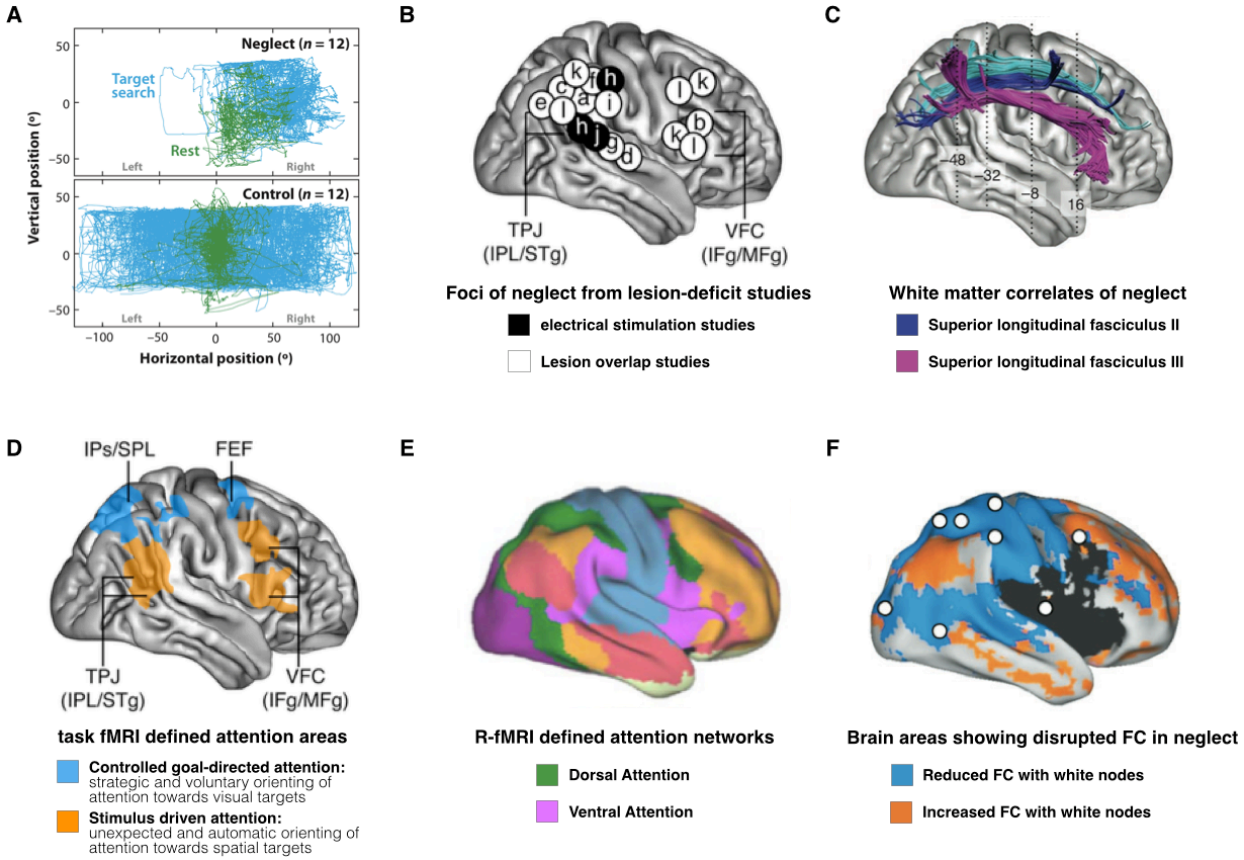

Figure 7-2. Structural and functional correlates of spatial bias in neglect patients.
A) Neglect is characterized in the laboratory by an ipsilesional gaze bias while searching for a target (Fruhmann Berger et al. 2008). B) Cortical areas associated with neglect in numerous studies (a) Vallar and Perani, 1986; b) Husain and Kennard, 1996; c) Leibovitch et al., 1998; d) Karnath et al, 2001; e) Mort et al., 2003; f) Doricchi and Tomaiuolo, 2003; g) Karnath et al., 2004; h) Thiebaut de Schotten et al., 2005; i) Corbetta et al ., 2005; j) Gharabaghi et al., 2006; k) Committeri et al., 2007; l) Verdon et al., 2010). C) White matter tracts associated with attention shifting and neglect. D) Dorsal and ventral attention areas described in Corbetta & Shulman 2003. E) Functional connectivity based whole brain parcellation from Yeo et al., 2011. F) Brain areas showing disruption FC in neglect patients compared to lesion-matched controls (Baldassarre et al., 2014).

This is not incompatible with evidence that the disruptive effects of a lesion are most pronounced in the brain system in which the lesion occurs (Nomura et al., 2010). In fact, because both functional brain systems and behavioral domains are interdependent, a reliable way to isolate

FC:behavior relationships is by comparing specific connections to specific behaviors across the population only after other connections and other behaviors have been covaried out. This approach was used to illustrate both the behavioral dissociation between motor and attention systems, but also their interdependence (Baldassarre et al., 2016). Thus, brain-wide patterns of abnormalities co-exist with more behaviorally specific patterns.

When FC-deficit relationships are compared across behavioral domains, another principle of connectomics emerges. Attention, spatial memory, verbal memory, language, motor and visual deficits were all best predicted by a decreased in connections between the hemispheres and an increase in connection strength (typically, a loss of anti-correlations) within a hemisphere (Chapter 4, Figure 4-4). Thus, a common correlate of behavioral deficits is reduction to homotopic integration and reduction in within-hemisphere segregation between normally dissociated networks. This same overall pattern of reduced homotopic integration and reduced within-hemisphere segregation predicted domain-general deficit.

Interestingly, transection of the corpus callosum has also been found to results in both an expected drop off in interhemispheric FC, but also an increase in within-hemisphere correlation in human (Johnston et al., 2008) and monkey studies (O'Reilly et al., 2013). This suggests that integration of RSNs across the hemispheres is linked to segregation of task-positive and task-negative RSNs within the hemispheres. The post-stroke reduction in integration and segregation can be thought of as resulting from a single disruptive process such as previously observed reductions in brain network modularity (Gratton et al., 2012).

In fact, the healthy brain's modular network organization appears to be critical for higher cognitive functions such as language and attention. Despite severe disruptions following stroke, the post-stroke brain is capable of returning to a state of modular organization in the course of recovery (Chapter 6). Research using calcium channel signaling in mice has been particularly important in demonstrating that widespread FC changes observed in humans likely reflect neural and not vascular disruption. Recently, neural activity following stroke was measured both globally and locally (1-2mm from the infarct) using optogenetic photostimulation (Lim et al., 2014). Lim and colleagues observed a global scaling (relative decrease) in connectivity acutely, that recovered with time.

One way to understand reduction in the modularity of the system is as a decrement in the variability of available neural states. In information theory, information capacity is the segregative ability of a system to encode distinct stimuli and can be measures as the range of distinct neural states available to the brain in response to different stimuli (Deco et al., 2015). A recent study used real data from stroke patients and controls to generate models of the brain network and then quantified information capacity by simulating thousands of different perturbations the network (Adhikari, under review). A significant decrease in information capacity was observed after stroke, and this decrease correlated with reductions in homotopic connectivity (in the real R-fMRI data) in multiple RSNs. If we think of the healthy brain as a set of networks that can flexibly interact to produce the tremendous range of behavioral responses, than a reduction in the variability of available neural states may explain the clustered deficit seen after stroke.

1.2 Limitations & Considerations

The hypothesis that clusters of correlated behavioral impairments in stroke reflect abnormal interactions at the neural level must be weighed against an alternative explanations for clustered structure - that behavioral covariance results from anatomical covariance caused by proximity or shared vascular supply of distinct brain areas. For instance, the left middle cerebral artery provides vascular supply to both Wernicke's area, and left central sulcus, thus occlusion of the MCA would produce apparently correlated language and right motor deficits. Thus, stroke is a crude tool for testing hypotheses about local computations. Even if a lesion is constrained to a single brain area, this problem might persist. Precise tools developed in the laboratory are sometimes able to differentiate modular units even within a brain area. For example, electrophysiology physiology studies within the frontal eye field (FEF) of the macaque suggest find that some cells in the FEF are active during saccades and a distinct but overlapping population of cells are involved in covert shifting of attention (Thompson et al., 2005).

In the case of subcortical and white matter lesions, this logic would also apply to distinct white matter tracts that pass in close proximity. In such cases, a relatively small area of ischemia is likely to affect multiple tracts. This principle likely further explains correlated deficit between behavioral domains (Corbetta 2015) and requires further exploration.

While anatomical proximity certainly must be considered, many of the behavioral relationships described are occurring between areas no obvious vascular overlap. For example, language and spatial memory deficits are correlated ($r = .59$), despite localizing to different hemispheres

(Corbetta et al., 2015). Moreover, the correlation of deficits is the same when a population of only subcortical lesions is compared to a population of only cortical lesions. But most importantly, this does not explain the above observations of distributed effects of stroke and the reproducible links between global connectivity changes and behavioral deficit.

Additionally, the contention may be raises that the famous case of bilateral temporal lobectomy, HM, indicates that the encoding of memories is localizable (Scoville and Milner, 1957). We do not dispute this. It is our view that medial temporal structures provide a critical input to cortical memory systems, but the results given in chapter 4 demonstrate that verbal and spatial memories performance (both encoding and retrieval) are better represented in the cerebral cortex by distributed connectivity rather than location. Even if all of the deficits explored in chapter 4 could be localized given precise enough lesions, this would not change the distinction that some were well predicted by distributed FC changes while others are not.

7.4 Conclusion

In chapter 1, we explored historical and more contemporary prospective on how behavior is represented in the brain. In the final chapter, we closed by reviewing how recent findings from stroke studies by our lab and others have led to new principles of behavioral representation. Principles of integration of brain organization described using resting fMRI [and the consequences of disrupting such a network] explain why behavioral deficits form reliable clusters across a stroke population. Differences in the centrality of networks in the brain graph explain why some deficits are highly localizable while others are best understood as disruptions

to multi-network synchrony. And principles of network modularity explain why common patterns reduced integration and segregation are seen across domains and systems. It is our hope that these principles of brain organization might be used, to built a new framework with which to understand behavioral variability in diseases, be they neurological, psychiatric, or developmental conditions, or genetic.

References

Adams, H.P., Bendixen, B.H., Kappelle, L.J., Biller, J., Love, B.B., Gordon, D.L., Marsh, E., 1993. Classification of subtype of acute ischemic stroke. Definitions for use in a multicenter clinical trial. TOAST. Trial of Org 10172 in Acute Stroke Treatment. Stroke 24, 35–41.

Adolphs, R., Tranel, D., Damasio, H., Damasio, A., 1994. Impaired recognition of emotion in facial expressions following bilateral damage to the human amygdala. Nature 372, 669–672. doi:10.1038/372669a0

Albert, N.B., Robertson, E.M., Miall, R.C., 2009. The Resting Human Brain and Motor Learning. Curr. Biol. 19, 1023–1027. doi:10.1016/j.cub.2009.04.028

Albert, R., Jeong, H., Barabási, A.-L., 2000. Error and attack tolerance of complex networks. Nature 406, 378–382. doi:10.1038/35019019

Alstott, J., Breakspear, M., Hagmann, P., Cammoun, L., Sporns, O., 2009. Modeling the impact of lesions in the human brain. PLoS Comput. Biol. 5, e1000408. doi:10.1371/journal.pcbi.1000408

Altamura, C., Reinhard, M., Vry, M.-S., Kaller, C.P., Hamzei, F., Vernieri, F., Rossini, P.M., Hetzel, A., Weiller, C., Saur, D., 2009. The longitudinal changes of BOLD response and cerebral hemodynamics from acute to subacute stroke. A fMRI and TCD study. BMC Neurosci. 10, 151. doi:10.1186/1471-2202-10-151

Amemiya, S., Kunimatsu, A., Saito, N., Ohtomo, K., 2013. Cerebral Hemodynamic Impairment: Assessment with Resting-State Functional MR Imaging. Radiology 130982. doi:10.1148/radiol.13130982

Amemiya, S., Kunimatsu, A., Saito, N., Ohtomo, K., 2012. Impaired hemodynamic response in the ischemic brain assessed with BOLD fMRI. NeuroImage 61, 579–590. doi:10.1016/j.neuroimage.2012.04.001

Andersson, J.L., Jenkinson, M., Smith, S., 2007. Non-linear optimisation. FMRIB technical report TR07JA1. Univ. Oxf. FMRIB Cent. Oxf. UK.

Arbeláez, A.M., Su, Y., Thomas, J.B., Hauch, A.C., Hershey, T., Ances, B.M., 2013. Comparison of Regional Cerebral Blood Flow Responses to Hypoglycemia Using Pulsed Arterial Spin Labeling and Positron Emission Tomography. PLoS ONE 8, e60085. doi:10.1371/journal.pone.0060085

Attwell, D., Buchan, A.M., Charpak, S., Lauritzen, M., MacVicar, B.A., Newman, E.A., 2010. Glial and neuronal control of brain blood flow. Nature 468, 232–243. doi:10.1038/nature09613

Baldassarre, A., Lewis, C.M., Committeri, G., Snyder, A.Z., Romani, G.L., Corbetta, M., 2012. Individual variability in functional connectivity predicts performance of a perceptual task. Proc. Natl. Acad. Sci. 109, 3516–3521. doi:10.1073/pnas.1113148109

Baldassarre, A., Ramsey, L., Hacker, C.L., Callejas, A., Astafiev, S.V., Metcalf, N.V., Zinn, K., Rengachary, J., Snyder, A.Z., Carter, A.R., Shulman, G.L., Corbetta, M., 2014a. Large-scale changes in network interactions as a physiological signature of spatial neglect. Brain awu297. doi:10.1093/brain/awu297

Baldassarre, A., Ramsey, L., Hacker, C.L., Callejas, A., Astafiev, S.V., Metcalf, N.V., Zinn, K., Rengachary, J., Snyder, A.Z., Carter, A.R., Shulman, G.L., Corbetta, M., 2014b. Large-scale changes in network interactions as a physiological signature of spatial neglect. Brain 137, 3267–3283. doi:10.1093/brain/awu297

Baldassarre, A., Ramsey, L., Hacker, C.L., Callejas, A., Astafiev, S.V., Metcalf, N.V., Zinn, K., Rengachary, J., Snyder, A.Z., Carter, A.R., Shulman, G.L., Corbetta, M., 2014c. Large-scale changes in network interactions as a physiological signature of spatial neglect. Brain awu297. doi:10.1093/brain/awu297

Baldassarre, A., Ramsey, L., Rengachary, J., Zinn, K., Siegel, J.S., Metcalf, N.V., Strube, M.J., Snyder, A.Z., Corbetta, M., Shulman, G.L., 2016. Dissociated functional connectivity profiles for motor and attention deficits in acute right-hemisphere stroke. Brain aww107. doi:10.1093/brain/aww107

Baldassarre, A., Ramsey, L., Rengachary, J., Zinn, K., Siegel, J.S., Strube, M., Corbetta, M., Shulman, G.L., n.d. Dissociated functional connectivity profiles for motor and attention deficits in acute right-hemisphere stroke. Brain In Press.

Barris, R.W., Schuman, H.R., 1953. Bilateral anterior cingulate gyrus lesions. Syndrome of the anterior cingulate gyri. Neurology 3, 44–52.

Bastian, M., Heymann, S., Jacomy, M., others, 2009. Gephi: an open source software for exploring and manipulating networks. ICWSM 8, 361–362.

Bates, E., Wilson, S.M., Saygin, A.P., Dick, F., Sereno, M.I., Knight, R.T., Dronkers, N.F., 2003. Voxel-based lesion–symptom mapping. Nat. Neurosci. 6, 448–450. doi:10.1038/nn1050

Bauer, A.Q., Kraft, A.W., Wright, P.W., Snyder, A.Z., Lee, J.-M., Culver, J.P., 2014. Optical imaging of disrupted functional connectivity following ischemic stroke in mice. NeuroImage. doi:10.1016/j.neuroimage.2014.05.051

Behzadi, Y., Restom, K., Liau, J., Liu, T.T., 2007. A component based noise correction method (CompCor) for BOLD and perfusion based fMRI. NeuroImage 37, 90–101. doi:10.1016/j.neuroimage.2007.04.042

Belliveau, J.W., Kennedy, D.N., McKinstry, R.C., Buchbinder, B.R., Weisskoff, R.M., Cohen, M.S., Vevea, J.M., Brady, T.J., Rosen, B.R., 1991. Functional mapping of the human visual cortex by magnetic resonance imaging. Science 254, 716–719. doi:10.1126/science.1948051

Bender-deMoll, S., McFarland, D.A., 2006. The art and science of dynamic network visualization. J. Soc. Struct. 7, 1–38.

Benjamini, Y., Hochberg, Y., 1995. Controlling the False Discovery Rate: A Practical and Powerful Approach to Multiple Testing. J. R. Stat. Soc. Ser. B Methodol. 57, 289–300.

Bertolero, M.A., Yeo, B.T.T., D'Esposito, M., 2015. The modular and integrative functional architecture of the human brain. Proc. Natl. Acad. Sci. 112, E6798–E6807. doi:10.1073/pnas.1510619112

Beume, L.-A., Martin, M., Kaller, C.P., Klöppel, S., Schmidt, C.S.M., Urbach, H., Egger, K., Rijntjes, M., Weiller, C., Umarova, R.M., 2016. Visual neglect after left-hemispheric lesions: a voxel-based lesion–symptom mapping study in 121 acute stroke patients. Exp. Brain Res. 1–13. doi:10.1007/s00221-016-4771-9

Blanke, O., Landis, T., Spinelli, L., Seeck, M., 2004. Out- of- body experience and autoscopy of neurological origin. Brain 127, 243–258. doi:10.1093/brain/awh040

Blicher, J.U., Stagg, C.J., O'Shea, J., Østergaard, L., MacIntosh, B.J., Johansen-Berg, H., Jezzard, P., Donahue, M.J., 2012. Visualization of Altered Neurovascular Coupling in Chronic Stroke Patients using Multimodal Functional MRI. J. Cereb. Blood Flow Metab. 32, 2044–2054. doi:10.1038/jcbfm.2012.105

Blondel, V.D., Guillaume, J.-L., Lambiotte, R., Lefebvre, E., 2008. Fast unfolding of communities in large networks. J. Stat. Mech. Theory Exp. 2008, P10008. doi:10.1088/1742-5468/2008/10/P10008

Boes, A.D., Prasad, S., Liu, H., Liu, Q., Pascual-Leone, A., Caviness, V.S., Fox, M.D., 2015. Network localization of neurological symptoms from focal brain lesions. Brain awv228. doi:10.1093/brain/awv228

Bonakdarpour, B., Parrish, T.B., Thompson, C.K., 2007. Hemodynamic response function in patients with stroke-induced aphasia: Implications for fMRI data analysis. NeuroImage 36, 322–331. doi:10.1016/j.neuroimage.2007.02.035

Brain, W.R., 1941. Visual orientation with special reference to lesions of the right cerebral hemisphere. Brain J. Neurol. 64, 244–272. doi:10.1093/brain/64.4.244

Broca, P., 1861. Remarks on the seat of the faculty of articulated language, following an observation of aphemia (loss of speech). Bull. Société Anat. 330–357.

Brodmann, K., 1909. Comparative Localization Studies in the Brain Cortex, its Fundamentals Represented on the Basis of its Cellular Architecture.

Brott, T., Adams, H.P., Olinger, C.P., Marler, J.R., Barsan, W.G., Biller, J., Spilker, J., Holleran, R., Eberle, R., Hertzberg, V., 1989. Measurements of acute cerebral infarction: a clinical examination scale. Stroke 20, 864–870. doi:10.1161/01.STR.20.7.864

Buckner, R.L., Andrews-Hanna, J.R., Schacter, D.L., 2008. The Brain's Default Network: Anatomy, Function, and Relevance to Disease. Ann. N. Y. Acad. Sci. 1124, 1–38. doi:10.1196/annals.1440.011

Buckner, R.L., Corbetta, M., Schatz, J., Raichle, M.E., Petersen, S.E., 1996. Preserved speech abilities and compensation following prefrontal damage. Proc. Natl. Acad. Sci. 93, 1249–1253.

Buckner, R.L., Krienen, F.M., Castellanos, A., Diaz, J.C., Yeo, B.T.T., 2011. The organization of the human cerebellum estimated by intrinsic functional connectivity. J. Neurophysiol. 106, 2322–2345. doi:10.1152/jn.00339.2011

Buckner, R.L., Krienen, F.M., Yeo, B.T.T., 2013. Opportunities and limitations of intrinsic functional connectivity MRI. Nat. Neurosci. 16, 832–837. doi:10.1038/nn.3423

Bullmore, E., Sporns, O., 2009. Complex brain networks: graph theoretical analysis of structural and functional systems. Nat. Rev. Neurosci. 10, 186–198. doi:10.1038/nrn2575

Bush, G., Luu, P., Posner, M.I., 2000. Cognitive and emotional influences in anterior cingulate cortex. Trends Cogn. Sci. 4, 215–222.

Buxbaum, L.J., Coslett, H.B., 2001. Specialised structural descriptions for human body parts: Evidence from autotopagnosia. Cogn. Neuropsychol. 18, 289–306. doi:10.1080/02643290126172

Buxbaum, L.J., Giovannetti, T., Libon, D., 2000. The Role of the Dynamic Body Schema in Praxis: Evidence from Primary Progressive Apraxia. Brain Cogn. 44, 166–191. doi:10.1006/brcg.2000.1227

Cambier, J., Elghozi, D., Strube, E., 1980. Lésions du thalamus droit avec syndrome de l'hémisphère mineur. Discussion du concept de négligence thalamique. Rev Neurol Paris 105–116.

Carrera, E., Tononi, G., 2014. Diaschisis: past, present, future. Brain 137, 2408–2422. doi:10.1093/brain/awu101

Carter, A.R., Astafiev, S.V., Lang, C.E., Connor, L.T., Rengachary, J., Strube, M.J., Pope, D.L.W., Shulman, G.L., Corbetta, M., 2010. Resting interhemispheric functional magnetic resonance imaging connectivity predicts performance after stroke. Ann. Neurol. 67, 365–375. doi:10.1002/ana.21905

Carter, A.R., Patel, K.R., Astafiev, S.V., Snyder, A.Z., Rengachary, J., Strube, M.J., Pope, A., Shimony, J.S., Lang, C.E., Shulman, G.L., Corbetta, M., 2012a. Upstream Dysfunction of Somatomotor Functional Connectivity After Corticospinal Damage in Stroke. Neurorehabil. Neural Repair 26, 7–19. doi:10.1177/1545968311411054

Carter, A.R., Shulman, G.L., Corbetta, M., 2012b. Why use a connectivity-based approach to study stroke and recovery of function? NeuroImage 62, 2271–2280. doi:10.1016/j.neuroimage.2012.02.070

Carter, C.S., Botvinick, M.M., Cohen, J.D., 1999. The Contribution of the Anterior Cingulate Cortex to Executive Processes in Cognition. Rev. Neurosci. 10. doi:10.1515/REVNEURO.1999.10.1.49

Carusone, L.M., Srinivasan, J., Gitelman, D.R., Mesulam, M.M., Parrish, T.B., 2002. Hemodynamic response changes in cerebrovascular disease: implications for functional MR imaging. Am. J. Neuroradiol. 23, 1222–1228.

Chang, T.-Y., Huang, K.-L., Ho, M.-Y., Ho, P.-S., Chang, C.-H., Liu, C.-H., Chang, Y.-J., Wong, H.-F., Hsieh, I.-C., Lee, T.-H., Liu, H.-L., 2016. Graph theoretical analysis of functional networks and its relationship to cognitive decline in patients with carotid stenosis. J. Cereb. Blood Flow Metab. 36, 808–818. doi:10.1177/0271678X15608390

Chan, M.Y., Park, D.C., Savalia, N.K., Petersen, S.E., Wig, G.S., 2014. Decreased segregation of brain systems across the healthy adult lifespan. Proc. Natl. Acad. Sci. 111, E4997–E5006. doi:10.1073/pnas.1415122111

Cheng, H.-L., Lin, C.-J., Soong, B.-W., Wang, P.-N., Chang, F.-C., Wu, Y.-T., Chou, K.-H., Lin, C.-P., Tu, P.-C., Lee, I.-H., 2012. Impairments in Cognitive Function and Brain Connectivity in Severe Asymptomatic Carotid Stenosis. Stroke 43, 2567–2573. doi:10.1161/STROKEAHA.111.645614

Cheung, V.C.K., Piron, L., Agostini, M., Silvoni, S., Turolla, A., Bizzi, E., 2009. Stability of muscle synergies for voluntary actions after cortical stroke in humans. Proc. Natl. Acad. Sci. 106, 19563–19568. doi:10.1073/pnas.0910114106

Cheung, V.C.K., Turolla, A., Agostini, M., Silvoni, S., Bennis, C., Kasi, P., Paganoni, S., Bonato, P., Bizzi, E., 2012. Muscle synergy patterns as physiological markers of motor cortical damage. Proc. Natl. Acad. Sci. 109, 14652–14656. doi:10.1073/pnas.1212056109

Choi, E.Y., Yeo, B.T.T., Buckner, R.L., 2012. The organization of the human striatum estimated by intrinsic functional connectivity. J. Neurophysiol. 108, 2242–2263. doi:10.1152/jn.00270.2012

Chollet, F., Dipiero, V., Wise, R.J.S., Brooks, D.J., Dolan, R.J., Frackowiak, R.S.J., 1991. The functional anatomy of motor recovery after stroke in humans: A study with positron emission tomography. Ann. Neurol. 29, 63–71. doi:10.1002/ana.410290112

Christen, T., Jahanian, H., Ni, W.W., Qiu, D., Moseley, M.E., Zaharchuk, G., 2015. Noncontrast mapping of arterial delay and functional connectivity using resting-state functional MRI: A study in Moyamoya patients. J. Magn. Reson. Imaging 41, 424–430. doi:10.1002/jmri.24558

Clark, L., Bechara, A., Damasio, H., Aitken, M.R.F., Sahakian, B.J., Robbins, T.W., 2008. Differential effects of insular and ventromedial prefrontal cortex lesions on risky decision-making. Brain 131, 1311–1322. doi:10.1093/brain/awn066

Cohen, R.A., Kaplan, R.F., Zuffante, P., Moser, D.J., Jenkins, M.A., Salloway, S., Wilkinson, H., 1999. Alteration of Intention and Self-Initiated Action Associated With Bilateral Anterior Cingulotomy. J. Neuropsychiatry Clin. Neurosci. 11, 444–453.

Connor, L.T., Albert, M.L., Helm-Estabrooks, N., Obler, L.K., 2000. Attentional Modulation of Language Performance. Brain Lang. 71, 52–55. doi:10.1006/brln.1999.2210

Corbetta, M., 2012. Functional connectivity and neurological recovery. Dev. Psychobiol. 54, 239–253. doi:10.1002/dev.20507

Corbetta, M., Kincade, M.J., Lewis, C., Snyder, A.Z., Sapir, A., 2005. Neural basis and recovery of spatial attention deficits in spatial neglect. Nat. Neurosci. 8, 1603–1610. doi:10.1038/nn1574

Corbetta, M., Patel, G., Shulman, G.L., 2008. The Reorienting System of the Human Brain: From Environment to Theory of Mind. Neuron 58, 306–324. doi:10.1016/j.neuron.2008.04.017

Corbetta, M., Ramsey, L., Callejas, A., Baldassarre, A., Hacker, C.D., Siegel, J.S., Astafiev, S.V., Rengachary, J., Zinn, K., Lang, C.E., Connor, L.T., Fucetola, R., Strube, M., Carter, A.R., Shulman, G.L., 2015. Common Behavioral Clusters and Subcortical Anatomy in Stroke. Neuron 85, 927–941. doi:10.1016/j.neuron.2015.02.027

Corbetta, M., Shulman, G.L., 2011. Spatial Neglect and Attention Networks. Annu. Rev. Neurosci. 34, 569–599. doi:10.1146/annurev-neuro-061010-113731

Corbetta, M., Shulman, G.L., 2002. Control of goal-directed and stimulus-driven attention in the brain. Nat. Rev. Neurosci. 3, 201–215. doi:10.1038/nrn755

Craddock, R.C., James, G.A., Holtzheimer, P.E., Hu, X.P., Mayberg, H.S., 2012. A whole brain fMRI atlas generated via spatially constrained spectral clustering. Hum. Brain Mapp. 33, 1914–1928. doi:10.1002/hbm.21333

Critchley, M., 1953. The parietal lobes. Williams and Wilkins, Oxford, England.

Dale, A.M., Fischl, B., Sereno, M.I., 1999. Cortical Surface-Based Analysis: I. Segmentation and Surface Reconstruction. NeuroImage 9, 179–194. doi:10.1006/nimg.1998.0395

Damasio, A.R., Damasio, H., Chui, H.C., 1980. Neglect following damage to frontal lobe or basal ganglia. Neuropsychologia 18, 123–132. doi:10.1016/0028-3932(80)90058-5

Damasio, H., Grabowski, T.J., Tranel, D., Hichwa, R.D., Damasio, A.R., 1996. A neural basis for lexical retrieval. Nature 380, 499–505. doi:10.1038/380499a0

Daumé III, H., 2009. Frustratingly easy domain adaptation. ArXiv Prepr. ArXiv09071815.

Deco, G., Tononi, G., Boly, M., Kringelbach, M.L., 2015. Rethinking segregation and integration: contributions of whole-brain modelling. Nat. Rev. Neurosci. 16, 430–439. doi:10.1038/nrn3963

de Haan, B., Rorden, C., Karnath, H.-O., 2013. Abnormal perilesional BOLD signal is not correlated with stroke patients' behavior. Front. Hum. Neurosci. 7, 669. doi:10.3389/fnhum.2013.00669

Derdeyn, C.P., 2007. Mechanisms of Ischemic Stroke Secondary to Large Artery Atherosclerotic Disease. Neuroimaging Clin. N. Am., Angioplasty and Stenting for Atherosclerotic Cerebrovascular Disease 17, 303–311. doi:10.1016/j.nic.2007.03.001

Derdeyn, C.P., Powers, W.J., Grubb, R.L., 1998. Hemodynamic effects of middle cerebral artery stenosis and occlusion. Am. J. Neuroradiol. 19, 1463–1469.

De Renzi, E., 1982. Disorders of space exploration and cognition. J. Wiley.

D'Esposito, M., Deouell, L.Y., Gazzaley, A., 2003. Alterations in the BOLD fMRI signal with ageing and disease: a challenge for neuroimaging. Nat. Rev. Neurosci. 4, 863–872. doi:10.1038/nrn1246

Ding, X., Li, C.-Y., Wang, Q.-S., Du, F.-Z., Ke, Z.-W., Peng, F., Wang, J., Chen, L., 2014. Patterns in default-mode network connectivity for determining outcomes in cognitive function in acute stroke patients. Neuroscience 277, 637–646. doi:10.1016/j.neuroscience.2014.07.060

Donahue, M.J., Strother, M.K., Hendrikse, J., 2012. Novel MRI Approaches for Assessing Cerebral Hemodynamics in Ischemic Cerebrovascular Disease. Stroke 43, 903–915. doi:10.1161/STROKEAHA.111.635995

Dosenbach, N.U.F., Fair, D.A., Miezin, F.M., Cohen, A.L., Wenger, K.K., Dosenbach, R.A.T., Fox, M.D., Snyder, A.Z., Vincent, J.L., Raichle, M.E., Schlaggar, B.L., Petersen, S.E., 2007. Distinct brain networks for adaptive and stable task control in humans. Proc. Natl. Acad. Sci. U. S. A. 104, 11073–11078. doi:10.1073/pnas.0704320104

Dosenbach, N.U.F., Visscher, K.M., Palmer, E.D., Miezin, F.M., Wenger, K.K., Kang, H.C., Burgund, E.D., Grimes, A.L., Schlaggar, B.L., Petersen, S.E., 2006. A Core System for the Implementation of Task Sets. Neuron 50, 799–812. doi:10.1016/j.neuron.2006.04.031

Doucet, G., Naveau, M., Petit, L., Delcroix, N., Zago, L., Crivello, F., Jobard, G., Tzourio-Mazoyer, N., Mazoyer, B., Mellet, E., Joliot, M., 2011. Brain activity at rest: a multiscale hierarchical functional organization. J. Neurophysiol. 105, 2753–2763. doi:10.1152/jn.00895.2010

Dronkers, N.F., Plaisant, O., Iba-Zizen, M.T., Cabanis, E.A., 2007. Paul Broca's historic cases: high resolution MR imaging of the brains of Leborgne and Lelong. Brain 130, 1432–1441. doi:10.1093/brain/awm042

Dubovik, S., Pignat, J.-M., Ptak, R., Aboulafia, T., Allet, L., Gillabert, N., Magnin, C., Albert, F., Momjian-Mayor, I., Nahum, L., Lascano, A.M., Michel, C.M., Schnider, A., Guggisberg, A.G., 2012. The behavioral significance of coherent resting-state oscillations after stroke. NeuroImage 61, 249–257. doi:10.1016/j.neuroimage.2012.03.024

Duffau, H., 2015. Stimulation mapping of white matter tracts to study brain functional connectivity. Nat. Rev. Neurol. 11, 255–265. doi:10.1038/nrneurol.2015.51

Fedorenko, E., Thompson-Schill, S.L., 2014. Reworking the language network. Trends Cogn. Sci. 18, 120–126. doi:10.1016/j.tics.2013.12.006

Feeney, D.M., Baron, J.C., 1986. Diaschisis. Stroke 17, 817–830. doi:10.1161/01.STR.17.5.817

Finger, S., 2004. Paul Broca (1824-1880). J. Neurol. 251. doi:10.1007/s00415-004-0456-6

Fischl, B., 2012. FreeSurfer. NeuroImage, 20 YEARS OF fMRI 20 YEARS OF fMRI 62, 774–781. doi:10.1016/j.neuroimage.2012.01.021

Fischl, B., Salat, D.H., Busa, E., Albert, M., Dieterich, M., Haselgrove, C., Van Der Kouwe, A., Killiany, R., Kennedy, D., Klaveness, S., others, 2002. Whole brain segmentation: automated labeling of neuroanatomical structures in the human brain. Neuron 33, 341–355.

Fischl, B., Sereno, M.I., Dale, A.M., 1999. Cortical Surface-Based Analysis: II: Inflation, Flattening, and a Surface-Based Coordinate System. NeuroImage 9, 195–207. doi:10.1006/nimg.1998.0396

Fischl, B., Sereno, M.I., Tootell, R.B.H., Dale, A.M., 1999. High-resolution intersubject averaging and a coordinate system for the cortical surface. HUM BRAIN MAPP 8, 272–284.

Fornito, A., Zalesky, A., Breakspear, M., 2015. The connectomics of brain disorders. Nat. Rev. Neurosci. 16, 159–172. doi:10.1038/nrn3901

Fox, M.D., Snyder, A.Z., Vincent, J.L., Corbetta, M., Van Essen, D.C., Raichle, M.E., 2005. The human brain is intrinsically organized into dynamic, anticorrelated functional networks. Proc. Natl. Acad. Sci. U. S. A. 102, 9673–9678. doi:10.1073/pnas.0504136102

Fox, P.T., Raichle, M.E., 1986. Focal physiological uncoupling of cerebral blood flow and oxidative metabolism during somatosensory stimulation in human subjects. Proc. Natl. Acad. Sci. 83, 1140–1144.

Ghoshal, S., Gokhale, S., Rebovich, G., Caplan, L.R., 2011. The neurology of decreased activity: abulia. Rev. Neurol. Dis. 8, e55–67.

Ghosh, S.S., Kakunoori, S., Augustinack, J., Nieto-Castanon, A., Kovelman, I., Gaab, N., Christodoulou, J.A., Triantafyllou, C., Gabrieli, J.D.E., Fischl, B., 2010. Evaluating the validity of volume-based and surface-based brain image registration for developmental cognitive neuroscience studies in children 4 to 11years of age. NeuroImage 53, 85–93. doi:10.1016/j.neuroimage.2010.05.075

Glasser, M.F., Sotiropoulos, S.N., Wilson, J.A., Coalson, T.S., Fischl, B., Andersson, J.L., Xu, J., Jbabdi, S., Webster, M., Polimeni, J.R., Van Essen, D.C., Jenkinson, M., 2013. The minimal preprocessing pipelines for the Human Connectome Project. NeuroImage 80, 105–124. doi:10.1016/j.neuroimage.2013.04.127

Goldman-Rakic, P.S., 1988. Topography of cognition: parallel distributed networks in primate association cortex. Annu. Rev. Neurosci. 11, 137–156.

Golland, P., Fischl, B., 2003. Permutation Tests for Classification: Towards Statistical Significance in Image-Based Studies, in: Taylor, C., Noble, J.A. (Eds.), Information Processing in Medical Imaging, Lecture Notes in Computer Science. Springer Berlin Heidelberg, pp. 330–341.

Gordon, E.M., Laumann, T.O., Adeyemo, B., Huckins, J.F., Kelley, W.M., Petersen, S.E., 2016. Generation and Evaluation of a Cortical Area Parcellation from Resting-State Correlations. Cereb. Cortex N. Y. N 1991 26, 288–303. doi:10.1093/cercor/bhu239

Gracco, V.L., Abbs, J.H., 1988. Central patterning of speech movements. Exp. Brain Res. 71, 515–526. doi:10.1007/BF00248744

Grant, E.G., Benson, C.B., Moneta, G.L., Alexandrov, A.V., Baker, J.D., Bluth, E.I., Carroll, B.A., Eliasziw, M., Gocke, J., Hertzberg, B.S., Katanick, S., Needleman, L., Pellerito, J.,

Polak, J.F., Rholl, K.S., Wooster, D.L., Zierler, R.E., 2003. Carotid Artery Stenosis: Gray-Scale and Doppler US Diagnosis—Society of Radiologists in Ultrasound Consensus Conference. Radiology 229, 340–346. doi:10.1148/radiol.2292030516

Gratton, C., Nomura, E.M., Pérez, F., D'Esposito, M., 2012. Focal Brain Lesions to Critical Locations Cause Widespread Disruption of the Modular Organization of the Brain. J. Cogn. Neurosci. 24, 1275–1285. doi:10.1162/jocn_a_00222

Grayson, D.S., Bliss-Moreau, E., Machado, C.J., Bennett, J., Shen, K., Grant, K.A., Fair, D.A., Amaral, D.G., 2016. The Rhesus Monkey Connectome Predicts Disrupted Functional Networks Resulting from Pharmacogenetic Inactivation of the Amygdala. Neuron 91, 453–466. doi:10.1016/j.neuron.2016.06.005

Grefkes, C., Fink, G.R., 2014. Connectivity-based approaches in stroke and recovery of function. Lancet Neurol. 13, 206–216. doi:10.1016/S1474-4422(13)70264-3

Grefkes, C., Fink, G.R., 2011. Reorganization of cerebral networks after stroke: new insights from neuroimaging with connectivity approaches. Brain 134, 1264–1276. doi:10.1093/brain/awr033

Greicius, M.D., Srivastava, G., Reiss, A.L., Menon, V., 2004. Default-mode network activity distinguishes Alzheimer's disease from healthy aging: Evidence from functional MRI. Proc. Natl. Acad. Sci. U. S. A. 101, 4637–4642. doi:10.1073/pnas.0308627101

Hacker, C.D., Laumann, T.O., Szrama, N.P., Baldassarre, A., Snyder, A.Z., 2013. Resting-State Network Estimation in Individual Subjects.

Hacker, C.D., Laumann, T.O., Szrama, N.P., Baldassarre, A., Snyder, A.Z., Leuthardt, E.C., Corbetta, M., 2013. Resting state network estimation in individual subjects. NeuroImage 82, 616–633. doi:10.1016/j.neuroimage.2013.05.108

Hall, C.N., Reynell, C., Gesslein, B., Hamilton, N.B., Mishra, A., Sutherland, B.A., O'Farrell, F.M., Buchan, A.M., Lauritzen, M., Attwell, D., 2014. Capillary pericytes regulate cerebral blood flow in health and disease. Nature 508, 55–60. doi:10.1038/nature13165

Hathout, G.M., Gopi, R.K., Bandettini, P., Gambhir, S.S., 1999. The lag of cerebral hemodynamics with rapidly alternating periodic stimulation: modeling for functional MRI. Magn. Reson. Imaging 17, 9–20. doi:10.1016/S0730-725X(98)00150-7

Hauck, E.F., Apostel, S., Hoffmann, J.F., Heimann, A., Kempski, O., 2004. Capillary Flow and Diameter Changes during Reperfusion after Global Cerebral Ischemia Studied by Intravital Video Microscopy. J. Cereb. Blood Flow Metab. 24, 383–391. doi:10.1097/00004647-200404000-00003

Hayes, S.M., Salat, D.H., Verfaellie, M., 2012. Default Network Connectivity in Medial Temporal Lobe Amnesia. J. Neurosci. 32, 14622–14629a. doi:10.1523/JNEUROSCI.0700-12.2012

He, B.J., Snyder, A.Z., Vincent, J.L., Epstein, A., Shulman, G.L., Corbetta, M., 2007. Breakdown of Functional Connectivity in Frontoparietal Networks Underlies Behavioral Deficits in Spatial Neglect. Neuron 53, 905–918. doi:10.1016/j.neuron.2007.02.013

Hier, D.B., Davis, K.R., Richardson, E.P., Mohr, J.P., 1977. Hypertensive putaminal hemorrhage. Ann. Neurol. 1, 152–159. doi:10.1002/ana.410010209

Hillis, A.E., Newhart, M., Heidler, J., Barker, P.B., Herskovits, E.H., Degaonkar, M., 2005. Anatomy of Spatial Attention: Insights from Perfusion Imaging and Hemispatial Neglect in Acute Stroke. J. Neurosci. 25, 3161–3167. doi:10.1523/JNEUROSCI.4468-04.2005

Hillis, A.E., Wityk, R.J., Barker, P.B., Beauchamp, N.J., Gailloud, P., Murphy, K., Cooper, O., Metter, E.J., 2002. Subcortical aphasia and neglect in acute stroke: the role of cortical hypoperfusion. Brain 125, 1094–1104. doi:10.1093/brain/awf113

Honey, C.J., Sporns, O., 2008. Dynamical consequences of lesions in cortical networks. Hum. Brain Mapp. 29, 802–809. doi:10.1002/hbm.20579

Howard, I.S., Ingram, J.N., Körding, K.P., Wolpert, D.M., 2009. Statistics of Natural Movements Are Reflected in Motor Errors. J. Neurophysiol. 102, 1902–1910. doi:10.1152/jn.00013.2009

Ingram, J.N., Körding, K.P., Howard, I.S., Wolpert, D.M., 2008. The statistics of natural hand movements. Exp. Brain Res. 188, 223–236. doi:10.1007/s00221-008-1355-3

Jahanshahi, M., 1998. Willed Action and Its Impairments. Cogn. Neuropsychol. 15, 483–533. doi:10.1080/026432998381005

Jiang, L., Xu, H., Yu, C., 2013. Brain Connectivity Plasticity in the Motor Network after Ischemic Stroke. Neural Plast. 2013. doi:10.1155/2013/924192

Johnston, J.M., Vaishnavi, S.N., Smyth, M.D., Zhang, D., He, B.J., Zempel, J.M., Shimony, J.S., Snyder, A.Z., Raichle, M.E., 2008. Loss of Resting Interhemispheric Functional Connectivity after Complete Section of the Corpus Callosum. J. Neurosci. 28, 6453–6458. doi:10.1523/JNEUROSCI.0573-08.2008

Jones, D.T., Mateen, F.J., Lucchinetti, C.F., Jack, C.R., Welker, K.M., 2011. Default Mode Network Disruption Secondary to a Lesion in the Anterior Thalamus. Arch. Neurol. 68. doi:10.1001/archneurol.2010.259

Jorge, R.E., Starkstein, S.E., Robinson, R.G., 2010. Apathy following stroke. Can. J. Psychiatry Rev. Can. Psychiatr. 55, 350–354.

Karnath, H.-O., Ferber, S., Himmelbach, M., 2001. Spatial awareness is a function of the temporal not the posterior parietal lobe. Nature 411, 950–953. doi:10.1038/35082075

Kelley, W.M., Miezin, F.M., McDermott, K.B., Buckner, R.L., Raichle, M.E., Cohen, N.J., Ollinger, J.M., Akbudak, E., Conturo, T.E., Snyder, A.Z., Petersen, S.E., 1998. Hemispheric Specialization in Human Dorsal Frontal Cortex and Medial Temporal Lobe for Verbal and Nonverbal Memory Encoding. Neuron 20, 927–936. doi:10.1016/S0896-6273(00)80474-2

Kimura, H., Kado, H., Koshimoto, Y., Tsuchida, T., Yonekura, Y., Itoh, H., 2005. Multislice continuous arterial spin-labeled perfusion MRI in patients with chronic occlusive cerebrovascular disease: A correlative study with CO2 PET validation. J. Magn. Reson. Imaging 22, 189–198. doi:10.1002/jmri.20382

Krainik, A., Hund-Georgiadis, M., Zysset, S., Cramon, D.Y. von, 2005. Regional Impairment of Cerebrovascular Reactivity and BOLD Signal in Adults After. Stroke 36, 1146–1152. doi:10.1161/01.STR.0000166178.40973.a7

Kumral, E., Evyapan, D., Balkir, K., 1999. Acute Caudate Vascular Lesions. Stroke 30, 100–108. doi:10.1161/01.STR.30.1.100

Lake, E.M.R., Bazzigaluppi, P., Stefanovic, B., 2016. Functional magnetic resonance imaging in chronic ischaemic stroke. Phil Trans R Soc B 371, 20150353. doi:10.1098/rstb.2015.0353

Lazar, R.M., Antoniello, D., 2008. Variability in recovery from aphasia. Curr. Neurol. Neurosci. Rep. 8, 497–502.

Lee, J.-M., Vo, K.D., An, H., Celik, A., Lee, Y., Hsu, C.Y., Lin, W., 2003. Magnetic resonance cerebral metabolic rate of oxygen utilization in hyperacute stroke patients. Ann. Neurol. 53, 227–232. doi:10.1002/ana.10433

Leibovitch, F.S., Black, S.E., Caldwell, C.B., Ebert, P.L., Ehrlich, L.E., Szalai, J.P., 1998. Brain-behavior correlations in hemispatial neglect using CT and SPECT The Sunnybrook Stroke Study. Neurology 50, 901–908. doi:10.1212/WNL.50.4.901

Leo, A., Handjaras, G., Bianchi, M., Marino, H., Gabiccini, M., Guidi, A., Scilingo, E.P., Pietrini, P., Bicchi, A., Santello, M., Ricciardi, E., 2016. A synergy-based hand control is encoded in human motor cortical areas. eLife 5, e13420. doi:10.7554/eLife.13420

Lewis, C.M., Baldassarre, A., Committeri, G., Romani, G.L., Corbetta, M., 2009. Learning sculpts the spontaneous activity of the resting human brain. Proc. Natl. Acad. Sci. 106, 17558–17563. doi:10.1073/pnas.0902455106

Liepert, J., Bauder, H., Miltner, W.H.R., Taub, E., Weiller, C., 2000. Treatment-Induced Cortical Reorganization After Stroke in Humans. Stroke 31, 1210–1216. doi:10.1161/01.STR.31.6.1210

Lim, D.H., LeDue, J.M., Mohajerani, M.H., Murphy, T.H., 2014. Optogenetic Mapping after Stroke Reveals Network-Wide Scaling of Functional Connections and Heterogeneous Recovery of the Peri-Infarct. J. Neurosci. 34, 16455–16466. doi:10.1523/JNEUROSCI.3384-14.2014

Longstreth, W.T., Manolio, T.A., Arnold, A., Burke, G.L., Bryan, N., Jungreis, C.A., Enright, P.L., O'Leary, D., Fried, L., 1996. Clinical Correlates of White Matter Findings on Cranial Magnetic Resonance Imaging of 3301 Elderly People The Cardiovascular Health Study. Stroke 27, 1274–1282. doi:10.1161/01.STR.27.8.1274

Luu, P., Tucker, D.M., Derryberry, D., Reed, M., Poulsen, C., 2003. Electrophysiological Responses to Errors and Feedback in the Process of Action Regulation. Psychol. Sci. 14, 47–53. doi:10.1111/1467-9280.01417

Lv, Y., Margulies, D.S., Cameron Craddock, R., Long, X., Winter, B., Gierhake, D., Endres, M., Villringer, K., Fiebach, J., Villringer, A., 2013. Identifying the perfusion deficit in acute stroke with resting-state functional magnetic resonance imaging. Ann. Neurol. 73, 136–140. doi:10.1002/ana.23763

MacIntosh, B.J., Lindsay, A.C., Kylintireas, I., Kuker, W., Günther, M., Robson, M.D., Kennedy, J., Choudhury, R.P., Jezzard, P., 2010. Multiple Inflow Pulsed Arterial Spin-Labeling Reveals Delays in the Arterial Arrival Time in Minor Stroke and Transient Ischemic Attack. Am. J. Neuroradiol. 31, 1892–1894. doi:10.3174/ajnr.A2008

Marcus, D.S., Harms, M.P., Snyder, A.Z., Jenkinson, M., Wilson, J.A., Glasser, M.F., Barch, D.M., Archie, K.A., Burgess, G.C., Ramaratnam, M., Hodge, M., Horton, W., Herrick, R., Olsen, T., McKay, M., House, M., Hileman, M., Reid, E., Harwell, J., Coalson, T., Schindler, J., Elam, J.S., Curtiss, S.W., Van Essen, D.C., 2013. Human Connectome Project informatics: Quality control, database services, and data visualization. NeuroImage 80, 202–219. doi:10.1016/j.neuroimage.2013.05.077

Marshall, R., 2004. The functional relevance of cerebral hemodynamics: why blood... : Current Opinion in Neurology [WWW Document]. LWW. URL http://journals.lww.com/co-neurology/Fulltext/2004/12000/The_functional_relevance_of_cerebral_hemodynamics_.10.aspx (accessed 9.1.16).

Massa, M.S., Wang, N., Bickerton, W.-L., Demeyere, N., Riddoch, M.J., Humphreys, G.W., 2015. On the importance of cognitive profiling: A graphical modelling analysis of domain-specific and domain-general deficits after stroke. Cortex 71, 190–204. doi:10.1016/j.cortex.2015.06.006

Mazzocchi, F., Vignolo, L.A., 1979. Localisation of Lesions in Aphasia: Clinical-CT Scan Correlations in Stroke Patients. Cortex 15, 627–653. doi:10.1016/S0010-9452(79)80051-9

McFie, J., Piercy, M.F., Zangwill, O.L., 1950. Visual-spatial agnosia associated with lesions of the right cerebral hemisphere. Brain J. Neurol. 73, 167–190.

Mega, M.S., Cohenour, R.C., 1997. Akinetic mutism: disconnection of frontal-subcortical circuits. Neuropsychiatry. Neuropsychol. Behav. Neurol. 10, 254–259.

Mega, M.S., Cummings, J.L., 1994. Frontal-subcortical circuits and neuropsychiatric disorders. J. Neuropsychiatry Clin. Neurosci. 6, 358–370.

Mennes, M., Kelly, C., Zuo, X.-N., Di Martino, A., Biswal, B.B., Castellanos, F.X., Milham, M.P., 2010. Inter-individual differences in resting-state functional connectivity predict task-induced BOLD activity. NeuroImage 50, 1690–1701. doi:10.1016/j.neuroimage.2010.01.002

Mesulam, M.-M., 1990. Large-scale neurocognitive networks and distributed processing for attention, language, and memory. Ann. Neurol. 28, 597–613. doi:10.1002/ana.410280502

Mitra, A., Snyder, A.Z., Hacker, C.D., Raichle, M.E., 2014. Lag structure in resting-state fMRI. J. Neurophysiol. 111, 2374–2391. doi:10.1152/jn.00804.2013

Mohr, J.P., Pessin, M.S., Finkelstein, S., Funkenstein, H.H., Duncan, G.W., Davis, K.R., 1978. Broca aphasia Pathologic and clinical. Neurology 28, 311–311. doi:10.1212/WNL.28.4.311

Mueller, S., Wang, D., Fox, M.D., Yeo, B.T.T., Sepulcre, J., Sabuncu, M.R., Shafee, R., Lu, J., Liu, H., 2013. Individual Variability in Functional Connectivity Architecture of the Human Brain. Neuron 77, 586–595. doi:10.1016/j.neuron.2012.12.028

Munkres, J., 1957. Algorithms for the Assignment and Transportation Problems. J. Soc. Ind. Appl. Math. 5, 32–38. doi:10.1137/0105003

Murphy, T.H., Corbett, D., 2009. Plasticity during stroke recovery: from synapse to behaviour. Nat. Rev. Neurosci. 10, 861–872. doi:10.1038/nrn2735

Muschelli, J., Nebel, M.B., Caffo, B.S., Barber, A.D., Pekar, J.J., Mostofsky, S.H., 2014. Reduction of motion-related artifacts in resting state fMRI using aCompCor. NeuroImage 96, 22–35. doi:10.1016/j.neuroimage.2014.03.028

Newman, M.E.J., 2004. Fast algorithm for detecting community structure in networks. Phys. Rev. E 69, 066133. doi:10.1103/PhysRevE.69.066133

Nishio, Y., Hashimoto, M., Ishii, K., Mori, E., 2011. Neuroanatomy of a neurobehavioral disturbance in the left anterior thalamic infarction. J. Neurol. Neurosurg. Psychiatry 82, 1195–1200. doi:10.1136/jnnp.2010.236463

Nomura, E.M., Gratton, C., Visser, R.M., Kayser, A., Perez, F., D'Esposito, M., 2010. Double dissociation of two cognitive control networks in patients with focal brain lesions. Proc. Natl. Acad. Sci. 107, 12017–12022. doi:10.1073/pnas.1002431107

Nudo, R.J., Milliken, G.W., 1996. Reorganization of movement representations in primary motor cortex following focal ischemic infarcts in adult squirrel monkeys. J. Neurophysiol. 75, 2144–2149.

Ojemann, J.G., Akbudak, E., Snyder, A.Z., McKinstry, R.C., Raichle, M.E., Conturo, T.E., 1997. Anatomic Localization and Quantitative Analysis of Gradient Refocused Echo-Planar fMRI Susceptibility Artifacts. NeuroImage 6, 156–167. doi:10.1006/nimg.1997.0289

Olivot, J.-M., Mlynash, M., Thijs, V.N., Kemp, S., Lansberg, M.G., Wechsler, L., Bammer, R., Marks, M.P., Albers, G.W., 2009. Optimal Tmax Threshold for Predicting Penumbral Tissue in Acute. Stroke 40, 469–475. doi:10.1161/STROKEAHA.108.526954

Onoda, K., Ishihara, M., Yamaguchi, S., 2012. Decreased functional connectivity by aging is associated with cognitive decline. J. Cogn. Neurosci. 24, 2186–2198.

O'Reilly, J.X., Croxson, P.L., Jbabdi, S., Sallet, J., Noonan, M.P., Mars, R.B., Browning, P.G.F., Wilson, C.R.E., Mitchell, A.S., Miller, K.L., Rushworth, M.F.S., Baxter, M.G., 2013. Causal effect of disconnection lesions on interhemispheric functional connectivity in rhesus monkeys. Proc. Natl. Acad. Sci. 110, 13982–13987. doi:10.1073/pnas.1305062110

Ovadia-Caro, S., Margulies, D.S., Villringer, A., 2014. The Value of Resting-State Functional Magnetic Resonance Imaging in. Stroke 45, 2818–2824. doi:10.1161/STROKEAHA.114.003689

Ovadia-Caro, S., Villringer, K., Fiebach, J., Jungehulsing, G.J., van der Meer, E., Margulies, D.S., Villringer, A., 2013. Longitudinal effects of lesions on functional networks after stroke. J. Cereb. Blood Flow Metab. 33, 1279–1285. doi:10.1038/jcbfm.2013.80

Owen, A.M., McMillan, K.M., Laird, A.R., Bullmore, E., 2005. N-back working memory paradigm: A meta-analysis of normative functional neuroimaging studies. Hum. Brain Mapp. 25, 46–59. doi:10.1002/hbm.20131

PAPEZ JW, 1937. A proposed mechanism of emotion. Arch. Neurol. Psychiatry 38, 725–743. doi:10.1001/archneurpsyc.1937.02260220069003

Park, C., Chang, W.H., Ohn, S.H., Kim, S.T., Bang, O.Y., Pascual-Leone, A., Kim, Y.-H., 2011. Longitudinal Changes of Resting-State Functional Connectivity During Motor Recovery After. Stroke 42, 1357–1362. doi:10.1161/STROKEAHA.110.596155

Parvizi, J., Rangarajan, V., Shirer, W.R., Desai, N., Greicius, M.D., 2013. The Will to Persevere Induced by Electrical Stimulation of the Human Cingulate Gyrus. Neuron 80, 1359–1367. doi:10.1016/j.neuron.2013.10.057

Paterson, A., Zangwill, O.L., 1944. Disorders of Visual Space Perception Associated with Lesions of the Right Cerebral Hemisphere. Brain 67, 331–358. doi:10.1093/brain/67.4.331

Perani, D., Vallar, G., Cappa, S., Messa, C., Fazio, F., 1987. Aphasia and Neglect After Subcortical Stroke. Brain 110, 1211–1229. doi:10.1093/brain/110.5.1211

Petersen, S.E., Fox, P.T., Posner, M.I., Mintun, M., Raichle, M.E., 1988. Positron emission tomographic studies of the cortical anatomy of single-word processing. Nature 331, 585–589. doi:10.1038/331585a0

Petersen, S.E., Sporns, O., 2015. Brain Networks and Cognitive Architectures. Neuron 88, 207–219. doi:10.1016/j.neuron.2015.09.027

Petzold, G.C., Murthy, V.N., 2011. Role of Astrocytes in Neurovascular Coupling. Neuron 71, 782–797. doi:10.1016/j.neuron.2011.08.009

Phan, T.G., Chen, J., Donnan, G., Srikanth, V., Wood, A., Reutens, D.C., 2010. Development of a new tool to correlate stroke outcome with infarct topography: A proof-of-concept study. NeuroImage 49, 127–133. doi:10.1016/j.neuroimage.2009.07.067

Pineiro, R., Pendlebury, S., Johansen-Berg, H., Matthews, P.M., 2002. Altered Hemodynamic Responses in Patients After Subcortical Stroke Measured by Functional MRI. Stroke 33, 103–109. doi:10.1161/hs0102.100482

Posner, M.I., Cohen, Y., 1984. Components of visual orienting. Atten. Perform. X Control Lang. Process. 32, 531–556.

Posner, M.I., Petersen, S.E., 1990. The Attention System of the Human Brain. Annu. Rev. Neurosci. 13, 25–42. doi:10.1146/annurev.ne.13.030190.000325

Posner, M., Petersen, S., Fox, P., Raichle, M., 1988. Localization of cognitive operations in the human brain. Science 240, 1627–1631. doi:10.1126/science.3289116

Power, J.D., n.d. Methods to detect, characterize, and remove motion artifact in resting state fMRI.

Power, J.D., Barnes, K.A., Snyder, A.Z., Schlaggar, B.L., Petersen, S.E., 2012. Spurious but systematic correlations in functional connectivity MRI networks arise from subject motion. NeuroImage 59, 2142–2154. doi:10.1016/j.neuroimage.2011.10.018

Power, J.D., Cohen, A.L., Nelson, S.M., Wig, G.S., Barnes, K.A., Church, J.A., Vogel, A.C., Laumann, T.O., Miezin, F.M., Schlaggar, B.L., Petersen, S.E., 2011. Functional network organization of the human brain. Neuron 72, 665–678. doi:10.1016/j.neuron.2011.09.006

Power, J.D., Mitra, A., Laumann, T.O., Snyder, A.Z., Schlaggar, B.L., Petersen, S.E., 2014. Methods to detect, characterize, and remove motion artifact in resting state fMRI. NeuroImage 84, 320–341. doi:10.1016/j.neuroimage.2013.08.048

Powers, W.J., Fox, P.T., Raichle, M.E., 1988. The effect of carotid artery disease on the cerebrovascular response to physiologic stimulation. Neurology 38, 1475–1475. doi:10.1212/WNL.38.9.1475

Powers, W.J., Press, G.A., Grubb, R.L., Gado, M., Raichle, M.E., 1987. The effect of hemodynamically significant carotid artery disease on the hemodynamic status of the cerebral circulation. Ann. Intern. Med. 106, 27–34.

Prabhakaran, S., Zarahn, E., Riley, C., Speizer, A., Chong, J.Y., Lazar, R.M., Marshall, R.S., Krakauer, J.W., 2007. Inter-individual Variability in the Capacity for Motor Recovery After Ischemic Stroke. Neurorehabil. Neural Repair. doi:10.1177/1545968307305302

Raichle, M.E., Plum, F., 1972. Hyperventilation and Cerebral Blood Flow. Stroke 3, 566–575. doi:10.1161/01.STR.3.5.566

Ramsey, L.E., Siegel, J.S., Baldassarre, A., Metcalf, N.V., Zinn, K., Shulman, G.L., Corbetta, M., 2016. Normalization of network connectivity in hemispatial neglect recovery. Ann. Neurol. n/a–n/a. doi:10.1002/ana.24690

Ramsey, L., Siegel, J.S., Strube, M., Shulman, G.L., Corbetta, M., n.d. Behavioral patterns of recovery and predictors of outcome post-stroke. In Prep.

Rehme, A.K., Volz, L.J., Feis, D.-L., Bomilcar-Focke, I., Liebig, T., Eickhoff, S.B., Fink, G.R., Grefkes, C., 2014. Identifying Neuroimaging Markers of Motor Disability in Acute Stroke by Machine Learning Techniques. Cereb. Cortex bhu100. doi:10.1093/cercor/bhu100

Reinhard, M., Roth, M., Guschlbauer, B., Harloff, A., Timmer, J., Czosnyka, M., Hetzel, A., 2005. Dynamic cerebral autoregulation in acute ischemic stroke assessed from spontaneous blood pressure fluctuations. Stroke J. Cereb. Circ. 36, 1684–1689. doi:10.1161/01.STR.0000173183.36331.ee

Rengachary, J., He, B.J., Shulman, G., Corbetta, M., 2011. A behavioral analysis of spatial neglect and its recovery after stroke. Front. Hum. Neurosci. 5, 29. doi:10.3389/fnhum.2011.00029

Roc, A.C., Wang, J., Ances, B.M., Liebeskind, D.S., Kasner, S.E., Detre, J.A., 2006. Altered Hemodynamics and Regional Cerebral Blood Flow in Patients With Hemodynamically Significant Stenoses. Stroke 37, 382–387. doi:10.1161/01.STR.0000198807.31299.43

Rosner, G., Graf, R., Kataoka, K., Heiss, W.D., 1986. Selective functional vulnerability of cortical neurons following transient MCA-occlusion in the cat. Stroke 17, 76–82. doi:10.1161/01.STR.17.1.76

Rossini, P.M., Altamura, C., Ferretti, A., Vernieri, F., Zappasodi, F., Caulo, M., Pizzella, V., Gratta, C.D., Romani, G.-L., Tecchio, F., 2004. Does cerebrovascular disease affect the coupling between neuronal activity and local haemodynamics? Brain 127, 99–110. doi:10.1093/brain/awh012

Rowland, D.J., Garbow, J.R., Laforest, R., Snyder, A.Z., 2005. Registration of [18F]FDG microPET and small-animal MRI. Nucl. Med. Biol. 32, 567–572. doi:10.1016/j.nucmedbio.2005.05.002

Rubinov, M., Sporns, O., 2010. Complex network measures of brain connectivity: Uses and interpretations. NeuroImage 52, 1059–1069. doi:10.1016/j.neuroimage.2009.10.003

Sacco, R.L., Benjamin, E.J., Broderick, J.P., Dyken, M., Easton, J.D., Feinberg, W.M., Goldstein, L.B., Gorelick, P.B., Howard, G., Kittner, S.J., Manolio, T.A., Whisnant, J.P., Wolf, P.A., 1997. Risk Factors. Stroke 28, 1507–1517. doi:10.1161/01.STR.28.7.1507

Salinet, A.S.M., Haunton, V.J., Panerai, R.B., Robinson, T.G., 2013. A systematic review of cerebral hemodynamic responses to neural activation following stroke. J. Neurol. 260, 2715–2721. doi:10.1007/s00415-013-6836-z

Salinet, A.S.M., Panerai, R.B., Robinson, T.G., 2014. The Longitudinal Evolution of Cerebral Blood Flow Regulation after Acute Ischaemic Stroke. Cerebrovasc. Dis. Extra 4, 186–197. doi:10.1159/000366017

Sapir, A., Kaplan, J.B., He, B.J., Corbetta, M., 2007. Anatomical Correlates of Directional Hypokinesia in Patients with Hemispatial Neglect. J. Neurosci. 27, 4045–4051. doi:10.1523/JNEUROSCI.0041-07.2007

Saur, D., Lange, R., Baumgaertner, A., Schraknepper, V., Willmes, K., Rijntjes, M., Weiller, C., 2006. Dynamics of language reorganization after stroke. Brain 129, 1371–1384. doi:10.1093/brain/awl090

Saxe, R., Powell, L.J., 2006. It's the Thought That Counts Specific Brain Regions for One Component of Theory of Mind. Psychol. Sci. 17, 692–699. doi:10.1111/j.1467-9280.2006.01768.x

Schroeter, M.L., Cutini, S., Wahl, M.M., Scheid, R., Yves von Cramon, D., 2007. Neurovascular coupling is impaired in cerebral microangiopathy—An event-related Stroop study. NeuroImage 34, 26–34. doi:10.1016/j.neuroimage.2006.09.001

Schummers, J., Yu, H., Sur, M., 2008. Tuned Responses of Astrocytes and Their Influence on Hemodynamic Signals in the Visual Cortex. Science 320, 1638–1643. doi:10.1126/science.1156120

Schwartz, W.J., 1978. A role for the dopaminergic nigrostriatal bundle in the pathogenesis of altered brain glucose consumption after lateral hypothalamic lesions. Evidence using the14C-labeled deoxyglucose technique. Brain Res. 158, 129–147. doi:10.1016/0006-8993(78)90010-0

Scoville, W.B., Milner, B., 1957. LOSS OF RECENT MEMORY AFTER BILATERAL HIPPOCAMPAL LESIONS. J. Neurol. Neurosurg. Psychiatry 20, 11–21.

Seeley, W.W., Menon, V., Schatzberg, A.F., Keller, J., Glover, G.H., Kenna, H., Reiss, A.L., Greicius, M.D., 2007. Dissociable Intrinsic Connectivity Networks for Salience Processing and Executive Control. J. Neurosci. 27, 2349–2356. doi:10.1523/JNEUROSCI.5587-06.2007

Sestieri, C., Corbetta, M., Romani, G.L., Shulman, G.L., 2011. Episodic Memory Retrieval, Parietal Cortex, and the Default Mode Network: Functional and Topographic Analyses. J. Neurosci. 31, 4407–4420. doi:10.1523/JNEUROSCI.3335-10.2011

Shen, K., Mišić, B., Cipollini, B.N., Bezgin, G., Buschkuehl, M., Hutchison, R.M., Jaeggi, S.M., Kross, E., Peltier, S.J., Everling, S., Jonides, J., McIntosh, A.R., Berman, M.G., 2015. Stable long-range interhemispheric coordination is supported by direct anatomical projections. Proc. Natl. Acad. Sci. 201503436. doi:10.1073/pnas.1503436112

Shih, A.Y., Friedman, B., Drew, P.J., Tsai, P.S., Lyden, P.D., Kleinfeld, D., 2009. Active dilation of penetrating arterioles restores red blood cell flux to penumbral neocortex after focal stroke. J. Cereb. Blood Flow Metab. 29, 738–751. doi:10.1038/jcbfm.2008.166

Siegel, J.S., Ramsey, L.E., Snyder, A.Z., Metcalf, N.V., Chacko, R.V., Weinberger, K., Baldassarre, A., Hacker, C.D., Shulman, G.L., Corbetta, M., 2016. Disruptions of network connectivity predict impairment in multiple behavioral domains after stroke. Proc. Natl. Acad. Sci. 201521083. doi:10.1073/pnas.1521083113

Siegel, J.S., Snyder, A.Z., Metcalf, N.V., Fucetola, R.P., Hacker, C.D., Shimony, J.S., Shulman, G.L., Corbetta, M., 2014. The circuitry of abulia: Insights from functional connectivity MRI. NeuroImage Clin. 6, 320–326. doi:10.1016/j.nicl.2014.09.012

Siegel, J.S., Snyder, A.Z., Ramsey, L., Shulman, G.L., Corbetta, M., 2015. The effects of hemodynamic lag on functional connectivity and behavior after stroke. J. Cereb. Blood Flow Metab. Off. J. Int. Soc. Cereb. Blood Flow Metab. doi:10.1177/0271678X15614846

Smith, D.V., Clithero, J.A., Rorden, C., Karnath, H.-O., 2013. Decoding the anatomical network of spatial attention. Proc. Natl. Acad. Sci. 110, 1518–1523. doi:10.1073/pnas.1210126110

Smith, E.E., Jonides, J., 1998. Neuroimaging analyses of human working memory. Proc. Natl. Acad. Sci. 95, 12061–12068. doi:10.1073/pnas.95.20.12061

Smith, S.M., Fox, P.T., Miller, K.L., Glahn, D.C., Fox, P.M., Mackay, C.E., Filippini, N., Watkins, K.E., Toro, R., Laird, A.R., Beckmann, C.F., 2009. Correspondence of the brain's functional architecture during activation and rest. Proc. Natl. Acad. Sci. 106, 13040–13045. doi:10.1073/pnas.0905267106

Smith, S.M., Hyvärinen, A., Varoquaux, G., Miller, K.L., Beckmann, C.F., 2014. Group-PCA for very large fMRI datasets. NeuroImage 101, 738–749. doi:10.1016/j.neuroimage.2014.07.051

Smith, S.M., Nichols, T.E., Vidaurre, D., Winkler, A.M., Behrens, T.E.J., Glasser, M.F., Ugurbil, K., Barch, D.M., Van Essen, D.C., Miller, K.L., 2015. A positive-negative mode of population covariation links brain connectivity, demographics and behavior. Nat. Neurosci. 18, 1565–1567. doi:10.1038/nn.4125

Stufflebeam, S.M., Liu, H., Sepulcre, J., Tanaka, N., Buckner, R.L., Madsen, J.R., 2011. Localization of focal epileptic discharges using functional connectivity magnetic resonance imaging. J. Neurosurg. 114, 1693–1697. doi:10.3171/2011.1.JNS10482

Suzuki, M., Sugimura, Y., Yamada, S., Omori, Y., Miyamoto, M., Yamamoto, J., 2013. Predicting Recovery of Cognitive Function Soon after Stroke: Differential Modeling of Logarithmic and Linear Regression. PLOS ONE 8, e53488. doi:10.1371/journal.pone.0053488

Swanson, L.W., 2000. Cerebral hemisphere regulation of motivated behavior. Brain Res. 886, 113–164.

Tallal, P., Miller, S.L., Bedi, G., Byma, G., Wang, X., Nagarajan, S.S., Schreiner, C., Jenkins, W.M., Merzenich, M.M., 1996. Language Comprehension in Language-Learning Impaired Children Improved with Acoustically Modified Speech. Science 271, 81–84. doi:10.1126/science.271.5245.81

Tambini, A., Ketz, N., Davachi, L., 2010. Enhanced Brain Correlations during Rest Are Related to Memory for Recent Experiences. Neuron 65, 280–290. doi:10.1016/j.neuron.2010.01.001

Thiebaut de Schotten, M., Dell'Acqua, F., Ratiu, P., Leslie, A., Howells, H., Cabanis, E., Iba-Zizen, M.T., Plaisant, O., Simmons, A., Dronkers, N.F., Corkin, S., Catani, M., 2015. From Phineas Gage and Monsieur Leborgne to H.M.: Revisiting Disconnection Syndromes. Cereb. Cortex bhv173. doi:10.1093/cercor/bhv173

Thompson, K.G., Biscoe, K.L., Sato, T.R., 2005. Neuronal Basis of Covert Spatial Attention in the Frontal Eye Field. J. Neurosci. 25, 9479–9487. doi:10.1523/JNEUROSCI.0741-05.2005

Uğurbil, K., Xu, J., Auerbach, E.J., Moeller, S., Vu, A.T., Duarte-Carvajalino, J.M., Lenglet, C., Wu, X., Schmitter, S., Van de Moortele, P.F., Strupp, J., Sapiro, G., De Martino, F., Wang, D., Harel, N., Garwood, M., Chen, L., Feinberg, D.A., Smith, S.M., Miller, K.L., Sotiropoulos, S.N., Jbabdi, S., Andersson, J.L.R., Behrens, T.E.J., Glasser, M.F., Van Essen, D.C., Yacoub, E., 2013. Pushing spatial and temporal resolution for functional and diffusion MRI in the Human Connectome Project. NeuroImage, Mapping the Connectome 80, 80–104. doi:10.1016/j.neuroimage.2013.05.012

Ullman, S., 1984. Visual routines. Cognition 18, 97–159. doi:10.1016/0010-0277(84)90023-4

Vaidya, C.J., Gordon, E.M., 2013. Phenotypic Variability in Resting-State Functional Connectivity: Current Status. Brain Connect. 3, 99–120. doi:10.1089/brain.2012.0110

Van Essen, D.C., Drury, H.A., Dickson, J., Harwell, J., Hanlon, D., Anderson, C.H., 2001. An Integrated Software Suite for Surface-based Analyses of Cerebral Cortex. J. Am. Med. Inform. Assoc. 8, 443–459. doi:10.1136/jamia.2001.0080443

van Meer, M.P., Marel, K. van der, Wang, K., Otte, W.M., Bouazati, S. el, Roeling, T.A.P., Viergever, M.A., Sprenkel, J.W.B. van der, Dijkhuizen, R.M., 2010a. Recovery of Sensorimotor Function after Experimental Stroke Correlates with Restoration of Resting-State Interhemispheric Functional Connectivity. J. Neurosci. 30, 3964–3972. doi:10.1523/JNEUROSCI.5709-09.2010

van Meer, M.P., van der Marel, K., Otte, W.M., Berkelbach van der Sprenkel, J.W., Dijkhuizen, R.M., 2010b. Correspondence between altered functional and structural connectivity in the contralesional sensorimotor cortex after unilateral stroke in rats: a combined resting-state functional MRI and manganese-enhanced MRI study. J. Cereb. Blood Flow Metab. 30, 1707–1711. doi:10.1038/jcbfm.2010.124

Várkuti, B., Guan, C., Pan, Y., Phua, K.S., Ang, K.K., Kuah, C.W.K., Chua, K., Ang, B.T., Birbaumer, N., Sitaram, R., 2013. Resting State Changes in Functional Connectivity Correlate With Movement Recovery for BCI and Robot-Assisted Upper-Extremity Training After Stroke. Neurorehabil. Neural Repair 27, 53–62. doi:10.1177/1545968312445910

Verdon, V., Schwartz, S., Lovblad, K.-O., Hauert, C.-A., Vuilleumier, P., 2009. Neuroanatomy of hemispatial neglect and its functional components: a study using voxel-based lesion-symptom mapping. Brain awp305. doi:10.1093/brain/awp305

Vignolo, L.A., Boccardi, E., Caverni, L., 1986. Unexpected CT-Scan Findings in Global Aphasia. Cortex 22, 55–69. doi:10.1016/S0010-9452(86)80032-6

Vijayaraghavan, L., Krishnamoorthy, E.S., Brown, R.G., Trimble, M.R., 2002. Abulia: a delphi survey of British neurologists and psychiatrists. Mov. Disord. Off. J. Mov. Disord. Soc. 17, 1052–1057. doi:10.1002/mds.10194

Vincent, J.L., Kahn, I., Snyder, A.Z., Raichle, M.E., Buckner, R.L., 2008. Evidence for a Frontoparietal Control System Revealed by Intrinsic Functional Connectivity. J. Neurophysiol. 100, 3328–3342. doi:10.1152/jn.90355.2008

Vincent, J.L., Snyder, A.Z., Fox, M.D., Shannon, B.J., Andrews, J.R., Raichle, M.E., Buckner, R.L., 2006. Coherent Spontaneous Activity Identifies a Hippocampal-Parietal Memory Network. J. Neurophysiol. 96, 3517–3531. doi:10.1152/jn.00048.2006

von Monakow, C., 1914. Die Lokalisation im Grosshirn: und der Abbau der Funktion durch kortikale Herde. Verlag von J.F. Bergmann.

Wang, D.J.J., Alger, J.R., Qiao, J.X., Gunther, M., Pope, W.B., Saver, J.L., Salamon, N., Liebeskind, D.S., 2013. Multi-delay multi-parametric arterial spin-labeled perfusion MRI in acute ischemic stroke — Comparison with dynamic susceptibility contrast enhanced perfusion imaging. NeuroImage Clin. 3, 1–7. doi:10.1016/j.nicl.2013.06.017

Wang, L., Yu, C., Chen, H., Qin, W., He, Y., Fan, F., Zhang, Y., Wang, M., Li, K., Zang, Y., Woodward, T.S., Zhu, C., 2010. Dynamic functional reorganization of the motor execution network after stroke. Brain 133, 1224–1238. doi:10.1093/brain/awq043

Ward, N.S., Brown, M.M., Thompson, A.J., Frackowiak, R.S.J., 2003. Neural correlates of motor recovery after stroke: a longitudinal fMRI study. Brain 126, 2476–2496. doi:10.1093/brain/awg245

Watson, B.D., Dietrich, W.D., Busto, R., Wachtel, M.S., Ginsberg, M.D., 1985. Induction of reproducible brain infarction by photochemically initiated thrombosis. Ann. Neurol. 17, 497–504. doi:10.1002/ana.410170513

Watson, R.T., Heilman, K.M., 1979. Thalamic neglect. Neurology 29, 690–690. doi:10.1212/WNL.29.5.690

Watson, R.T., Valenstein, E., Heilman, K.M., 1981. Thalamic neglect. Possible role of the medial thalamus and nucleus reticularis in behavior. Arch. Neurol. 38, 501–506.

Weerd, M. de, Greving, J.P., Hedblad, B., Lorenz, M.W., Mathiesen, E.B., O'Leary, D.H., Rosvall, M., Sitzer, M., Buskens, E., Bots, M.L., 2010. Prevalence of Asymptomatic Carotid Artery Stenosis in the General Population An Individual Participant Data Meta-Analysis. Stroke 41, 1294–1297. doi:10.1161/STROKEAHA.110.581058

Wernicke, C., 1885. Some new studies on aphasia. Fortschr Med 824–830.

Wernicke, C., 1874. The aphasic symptom complex: a psychological study on a neurological basis. Boston Studies in the Philosophy of Science.

Winship, I.R., Murphy, T.H., 2009. Remapping the Somatosensory Cortex after Stroke: Insight from Imaging the Synapse to Network. The Neuroscientist 15, 507–524. doi:10.1177/1073858409333076

Wolf, T.J., Baum, C., Connor, L.T., 2009. Changing Face of Stroke: Implications for Occupational Therapy Practice. Am. J. Occup. Ther. Off. Publ. Am. Occup. Ther. Assoc. 63, 621–625.

Wong, K.S., Huang, Y.N., Gao, S., Lam, W.W.M., Chan, Y.L., Kay, R., 1998. Intracranial stenosis in Chinese patients with acute stroke. Neurology 50, 812–813. doi:10.1212/WNL.50.3.812

Wu, J., Quinlan, E.B., Dodakian, L., McKenzie, A., Kathuria, N., Zhou, R.J., Augsburger, R., See, J., Le, V.H., Srinivasan, R., Cramer, S.C., 2015. Connectivity measures are robust biomarkers of cortical function and plasticity after stroke. Brain awv156. doi:10.1093/brain/awv156

Yemisci, M., Gursoy-Ozdemir, Y., Vural, A., Can, A., Topalkara, K., Dalkara, T., 2009. Pericyte contraction induced by oxidative-nitrative stress impairs capillary reflow despite successful opening of an occluded cerebral artery. Nat. Med. 15, 1031–1037. doi:10.1038/nm.2022

Yeo, B.T.T., Krienen, F.M., Eickhoff, S.B., Yaakub, S.N., Fox, P.T., Buckner, R.L., Asplund, C.L., Chee, M.W.L., 2015. Functional Specialization and Flexibility in Human Association Cortex. Cereb. Cortex 25, 3654–3672. doi:10.1093/cercor/bhu217

Yeo, B.T.T., Krienen, F.M., Sepulcre, J., Sabuncu, M.R., Lashkari, D., Hollinshead, M., Roffman, J.L., Smoller, J.W., Zöllei, L., Polimeni, J.R., Fischl, B., Liu, H., Buckner, R.L., 2011. The organization of the human cerebral cortex estimated by intrinsic functional connectivity. J. Neurophysiol. 106, 1125–1165. doi:10.1152/jn.00338.2011

Zhang, J., Meng, L., Qin, W., Liu, N., Shi, F.-D., Yu, C., 2014. Structural Damage and Functional Reorganization in Ipsilesional M1 in Well-Recovered Patients With Subcortical. Stroke 45, 788–793. doi:10.1161/STROKEAHA.113.003425